INFORMATION TO USERS

This manuscript has been reproduced from the microfilm master. UMI films the text directly from the original or copy submitted. Thus, some thesis and dissertation copies are in typewriter face, while others may be from any type of computer printer.

The quality of this reproduction is dependent upon the quality of the copy submitted. Broken or indistinct print, colored or poor quality illustrations and photographs, print bleedthrough, substandard margins, and improper alignment can adversely affect reproduction.

In the unlikely event that the author did not send UMI a complete manuscript and there are missing pages, these will be noted. Also, if unauthorized copyright material had to be removed, a note will indicate the deletion.

Oversize materials (e.g., maps, drawings, charts) are reproduced by sectioning the original, beginning at the upper left-hand corner and continuing from left to right in equal sections with small overlaps.

Photographs included in the original manuscript have been reproduced xerographically in this copy. Higher quality 6" x 9" black and white photographic prints are available for any photographs or illustrations appearing in this copy for an additional charge. Contact UMI directly to order.

Bell & Howell Information and Learning
300 North Zeeb Road, Ann Arbor, MI 48106-1346 USA
800-521-0600

Characterizations and applications of thiol monolayers adsorbed at gold electrodes

by

Garry Brent Dawson

A dissertation submitted to the graduate faculty

in partial fulfillment of the requirements for the degree of

DOCTOR OF PHILOSOPHY

Major: Analytical Chemistry (Biomolecular Sciences)

Major Professor: Marc D. Porter

Iowa State University

Ames, Iowa

2001

UMI Number: 3003236

UMI Microform 3003236

Bell & Howell Information and Learning Company
300 North Zeeb Road
P.O. Box 1346
Ann Arbor, MI 48106-1346

Graduate College
Iowa State University

This is to certify that the Doctoral dissertation of

Garry Brent Dawson

has met the dissertation requirements of Iowa State University

Signature was redacted for privacy.

Major Professor

Signature was redacted for privacy.

For the Major Program

Signature was redacted for privacy.

For the Graduate College

TABLE OF CONTENTS

ACKNOWLEDGEMENTS

The work described in this dissertation was the result of not only many hours of hard work, but also many years of advice, encouragement, and support by coworkers, friends, and family. When questions, doubts, and times of loneliness arose, I always could find someone to listen and give support. It is because of them that this work has reached a state of closure and to them all credit is due.

The Porter Group has always maintained a sense of community and creativity and has been a pleasant environment in which to work. This atmosphere is due largely to the personality of Marc Porter and his ability to smooth out any conflict that arises from the heterogeneity of personalities and backgrounds present in the lab. Through his leadership, the group members realize that we are caught in a 'web of mutuality' where the success of one is tied to the success of all. Two group members who are particularly adept at nurturing others are Chuanjian Zhong and Bob Lipert. Their ability to explain complex phenomena in simple terms is complemented by their ability to encourage students to be their best. This work is built upon the work and advice of the previous electrochemists in the group particularly that of Neal Simmons and Season Wong who are good scientists and better friends. Without the friendship, direction, and employment advice of Janese O'Brien, Jeremy Kenseth, Becky Staedtler, I would have lost focus along the way and continually wallowed in self-pity. Thanks for keeping me mentally on track.

Without the good friends that I have made in Ames, I would not have stayed for six years. Coffee and long conversations with Laurie Cardoza and Jennifer Harnisch have maintained my emotional stability and self-esteem. You have shown me unconditional friendship, and you deserve all the happiness that this life can bring. Desiree Grubisha and

Steph Syverson were always there to listen to me complain about everything. I am sure that our conversations reduced my stress level and prolonged my life. Barbara Woods and Rev. David Russell and all of the members of First Baptist Church have provided advice, love, and support in all things spiritual and have taught me how to serve others. I will truly miss all of you.

In conclusion, I thank my family for giving me long distance support for all of my life, especially the last six years. My mother Jerrie Dawson and my father Sam always stressed the importance of education, and I think that I might have listened a little too well. My sister, Myra Smith, and my cousin Bentley Sweeton have always understood me, and the things, I do even when others don't. I am glad that you are never more than a phone call away.

GENERAL INTRODUCTION

Overview of Monolayer Structure

Self-assembled monolayers (SAMs) of thiols $X(CH_2)_nSH$, sulfides $X(CH_2)_nS(CH_2)_mY$, and disulfides $X(CH_2)_nSS(CH_2)_mY$ at gold have been extensively studied over the past two decades.[1,2] These monolayers possess a common orientation and definable structural regions that include a head group, spacer region, and terminal group. These films can be utilized to control interfacial properties as well as act as platforms for analytical sensors. The following paragraphs provide background on the structure and properties of thiolate monolayers at gold electrodes, discuss the current consensus on the hydrogen-containing product of monolayer formation, and describe examples of electrochemical detection schemes that utilize these systems.

Monolayers prepared from thiols and disulfides at gold surfaces have been shown to form stable structures due to a balance of enthalpic and entropic forces.[3] Through temperature programmed desorption experiments, the strength of the Au-S bond was found to be 44 kcal/mol,[4] and this relatively strong coordinate covalent bond helps to counteract unfavorable entropy changes that occur when the precursor is removed from solution. In the case of a thiol precursor, the S-H bond cleaves,[5] and the adsorbed species is a thiolate. For disulfides, the relatively weak S-S bond cleaves, and each molecular fragment adsorbs as a thiolate producing two Au-S bonds. Furthermore, the all-*trans* carbon backbone of the alkyl chain tilts to maximize van der Waals interactions among the methylene groups adding stability to the structures.[4,6,7] Diffraction techniques and *ab initio* calculations have provided

further insight into the structure of monolayer at gold substrates.[8,9] The lattice constant found by low energy helium diffraction, 5.01 Å, was in good agreement with that found by an electron diffraction study.[9] *Ab initio* calculations have determined the threefold hollow site to be the favored adsorption site on the Au (111) surface, and it is generally assumed that thiolates adopt a $\sqrt{3}$ x $\sqrt{3}$ R30° overlayer structure at the threefold hollow sites with a 30° tilt from the surface normal.[8] A later study found a c (4x2) superlattice for the $\sqrt{3}$ x $\sqrt{3}$ R30° overlayer structure of octadecanethiol on a Au (111) surface. The unit cell was speculated to contain four thiol chains; two with clockwise chain twists and two with counterclockwise chain twists.[7]

Monolayer technology allows one to control properties such as friction, capacitance, and ion permeability through the spontaneous adsorption of species with a variety of terminal functional groups such as $-CH_3$, $-CF_3$, -COOH, and $-COOCH_3$. Specifically, varying the identity of these terminal groups, one can manipulate the properties of the films. Whitesides and co-workers have used contact angle measurements to determine the differences in surface free energy of different alkanethiols.[10] Porter and coworkers have also shown that the interfacial friction and adhesion changes with functional group identity using the atomic force microscope (AFM).[11]

Further control over interfacial properties can be realized through the use of mixed monolayers. Monolayers of mixed characteristics can be formed by using a sulfide or disulfide where X and Y are not the same,[12,13] co-assembling a monolayer with two sulfur-containing species in the formation solution,[14,15] or preparing a monolayer of one species and removing a fraction of the species from the surface by photo-oxidation[16] and replacing it

with another species. Ideally mixed monolayers form structures where the thiols are homogeneously mixed on the surface; usually, however the structures form with some degree of phase segregation. When monolayers are formed from two components in solution or from the homolytic S-S bond cleavage of an asymmetric disulfide, a homogeneous surface is formed with properties different from each independent thiol.[17] Phase-segregated surfaces can be formed by partially replacing one thiol with another after photo-oxidation. These surfaces will show characteristics of one or both thiols depending on the spatial resolution of the technique used for the interrogation. Furthermore, patterning techniques allow one to control surface properties in micron-sized domains across the surface.[18]

Many techniques have been used to characterize these systems, and the findings of some of the more important electrochemical and spectroscopic studies will be discussed in the next few paragraphs, followed by discussions of the fate of the sulfhydryl hydrogen and of some electrochemical applications of monolayers that have been recently developed.

Findings from Electrochemical Measurements

Through the use of voltammetry and chronoamperometry, much has been learned about the structure and stability of alkanethiolate monolayers at gold. Porter et al. reported the blocking nature of alkanethiol films using two ionic redox probes. From their data, they speculated that electron transfer occurred via a tunneling process through the film. Specifically, a plot of the reciprocal capacitance versus number of methylene units gave a slope of 0.055 $cm^2/\mu F$ and an intercept of 0.1 μF.[19] The relative ionic permeability, as determined by cyclic voltammetry, was reported by Chidsey and co-workers, and when these data were compared with measured contact angles of the surfaces important differences were noted. Specifically, the ionic permeability for a series of monolayers was shown to increase

in the following order: $CF_3(CF_2)_7(CH_2)_2SH < CH_3(CH_2)_9SH < HOCH_2(CH_2)_{10}SH < NC(CH_2)_{10}SH < HO_2C(CH_2)_{10}SH$, while the cyano-terminated film gave a water contact angle that was higher than the hydroxy terminated one.[20] These differences were attributed to the small size of the hydroxy terminus and hydrogen bonding of the hydroxy-terminated film.

Monolayers have been shown to be unstable under the effects of applied potential due to reductive and oxidative desorption of the films.[21] Creager and Groat reported the instability of dodecanethiolate monolayers in propylene carbonate in the 0.0-0.8 V vs. Ag/AgCl potential range,[22] yet the stability of the monolayers was enhanced by adding 50 μM dodecanethiol to the solution during the voltammetric scans. While no size selectivity was noticed in the heterogeneous electron transfer to several redox probes, electron transfer to charged species was slower than to neutral ones. Everett et al. showed the instability of monolayers in methylene chloride solutions at potentials less that -0.8 V vs. Ag/AgCl and greater than 0.6 V.[23]

Open circuit measurements have proven useful in efforts to determine the mechanism of monolayer formation. Majda and co-workers performed open circuit potential measurements during the transfer of a Langmuir film of a thiol/alcohol monolayer to a gold surface.[24] From these measurements, they speculated that the formal partial charge number per thiol was 0.28-0.38 e^- and not $1e^-$ as Porter and coworkers concluded.[21] Experiments at rough surfaces, such as gold foil, led to higher numbers of the formal partial charge possibly indicating that a different amount of adsorption was taking place at these substrates. It is highly likely that identical surface concentrations are not realized in the different experiments due to the different thermodynamic forces present in the two preparation methods.

Furthermore, the assumption that similar levels of double layer charging are active in alcohols and thiols may not be valid. In a later study, Porter and co-workers showed that the shifts in open circuit potential upon the adsorption of thiols were much lower than expected and demonstrated that a concomitant reductive reaction was highly probable.[25]

Electrochemical Reductive Desorption (ERD)

While applying a large cathodic potential to monolayer-coated electrode can induce instability, the current-potential curves recorded during this process can give much insight into the structure and formation of the monolayer. During ERD, potential scans are initiated at a potential where the monolayer is stable (i.e., > -0.2 V vs. Ag/AgCl). The potential is then scanned negatively to induce the reductive cleavage of the gold-thiolate bond and the subsequent desorption of the thiolate species. The observed peak seen in the current trace is due to both the faradaic and the capacitive processes. When the scan is reversed, an oxidative re-deposition wave is seen for the desorbed thiolate whose magnitude increases proportionally with increased thiol chain length. Typically alkaline solutions are used to move the solvent reduction potential to a more negative value (i.e., -1.4 V vs. Ag/AgCl for pH 13.7), and such conditions increase the solubility of the desorbed species.[26,27]

Much of the work described in this dissertation utilizes ERD to probe the monolayer structure and formation kinetics. Additionally, this technique can give insight into the coverage, structural order, and the strength of the gold-sulfur bond of the adlayer, as well as the crystallinity of the surface.[21,28,29] The integrated area under the desorption wave is related to the surface coverage of the monolayer. When the reduction reaction is assumed to have an electron to thiolate ratio of 1, the following equation applies:

$$\Gamma = \frac{Q_f}{FA} \tag{1}$$

where Q_f is the integrated charge, F is the Faraday (96,486 C / mole e-) and A is the real area of the electrode. A is calculated by multiplying the geometric area of the electrode by a roughness factor which is typically 1.1-1.2 for annealed substrates and 1.3-1.4 for unannealed substrates. The integrated charge, Q_f, is the difference between the total integrated charge, Q_T, and the capacitive charge, Q_C, which is estimated to be 0.1-0.2 Q_T through calculations based on a Frumkin model.[30,31] Porter and co-workers first demonstrated the viability of this method for determining surface coverage.[32] They formed monolayers of a thiol terminated with a ferrocene moiety and found the calculated charge from reductive desorption to be comparable to that found for the reversible heterogeneous electron transfer to the tethered species.

The peak potential for desorption of the monolayer is indicative of the strength of the interaction between the sulfur and the gold atoms and potential of zero charge (pzc) of the gold electrode. A strong interaction between the gold and the sulfur moves the peak potential negatively, and this fact has been used to explain the more negative peak potentials seen for the desorption of thiols from the pseudo-four-fold hollow sites of the Au(110) surfaces in comparison to that from the three-fold hollow sites of the Au(111) terraces. Furthermore, the pzc of the Au (111) surface is 200 mV positive of the pzc of the Au (110) surface which also argues that the potential for the reductive cleavage of the Au-S would be more negative for the Au (110) surface.

The peak potential will also move negatively as the interactions between the chains of the adlayer increase due to decreased ionic permeability. For longer chain thiols a higher

potential gradient is needed to bring counter ions into the film before the monolayer can be desorbed. Specifically, a -20 mV / methylene unit shift in desorption peak potential was recorded for a homologous series of alkanethiols.[21]

The dependence of the peak potential on chain-chain interactions and the nature of the adsorption site gives rise to changes in the shape of the desorption wave. Desorption waves for heterogeneous unannealed surfaces are broadened due to the presence of differently sized domains on the terraces and steps of the gold surface, yielding multiple, broad peaks for the desorption of thiols from small domains on the terraces and steps.[28,33] For annealed surfaces possessing thiolate domains as large as 600 nm^2,[34] the full width at half maximum (fwhm) is typically < 90 mV for desorption of alkanethiols and is indicative of attractive interactions among the adsorbates in similarly sized domains.[35] Undecanethiol and longer chain homologs exhibit a split desorption peak, with the separation of the two components being less than 100 mV.[29] This "fine structure" has been attributed to the difference in domain sizes and the topography of the substrate.[36]

By monitoring the rate of the decay of the current after a potential step has been applied to the monolayer-coated electrode, one can gain mechanistic insights into the nature of the desorption process. The mechanism has been shown to involve three steps-- creation of etch centers by reduction of a thiolate located at a domain boundary, removal of the reduced thiol, and further reduction of the thiol around the etch center.[37,38] The rate of the first step is dependent on the surface tension of the film and the magnitude of the overpotential, whereas the second and third steps are dependent on the extent of chain-chain interactions and the overpotential, respectively. The rates of the first two steps will decrease with increasing chain lengths with the third step being independent of chainlength. The rate

of the first and third steps will increase with increasing overpotential with the second step being independent of chain length.

By combining ERD with other techniques, one can shed light on both the adsorption and desorption processes. Schneider and Buttry performed electrochemical quartz crystal microbalance experiments to investigate monolayer formation and desorption processes in several organic solvents.[39] Their studies showed that multi-layers of long chain thiols initially formed in acetonitrile, however multi-layers were not formed when dimethylformamide(DMF) was used as the solvent. While the frequency changes correlated to the partial monolayer formation in DMF, the total integrated charge was greater than that expected for a 1 e^- reduction process of a single monolayer. From their desorption experiments, they concluded that, due to the high capacitance at gold electrodes in DMF a considerable fraction of the measured charge could be attributed to the non-faradaic processes; hence, ERD is not a reliable measure of surface coverage. This study illustrates that caution should be exercised in using ERD coverage data obtained under conditions where the capactive currents could be larger than the 18 $\mu C/cm^2$ estimated by Zhong and Porter.[40] Shimazu and co-workers, also using electrochemical quartz crystal microgravimetry (EQCM) techniques, determined that the ERD process was accompanied by the simultaneous adsorption of a cation from the electrolyte solution, which explained discrepancies in the experimental and expected value of mass change per molecule and the expected one.[41] Through the use of in-situ infrared spectroscopy, Morin and coworkers described the ERD process as involving two steps with the first being reduction of the thiol to a thiolate species followed by the formation of micelles giving rise to a capacitive current.

Many uses of the desorption technique have been demonstrated since its original description. Weisshaar, Lamp, and Porter showed that the extent of self-assembly can be manipulated by controlling the potential applied to the monolayer.[42] Holding the potential in the region of thiolate desorption in the presence of a thiolate in solution formed partial monolayers. In another study, an array of microelectrodes was formed by selectively desorbing mercaptopropionic acid (MPA) from a mixed monolayer composed of MPA and hexadecanethiol. The electrochemical behavior of the array further confirmed that the original surface was homogeneous and not phase-segregated.[43] ERD was used to confirm that homogeneously mixed monolayers of two thiolate components were created when two asymmetric disulfide precursors [$(CH_3(CH_2)_9$-S-S$(CH_2)_2(CF_2)_5CF_3$ and $CH_3(CH_2)_3$-S-S-$(CH_2)_{15}CH_3$] were used.[13] The mixed and single component thiolate monolayers exhibited different desorption potentials indicating that little phase segregation had occurred. Wang and co-workers used reductive desorption to remove thiol-modified single and double stranded DNA from gold microelectrode surfaces. The authors proposed that this technique could be used to deliver nonviral DNA to patients *in vivo*.[44]

Findings from X-ray Photoelectron Spectroscopy

X-ray photoelectron spectroscopy (XPS) uses X-rays to the remove core electrons from the atoms on the surface. The kinetic energy of these electrons is not only representative of the atoms on the surface but also their oxidation states. Furthermore, as the angle between the surface and the energy analyzer approaches the surface normal, the electrons from atoms buried beneath the surface are preferentially sampled. Therefore, one can perform depth profiling of a few nanometers[45] by varying the takeoff angle.

In the case of organosulfur monolayers, XPS has been used to determine the oxidation of the sulfur atom on the surface and its location in the film. Due to the area (diameter > 100 μm) irradiated by the x-ray beam, this technique gives the average chemical state of elements present on the surface, yet is insensitive to microscopic differences that might arise on surfaces composed of two or more different thiols. Furthermore, the inherent spectral resolution of the technique prevents the determination of the nature of the adsorption site on the surface due to the small differences in binding that exists between step and terrace binding sites.

Nevertheless, a significant amount of valuable information has been gained with this technique. In an early study, XPS was used to confirm the desorption of a hexadecyl disulfide monolayer when it was heated above 225 °C.[46] Additionally, XPS has been employed to confirm the differences in the binding of methanethiol and dimethyl disulfide from the gas phase. Specifically dimethyl disulfide was shown to form a stable monolayer with an S (2p) binding energy of 162.7, whereas methanethiol-modified surfaces contained this peak only after long exposure to the X-ray source.[4] Films formed from disulfides and thiols were found to have similar spectra in the S (2p) binding region indicating that a similar thiolate species is present on the surface.[47] As a final example, Bain et al. reported on a change in atomic percentages when takeoff angles were varied.[10] A maximum of 4 % (atomic) was reported for sulfur at a 90° takeoff angle indicating that the sulfur atoms located at the gold surface are greatly attenuated by the alkyl chains which are closer the to the energy analyzer.

XPS measurements have also been quite useful in determining surface compositions of mixed monolayers. In one study, the O (2p) signal was shown to increase with the mole

fraction of an alcohol-terminated thiol present in solution that also contained a methyl-terminated species.[14] In a exchange-replacement study, monolayers formed from $HO(CH_2)_{16}SS(CH_2)_3CF_3$ were shown to lose fluorine preferentially from the surface when placed in a solution of $HS(CH_2)_{16}CN$, and this loss was attributed to an exchange-replacement mechanism.[17]

Furthermore, similarities and differences in the structure of sulfide and thiolate monolayers have been explored by with XPS. In one report, data from the C (1s), O (2p), and S (2p) binding regions confirmed the expected monolayer composition formed from alkyl sulfides.[12] Porter and co-workers used XPS to show that monolayers formed from purified alkyl sulfides gave lower intensities and different binding energies in the S (2p) region than those formed from equivalent disulfide and thiol precursors. This difference was attributed to relatively weaker bond formed between the gold surface and the sulfur in the sulfide monolayers.

Several experiments using XPS have shown the presence of two oxidation states of sulfur. In a study using two different x-ray sources and multiple takeoff angles these different states were interpreted to be due to adsorbed disulfide with each of the two sulfurs located at different type of adsorption sites.[48] In another study, these two forms of sulfur were attributed to bound thiolate and unbound thiol and disulfide.[49] Taken together, the studies summarized above have demonstrated the utility of XPS in determining average surface elemental composition and the change of oxidation state of the sulfur molecule during the adsorption of thiols and disulfides.

Findings From Infrared Reflection Absorption Spectroscopy (IRRAS)

Chemical functionality and orientation information of monolayer samples can be gained through the use of grazing angle infrared reflection absorption spectroscopy. For monolayers on gold, the *p*-polarized light strikes the surface at a high angle of incidence with respect to the surface normal. The negative logarithm of the ratio of the sample reflectance signal and the background reflectance signal for each wavelength is then plotted. Surface selection rules state that dipole transitions parallel to the surface will not be excited since the due to the use of light polarized in the plane of incidence.[50] Therefore, the closer the transition dipole of a vibration coincides to the surface normal, the stronger the absorbance of the vibration. When compared to bulk spectra, the monolayer spectrum can provide much information on the orientation of the molecules in the film.[51] Furthermore, the position of certain bands shift as the crystallinity of the film changes (see below).

Chain geometry, tilt and twist angles, and the extent of chain-chain interactions have been determined by IRRAS data. In one of the earliest studies, Nuzzo and Allara confirmed the all *trans* configuration of the monolayer alkyl chains by reporting the presence of a series of sharp bands (i.e., the progression bands) in the 1200-1350 cm^{-1} region of the spectrum.[52] The methylene chains of monolayers formed from hexadecyl disulfide were determined to be in a highly crystalline state, as they are when dispersed in a potassium bromide (KBr) matrix, due to the similar positions for the symmetric and asymmetric methylene stretches.[46] Also, the infrared data were used to predict a 37° tilt angle from the surface normal for the alkyl chains of the hexadecyl disulfide monolayer, which was confirmed by an electron diffraction study.[9] The twist angle was found to be 55° for hexadecyl disulfide, and a model of disulfide

bond cleavage was proposed. In this study, spectroscopic measurements also demonstrated the stability of the films upon exposure to organic solvents.

The variable length of the methylene chain gives rise to many notable changes in the IRRAS spectra. Studies of monolayers formed from thiols of different chain lengths showed a progression from a liquid-like to a more crystalline environment in going from butyl mercaptan to docosyl mercaptan.[19] Specifically, the C-H stretching vibrations move to lower wave numbers with increased order in the polymethylene chains. While the intensity of the methylene stretches is expected to decrease with decreasing chain length, the measured decrease is much larger than expected one. This larger decrease is attributed to lower surface coverages and decreased film order for shorter chainlength thiols. Additionally, the intensity of the asymmetric methyl stretch alternates when the number of methylene units in the chain is increased by one. This behavior, termed the odd-even effect, is attributed to the change in the orientation of the dipole moment of the methyl group when the chain length is either an even or odd numbered.[53]

Like XPS, IRRAS has shown differences in monolayers formed from sulfides and thiols. For example, Troughton et al. reported the IRRAS spectra for several monolayers formed from alkyl sulfides.[12] The positions for the symmetric and asymmetric stretches were much higher than those reported for the equivalent thiol precursors, indicating more disorder in the films formed from the sulfide.

IRRAS has also been used to illustrate the manner in which the substrate affects the monolayer structure. A comparison of the IRRAS data for thiolate monolayers on Au, Ag, and Cu indicates smaller tilt angles for the films on Cu and Ag than those seen on Au and demonstrates that the substrate-adsorbate interaction can determine the tilt angle of the

methylene chains.[54] A thorough study of the infrared spectra for thiol monolayers at Au (100) and Au (111) resulted in discovery of important differences in the structures seen at the two substrates. Monolayers at Au (100) showed a much smaller tilt angle (14°) and the absence of an odd even effect for the symmetric and asymmetric methyl stretches.[55] These data helped to explain how the chains accommodate the c (2x2) overlayer structure imposed by the cubic lattice.

The effect of monolayer endgroup on methylene chain organization has also been probed by IRRAS. Monolayers derivatized with a variety of functional groups ($X(CH_2)_{15}SH$ ($X = CH_3$, CH_2OH, CO_2H, CO_2CH_3, and $CONH_2$) were prepared and characterized with infrared spectroscopy.[53] The similarities in the spectra in the high-energy regions and calculated tilt and twist angles indicated that the nature of the terminal group did not influence the packing of the methylene chains.

Manipulation of monolayer temperature produced distinct changes in the recorded spectra as reported by Nuzzo et al.[56] The differences reported for the spectra of a monolayer formed from a docosyl thiol precursor taken over a large temperature range (80-420 K) were attributed to the increase in the number of *gauche* kinks present in the films at higher temperatures. Moreover, the splitting of the scissoring band of the methylene groups supports rotational distortions and/or differences in tilt directions to maximize chain interactions while accommodating the sulfur-sulfur spacing prescribed by the substrate.

To summarize briefly, IRRAS is highly sensitive to the order and orientation of thiolate monolayers on gold surfaces and has demonstrated increased disorder in shorter chainlength thiolate monolayers. Furthermore, changes in film composition and reactivity upon exposure to chemical reagents can be monitored by following spectral changes with

increased exposure times.[44] Finally, the ever-increasing spatial resolution of the technique will extend its applicability in compositional analysis of mixed monolayers.[57]

Fate of the Sulfhydryl Proton

Based on results from XPS,[47] IRRAS,[19] Fourier transform mass spectrometry,[58] electrochemistry and Raman spectroscopy,[5,21] it is generally recognized that the predominant sulfur species on the surface is a thiolate. The absence of an S-H stretch in the Raman or infrared spectrum of monolayers points to cleavage of the bond, but the fate of the hydrogen has not been clearly established. Initial efforts to detect H^+ in conductivity measurements showed no detectable change in ionic strength.[3] Furthermore, an initial attempt to detect the evolution of hydrogen during monolayer formation with gas chromatography coupled with thermal conductivity detection was only partially successful.[59] Moreover, recent *ab initio* calculations have shown that the formation of molecular hydrogen would work to stabilize the adsorbed thiolate by 1-3 kcal/mol.[60] Thin layer spectroscopic data presented in Chapter 5 will show unequivocally that H^+ is generated in the adsorption process in aqueous solutions.

Monolayer Applications in Electrochemical Detection Schemes

Self-assembled monolayers at gold have become widely used as electrochemical sensing platforms because they provide a convenient mode of attaching modifying coatings to electrode surfaces to manipulate the selectivity and/or sensitivity of the analysis. Specifically, thiolate monolayers function as ligands or hosts for electroactive species and selectively permeable barriers. Much of the work in using monolayers in electrochemical, as

well as optical and piezoelectric, sensors has been recently reviewed by Reinhoudt and co-workers.[61] The following paragraphs describe a few examples of the novel detection schemes that utilize thiolate monolayers at gold electrodes.

Through specific interactions between the terminal groups of the monolayer and solution analytes, increased sensitivity and selectivity in electrochemical detection can be realized. Steinberg and Rubinstein demonstrated the highly sensitive and selective determination of Cu^{2+}, Pb^{2+}, and Zn^{2+} in the presence of Fe^{2+}.[62] In this scheme, 2,2'-thiobis(ethyl acetoacetate)/octadecyl silane films at gold were used to preconcentrate the metal ions for voltammetric detection. Detection limits of 10^{-7} M were achieved for Cu^{2+} with a dynamic range of four orders of magnitude. Rojas et al. showed that β-cyclodextran molecules could be immobilized on a surface after attaching thiol tethers. These hosts were shown to effectively complex electroactive guest molecules, such as ferrocenes, which were later displaced by guests with higher affinity constants.[63] Murakami and co-workers described an alternate method to detect sugars using boronic acid terminated thiols. They synthesized disulfide molecules, which contained a viologen group and were terminated with a phenyl boronic acid group. When the sugar was complexed by the boronic acid group, a negative shift in the viologen reduction wave was recorded.[64] A similar study noted that electron transfer between boronic acid-terminated monolayers on gold and a redox species in solution was also blocked upon the addition of a sugar or a glycoprotein.[65]

The permeability and electronic charge of thiolate monolayers has been shown to give selectivity to gold electrodes in a variety of detection formats. Wang and co-workers demonstrated the utility of monolayer modified electrodes in an amperometric detection scheme for flow injection analysis.[66] As the chain length of the adsorbed thiolate increased,

the detection current for the analytes decreased, while the magnitude of the decrease was unique for the analyte. Specifically, alkanethiols with chain lengths of 12 or more methylene units could significantly attenuate the oxidative current for ferrocyanide and ascorbic acid, though oxidative currents for chlorpromazine and dopamine showed only partial attenuation. Moreover, experiments performed over a six-hour period under hydrodynamic conditions demonstrated the long term stability of the monolayer modified electrodes. Additionally, Brajter-Toth and coworkers utilized the permselectivity of thioctic acid monolayers to ionic redox couples deposited on gold ultra microelectrodes to determine the pK_a of the acid.[67] This same group demonstrated that electrodes coated with mixed monolayers of acid- and methyl-terminated thiols had lower sensitivies to catecholamine and quinone probes than to $Ru(NH_3)_6^{3+}$, regardless of the surface concentration of each thiolate species.[68] These studies showed that many factors, such as molecular shape and redox mechanism, could influence electrochemical detection of analytes at monolayer-coated electrodes. In a recent study, Ward and co-workers demonstrated the enhanced selectivity of a voltammetric microelectrode array consisting of electrodes coated with different chainlength thiols. Though the results had to be obtained in a serial fashion, the ability to determine electroactivity in the absence of a concomitant pH change made it far superior to similar strategies using fluorescent detection.[69] Finally, Gadzekpo et al. described the detection of protamine by its ability to inhibit the diffusion of redox probes to a gold surface coated with a thioctic acid monolayer.[70]

Microelectrode pH sensors have been developed through the formation of mixed monolayers. In an early paper, Wrighton and co-workers described a micro scale pH sensor based on monolayer technology where quinone and ferrocene terminated thiols were co-

immobilized, and changes in the position of the redox wave for the quinone relative to that of the ferrocene were measured.[71] This strategy had internal calibration (the ferrocene redox couple) and could accurately determine pH over an 8 unit range. In a similar study, Willner and co-workers modified a quinone-containing sulfide monolayer with a ferrocene derivative for pH determination.[72]

Several groups have also utilized derivatized porphyrin molecules as surface-bound redox mediators for the catalytic determination of dissolved gases. Porter and co-workers presented the utility of a cobalt porphyrin monolayer for the determination of dissolved oxygen. Cobalt tetraphenyl and diphenyl etio porphyrins were derivatized with one and two thiols and were shown to be catalytic towards the reduction of oxygen, though a diluent alkanethiol was needed to produce an active film in the case of the singly derivatized porphyrin.[73] In a similar study, a tetra-thiolated cobalt porphyrin was used to form monolayers catalytic towards reduction of oxygen to hydrogen peroxide. These monolayers were found to be more active and durable than nonspecifically adsorbed cobalt tetraphenyl porphyrins at carbon electrodes.[74] In a later study, porphyrins were attached to monolayers through the axial ligation of the metal by nitrogen containing molecules such as pyridinethiol and *p*-aminothiophenol. While this method is widely applicable and easy to use, the redox activity of the layer was not reported and could be compromised due to the presence of the axial ligands.[75,76]

The highly selective hybridization of complementary DNA strands has also been detected through faradaic and capacitive detection schemes that use immobilized monolayers of thiolated oligonucleotides. Umezawa and co-workers recently described the detection of a single base pair mismatch by monitoring the electrode response to a solution phase redox

couple.[77] The binding of the complementary strand produced an electrostatic repulsion between the electrode surface and the ferricyanide redox probe which effectively blocked access to the surface. With the mismatched oligonucleotide, ion channels are present and provide access to the electrode surface. Berggren et al. performed initial studies involving the capacitive detection of DNA hybridization. While they found the technique highly sensitive, it was not selective enough to distinguish between the true complement and similar strands of DNA, and it also lacked reproducibility. The authors suggested that the use of peptide nucleic acids (PNAs) would decrease the non-specific adsorption and increase selectivity.[78]

While many methods using biological molecules are highly developed, spontaneously adsorbed monolayers offer many potential improvements over the established detection methods due to their ease of preparation and tunability of characteristics. Taniguchi first used a bipyridyl disulfide monolayer to function as a promoter for the electron transfer between cytochrome *c* and a gold electrode,[79] and since that time, it has been recognized that monolayers can often prevent the denaturation of enzymes that occurs at high free energy metal surfaces.[80] Furthermore, organic monolayers can provide a fixed tunneling distance for electron transfer between electrode and protein.[81] Also through the proper choice of monolayer terminal group, an enzyme can be properly aligned for optimum electron transfer through site specific attachment to the monolayer.[82]

Dissertation Organization

The body of this dissertation is divided into six chapters, following the general introduction. Each chapter is presented as a separate manuscript. Chapter 1 describes the use of sulfonate-terminated monolayers in redox amplification schemes. X-ray photoelectron spectroscopy (XPS), infrared reflection absorption spectroscopy (IRRAS), and electrochemical reductive desorption (ERD) data are presented which give insight into the structure of this novel monolayer. The responses of the electrode to the neurotransmitter dopamine and a common interfering species are reported and explained.

Chapter 2 describes several attempts to selectively determine nitric oxide (NO), a molecule important in cellular signaling pathways, using monolayer-coated electrodes. Chapter 3 describes the use of ERD to monitor the kinetics of monolayer formation at annealed and unannealed gold surfaces. The growth isotherms for the processes are given and compared to data found with other techniques. Chapter 4 explains a re-examination of the reductive desorption of butanethiolate from annealed surfaces showing the variety of voltammetric curves seen for this system. Chapter 5 details experiments that detect pH changes during monolayer formation using thin-layer spectroscopy. The last chapter provides a prospectus for the use of monolayers in electrochemical detection systems.

References

(1) Zhong, C.-J.; Porter, M. D. *Anal. Chem.* **1995,** *67,* 709 A-715 A.

(2) Ulman, A. *Chem. Rev.* **1996,** *96,* 1533-1554.

(3) Schessler, H. M.; Karpovich, D. S.; Blanchard, G. J. *J. Am. Chem. Soc.* **1996,** *118,* 9645-9651.

(4) Nuzzo, R. G.; Zegarski, B. R.; Dubois, L. H. *J. Am. Chem. Soc.* **1987,** *109,* 733-740.

(5) Bryant, M. A.; Pemberton, J. E. *J. Am. Chem. Soc.* **1991,** *113,* 8284-8293.

(6) Chidsey, C. E. D.; Liu, G.-Y.; Rowntree, P.; Scoles, G. *J. Chem. Phys.* **1989,** *91,* 4421-4423.

(7) Camillone III, N.; Chidsey, C. E. D.; Liu, G.-y.; Scoles, G. *J. Chem. Phys.* **1993,** *98,* 3503-3511.

(8) Sellers, H.; Ulman, A.; Shnidman, Y.; Eilers, J. E. *J. Am. Chem. Soc.* **1993,** *115,* 9389-9401.

(9) Strong, L.; Whitesides, G. M. *Langmuir.* **1988,** *4,* 546-558.

(10) Bain, C. D.; Troughton, E. B.; Tao, Y.-T.; Evall, J.; Whitesides, G. M.; Nuzzo, R. G. *J. Am. Chem. Soc.* **1989,** *111,* 321-335.

(11) Green, J.-B. D.; McDermott, M. T.; Porter, M. D.; Siperko, L. M. *J. Phys. Chem.* **1995,** *99,* 10960-10965.

(12) Troughton, E. B.; Bain, C. D.; Whitesides, G. M.; Nuzzo, R. G.; Allara, D. L.; Porter, M. D. *Langmuir.* **1988,** *4,* 365-385.

(13) Azehara, H.; Yoshimoto, S.; Hokari, H.; Akiba, U.; Taniguchi, I.; Fujihira, M. *J. Electroanal. Chem.* **1999,** *473,* 68-74.

(14) Bain, C. D.; Evall, J.; Whitesides, G. M. *J. Am. Chem. Soc.* **1989,** *111,* 7155-7164.

(15) Bain, C. D.; Whitesides, G. M. *J. Am. Chem. Soc.* **1989,** *111,* 7164-7175.

(16) Tarlov, M. J.; Burgess, D. R. F.; Gillen, G. *J. Am. Chem. Soc.* **1993,** *115,* 5305-6.

(17) Biebuyck, H. A.; Whitesides, G. M. *Langmuir.* **1993,** *9,* 1766-1770.

(18) Kumar, A.; Whitesides, G. M. *Appl. Phys. Lett.* **1993,** *63,* 2002-4.

(19) Porter, M. D.; Bright, T. B.; Allara, D. L.; Chidsey, C. E. D. *J. Am. Chem. Soc.* **1987,** *109,* 3559-3568.

(20) Chidsey, C. E. D.; Loiacono, D. N. *Langmuir.* **1990,** *6,* 682-691.

(21) Widrig, C. A.; Chung, C.; Porter, M. D. *J. Electroanal. Chem.* **1991,** *310,* 335-359.

(22) Groat, K. A.; Creager, S. E. *Langmuir.* **1993,** *9,* 3668-3675.

(23) Everett, W. R.; Welch, T. L.; Reed, L.; Fritsch-Faules, I. *Anal. Chem.* **1995,** *67,* 292-298.

(24) Krysinski, P.; Chamberlain II, R. V.; Majda, M. *Langmuir.* **1994,** *10,* 4286-4294.

(25) Zhong, C.-J.; Woods, N. T.; Dawson, G. B.; Porter, M. D. *Electrochem. Commun.* **1999,** *1,* 17-21.

(26) Yang, D.-F.; Wilde, C. P.; Morin, M. *Langmuir.* **1996,** *12,* 6570-6577.

(27) Yang, D.-F.; Wilde, C. P.; Morin, M. *Langmuir.* **1997,** *13,* 243-249.

(28) Walczak, M. M.; Alves, C. A.; Lamp, B. D.; Porter, M. D. *J. Electroanal. Chem.* **1995,** *396,* 103-114.

(29) Zhong, C.-J.; Porter, M. D. *J. Electroanal. Chem.* **1997,** *425,* 147-153.

(30) Zhong, C.-J. *Voltammetric simulations of electrochemical reductive desorption (ERD) of self-assembled monolayers at gold electrodes.* **1993,** *preprint.*

(31) Frumkin, A. N.; Damaskin, B. B. In Modern Aspects of Electrochemistry; Bockris, J. O. M., Conway, B. E., Eds.; Butterworths: London, 1964; Vol. 3, pp 149-223.

(32) Walczak, M. M.; Popenoe, D. D.; Deinhammer, R. S.; Lamp, B. D.; Chung, C.; Porter, M. D. *Langmuir.* **1991,** *7,* 2687-2693.

(33) Wong, S.-S.; Porter, M. D. *J. Electroanal. Chem.* **2000,** *485,* 135-143.

(34) Widrig, C. A.; Alves, C. A.; Porter, M. D. *J. Am. Chem. Soc.* **1991,** *113,* 2805-2810.

(35) Brown, A. P.; Anson, F. C. *Anal. Chem.* **1977,** *49,* 1589-1595.

(36) Wong, S.-S.; Porter, M. D. *J. Electroanal. Chem.* **2000,** *485,* 135-143.

(37) Yang, D.-F.; Morin, M. *J. Electroanal. Chem.* **1998,** *441,* 173-181.

(38) Yang, D.-F.; Morin, M. *J. Electroanal. Chem.* **1997,** *429,* 1-5.

(39) Schneider, T. W.; Buttry, D. A. *J. Am. Chem. Soc.* **1993,** *115,* 12391-12397.

(40) Zhong, C.-J.; Porter, M. D. *J. Am. Chem. Soc.* **1994,** *116,* 11616-11617.

(41) Kawaguchi, T.; Yasuda, H.; Shimazu, K.; Porter, M. D. *Langmuir.* **2000,** *17.*

(42) Weisshaar, D. E.; Lamp, B. D.; Porter, M. D. *J. Am. Chem. Soc.* **1992,** *114,* 5860-5862.

(43) Nishizawa, M.; Sunagawa, T.; Yoneyama, H. *J. Electroanal. Chem.* **1997,** *436,* 213-218.

(44) Wang, J.; Rivas, G.; Jiang, M.; Zhang, X. *Langmuir.* **1999,** *15,* 6541-6545.

(45) Ratner, B. D.; Castner, D. G. In Surface Analysis: the principal techniques; Vickerman, J. C., Ed.; John Wiley & Sons: New York, 1997, pp 43-98.

(46) Nuzzo, R. G.; Fusco, F. A.; Allara, D. L. *J. Am. Chem. Soc.* **1987,** *109,* 2538-2368.

(47) Bain, C. D.; Biebuyck, H. A.; Whitesides, G. M. *Langmuir.* **1989,** *5,* 723-727.

(48) Zubragel, C.; Deuper, C.; Schneider, F.; Neumann, M.; Grunze, M.; Schertel, A.; Woll, C. *Chem. Phys. Lett.* **1995,** *238,* 308-312.

(49) Castner, D. G.; Hinds, K.; Grainger, D. W. *Langmuir.* **1996,** *12,* 5083-5086.

(50) Greenler, R. G. *J. Chem. Phys.* **1966,** *44,* 310-355.

(51) Porter, M. D. *Anal. Chem.* **1988,** *60,* 1143A-1155A.

(52) Nuzzo, R. G.; Allara, D. L. *J. Am. Chem. Soc.* **1983,** *105,* 4481-4483.

(53) Nuzzo, R. G.; Dubois, L. H.; Allara, D. L. *J. Am. Chem. Soc.* **1990,** *112,* 558-569.

(54) Laibinis, P. E.; Whitesides, G. M.; Allara, D. L.; Tao, Y.-T.; Parikh, A. N.; Nuzzo, R. G. *J. Am. Chem. Soc.* **1991,** *113,* 7152-7167.

(55) Dubois, L. H.; Zegarski, B. R.; Nuzzo, R. G. *J. Chem. Phys.* **1993,** *98,* 678-688.

(56) Nuzzo, R. G.; Korenic, E. M.; Dubois, L. H. *J. Chem. Phys.* **1990,** *93,* 767-773.

(57) Schuth, F. *J. Phys. Chem.* **1992,** *96,* 7493-7496.

(58) Li, Y.; Huang, J.; Robert T. McIver, J.; Hemminger, J. C. *J. Am. Chem. Soc.* **1992,** *114,* 2482-2432.

(59) Smith, E. L.; Yin, W. Y.; Ramos, J. *Direct observation of molecular hydrogen during formation of thiolate films on the surface of oxide supported gold nanoparticles.* **1999,** *preprint.*

(60) Gronbeck, H.; Curioni, A.; Andreoni, W. *J. Am. Chem. Soc.* **2000,** *122,* 3839-3842.

(61) Flink, S.; Veggel, F. C. J. M. v.; Reinhoudt, D. N. *Adv. Mater.* **2000,** *12,* 1315-1328.

(62) Steinberg, S.; Rubinstein, I. *Langmuir.* **1992,** *8,* 1183-1187.

(63) Rojas, M. T.; Koniger, R.; Stoddart, J. F.; Kaifer, A. E. *J. Am. Chem. Soc.* **1995,** *117,* 336-343.

(64) Murakami, H.; Akiyoshi, H.; Wakamatsu, T.; Sagara, T.; Nakashima, N. *Chem. Lett.* **2000,** *2000,* 940-941.

(65) Kanayama, N.; Kitano, H. *Langmuir.* **2000,** *16,* 577-583.

(66) Wang, J.; Wu, H.; Angnes, L. *Anal. Chem.* **1993,** *65,* 1893-1896.

(67) Cheng, Q.; Brajter-Toth, A. *Anal. Chem.* **1996,** *68,* 4180-4185.

(68) Cheng, Q.; Brajter-Toth, A. *Anal. Chem.* **1995,** *67,* 2767-2775.

(69) Sullivan, M. G.; Utomo, H.; Fagan, P. J.; Ward, M. D. *Anal. Chem.* **1999,** *71,* 4369-4375.

(70) Gadzekpo, V. P. Y.; Xiao, K. P.; Aoki, H.; Buhlmann, P.; Umezawa, Y. *Anal. Chem.* **1999,** *71,* 5109-5115.

(71) Hickman, J. J.; Ofer, D.; Laibinis, P. E.; Whitesides, G. M.; Wrighton, M. S. *Science.* **252,** *252,* 688-691.

(72) Lahav, M.; Katz, E.; Willner, I. *Electroanalysis.* **1998,** *10,* 1159-1162.

(73) Zak, J.; Yuan, H.; Ho, M.; Woo, L. K.; Porter, M. D. *Langmuir.* **1993,** *9,* 2772-2774.

(74) Hutchison, J. E.; Postlewaite, T. A.; Murray, R. W. *Langmuir.* **1993,** *9,* 3277-3283.

(75) Kalyuzhny, G.; Vaskevich, A.; Ashkenasy, G.; Shanzer, A.; Rubinstein, I. *J. Phys. Chem. B.* **2000,** *104,* 8238-8244.

(76) Offord, D. A.; Sachs, S. B.; Ennis, M. S.; Eberspacher, T. A.; Griffin, J. H.; Chidsey, C. E. D.; Collman, J. P. *J. Am. Chem. Soc.* **1998,** *120,* 4478-4487.

(77) Aoki, H.; Buhlmann, P.; Umezawa, Y. *Electroanalysis.* **2000,** *12,* 1272-1276.

(78) Berggren, C.; Stalhandske, P.; Brundell, J.; Johansson, G. *Electroanalysis.* **1999,** *11,* 156-160.

(79) Taniguchi, I.; Toyosawa, K.; Yamaguchi, H.; Yasukouchi, K. *J. Electroanal. Chem.* **1982,** *140,* 187-193.

(80) Maeda, Y.; Yamamoto, H.; Kitano, H. *J. Phys. Chem.* **1995,** *99,* 4837-4841.

(81) Avila, A.; Gregory, B. W.; Niki, K.; Cotton, T. M. *J. Phys. Chem. B.* **2000,** *104,* 2759-2766.

(82) Lee, J. E.; Saavedra, S. S. *Langmuir.* **1996,** *12,* 4025-4032.

CHAPTER 1. AMPEROMETRIC AMPLIFICATION OF DOPAMINE BY ASCORBATE AT GOLD ELECTRODES COATED WITH MONOLAYERS OF 10-MERCAPTOSULFONIC ACID

A paper to be submitted to *Electroanalysis*

Zhongmin Hu, G. Brent Dawson, Robin L. McCarley, and Marc D. Porter

Abstract

The possibility of using ascorbic acid to recycle dopamine at 10-mercaptodecanesulfonic acid (MDS) monolayer-coated gold electrodes was investigated. Initially, the MDS monolayers were characterized with infrared spectroscopy, X-ray photoelectron spectroscopy, and electrochemical reductive desorption, the results of which showed that the monolayer exists as a loosely packed array of methylene chains. Electrochemical investigations showed that, compared with bare electrodes, the response of the MDS-modified gold electrodes for dopamine is only slightly compromised while that for ascorbic acid is effectively suppressed. This finding indicates that the monolayer is permeable to dopamine but resistant to ascorbic acid. The preferential permeation of dopamine with respect to ascorbic acid is attributed to the high negative charge density of the sulfonate terminus of the monolayer and the hydrophilicity of ascorbic acid due to its hydroxy groups. The results indicated that, because of the effective suppression of the heterogeneous oxidation of ascorbic acid at the monolayer-modified electrode, the observed current for the oxidation of dopamine was amplified by its regeneration upon reaction with solution-phase ascorbic acid.

Introduction

Amperometry has been used for the low level detection of a variety of analytes.[1,2] Unfortunately, the effectiveness of this technique is often compromised by the simultaneous oxidation/reduction of more than one of the components in a sample. As an approach to overcome this limitation, several laboratories have coated electrode surfaces with thin polymer films or organic monomolecular assemblies. These coatings modify the partitioning and/or accessibility of interfering species to the electrode surface, enhancing the selectivity and/or sensitivity.[3]

Polymer films on an electrode surface may not only change the electron transfer mechanism, but also may prove beneficial to electroanalysis in several other ways. For example, anionic polymer films such as Nafion® can pre-concentrate cations, translating to detection limits lower than those attainable at an uncoated electrode while at the same time providing a level of discrimination based on charge.[3] The preconcentrated cations are then electrolyzed through an electron hopping mechanism that can be described by finite diffusion models. Thus, the thicker the film, the larger the amount of pre-concentrated analyte and the lower the detection limit. However, the comparatively low diffusion coefficients of molecular species through polymer films, (e.g., the diffusion coefficient of dopamine in Nafion® is 1.5×10^{-9} cm^2 s^{-1} versus 6×10^{-6} cm^2 s^{-1} in an aqueous solution[4,5]), reduces the ability of thicker films to respond efficiently to dynamic changes in cation concentration.

Alternatively, self-assembled monolayers[6-10] particularly thiols and disulfides chemisorbed at gold, have several characteristics which are attractive for use as systems for electrode modification. These films are easily prepared, stable over a range of chemical environments, and can be used to discriminate one analyte from another in the same manner

as polymer films, while having a thickness of only one molecular layer.[11-17] With these systems, both the tail group and the methylene spacer work cooperatively to exclude interfering species from the surface of the electrode.[18-28] For example, carboxylic acid-terminated monolayers provide excellent barriers to anions in alkaline electrolytes (pH > 7.5), while only minimally reducing the mass transfer of cations to the underlying electrode.

The selective nature of these films can also be exploited in redox recycling schemes where an analyte is oxidized/reduced by a sacrificial species in solution after being reduced/oxidized at the electrode surface. In these schemes, the direct heterogeneous electrolysis of the sacrificial species must be blocked by the monolayer. As shown in Scheme 1,[29] Creager and co-workers recently used a gold-bound dodecanthiol monolayer to amplify the detection of hydroxymethyl ferrocene (HMF). Due to its inherent hydrophobicity, HMF can therefore be oxidized at the underlying electrode, and then recycled by the homogeneous electron transfer reaction of its oxidized form (i.e., hydroxymethyl ferrocenium ion). Using these reactants, a limit of detection of 60,000 molecules was realized. Importantly, this level of amplification cannot be readily achieved using polymer-coated electrodes since the mass transfer of analyte through the entangled network of the coating limits the recycling rate.

In this report, we investigate the possibility of extending this concept to biological redox processes by using a common interfering species in biological systems, ascorbic acid, as the sacrificial species to amplify the current due to the oxidation of the neurotransmitter, dopamine. The goal is to assess the feasibility of the concept, and based on the findings, identify issues that need to be addressed for its probable exploitation in key applications (e.g., monitoring hormone release and determination of blood glucose). Scheme 2 shows the

set of electron transfer reactions that lead to the amplification of the current for the oxidation of dopamine. First, dopamine is oxidized at the electrode to its quinone form, which is then reduced in the solution in the immediate vicinity of the electrode by ascorbic acid, the oxidized form of which undergoes an irreversible hydration reaction to form the 2,3 diketogulonic acid. The homogeneous reaction regenerates dopamine, which can again be reduced at the electrode, with the extent of the amplification being determined by the number of recycling steps. To impart selectivity to the gold electrode surface, we used a monolayer terminated with a sulfonate group. The following sections present the results from the characterization of this monolayer by infrared reflection absorption spectroscopy (IRRAS), X-ray photoelectron spectroscopy (XPS), and electrochemical reductive desorption (ERD) followed by a detailed examination of the amplification scheme. Earlier efforts have used similar approaches[30,31] for the determination of dopamine in the presence of ascorbic acid at a glassy carbon electrode in the presence of surfactant modifiers[32] and at enzyme modified electrodes.[33,34] We envision that the use of monolayers will impart a fast temporal to such amplification techniques.

Experimental

Chemicals

Solid 10-mercaptodecanesulfonic acid, sodium salt (MDS) was synthesized using a method reported by Mandler.[35] Briefly, 1,10-dibromodecane (Aldrich) was reacted with sodium sulfite (Fisher Scientific) to form 10-bromodecanesulfonic acid, sodium salt. The thiol group was introduced by nucleophilic substitution with thiourea (Baker) through the

formation of 10-S-thiouronium decanesulfonate, which was then converted to the corresponding thiol by hydrolysis under alkaline conditions. The hydrolyzed product was recrystallized twice from a minimum amount of boiling water, with the addition of a small amount of ethanol after product dissolution (~15% (v/v) ethanol:water mixture), to promote crystallization. All of the reactions were performed under a nitrogen atmosphere using standard inert atmospheric techniques.

Dopamine, L-ascorbic acid, 1-decanethiol were purchased from Aldrich. Phosphate buffer, prepared from sodium phosphate, monobasic (Fisher Scientific) and adjusted with NaOH or phosphoric acid, was used to control the pH of the electrolyte solutions. All chemicals used were of analytical or higher grade. All of the solutions were prepared with water purified by a Millipore Milli-Q water system.

Electrode and Monolayer Preparation

Electrodes were prepared either by the vapor deposition of gold onto mica or glass slides with a cryopumped Edwards E360A coating system, or by polishing and cleaning commercially available gold (1.6 mm) electrodes. Prior to gold deposition, the pre-cleaned glass slides were first primed with 15 nm of chromium at the deposition rate of 0.1 nm/s. For the electrochemical desorption experiments, the substrates were prepared by vapor deposition of ~300 nm of gold onto freshly cleaved mica slides (Asheville-Schoonmaker Mica), as described previously.[36] These films were subsequently annealed at 300 °C for 4 h, a process that yields a surface composed of atomically smooth Au (111) terraces.[36-42] The deposition rate of gold, on both glass and mica, was 0.2 nm/s. The commercial electrodes were first cleaned in Piranha (3:1 98% H_2SO_4: 30% H_2O_2) solution and rinsed with deionized water, and then polished with 0.05 μm Micropolish® II alumina (Buehler) slurry. **Warning**

Piranha solution can react violently with organic compounds and should be neutralized immediately after use.

MDS-based monolayers were assembled on the gold electrodes via overnight incubation in 0.1 M perchloric acid solutions which contained either 1 mM MDS and 1 mM MES, respectively. Decanethiolate monolayers were also formed via incubation overnight, but in a 1 mM decanethiol solution of ethanol. After emersion, the monolayer-coated electrodes were rinsed with deionized water, and dried with nitrogen.

Infrared Spectroscopy

IR spectra were acquired using a Magna 750 FT-IR spectrometer (Nicolet), equipped with a liquid nitrogen-cooled HgCdTe detector. Monolayer spectra were obtained, under the purge of nitrogen, in an external reflection mode using *p*-polarized light incident at 82° with respect to the surface normal. The spectra are reported as –log (R/R_o), where R is the reflectance of the sample and R_o is the reflectance of a *n*-octadecanethiol-d_{37} monolayer. For both sample and reference, the reflectance is the average of 512 scans. Spectra of MDS in KBr matrix were obtained in transmission mode as the average of 100 scans. All spectra were collected at a 2 cm^{-1} resolution and one level of zero filling with Happ-Genzel apodization.

X-Ray Photoelectron Spectroscopy

XPS characterizations were carried out with a Physical Electronics Industries 5500 surface analysis system equipped with a hemispherical analyzer, toroidal monochromator, and multi-channel detector. The sampling area was 2 mm^2. Monochromatic Al $K\alpha$ radiation with an energy of 1486.6 eV at 300 W was used for excitation. A pass energy of 29.35 eV

was used with a resolution of ~0.3 eV. Photoelectrons were collected at 45° with respect to the surface normal. Acquisition times were typically less than 10 min. The Au ($4f_{7/2}$) emission band served as an internal reference for binding energies. During analysis, the base pressure of the XPS chamber was less than 9×10^{-10} Torr.

Electrochemical Measurements

Reductive desorption measurements were carried out using an EG&G 263A potentiostat/galvanostat or a CV-27 potentiostat (Bioanalytical Systems) and a conventional three-electrode cell, with a Ag/AgCl (3 M NaCl) electrode (Bioanalytical Systems) as the reference electrode and a platinum coil as the auxiliary electrode. The geometric area of the working electrode, 0.61 cm^2, was defined by an O-ring that served as a gasket for mounting the electrode to the electrochemical cell. The supporting electrolyte was 0.5 M KOH aqueous solution, which was deoxygenated with argon just prior to carrying out the electrochemical measurements. Dopamine and ascorbic acid solutions were freshly prepared in deoxygenated supporting electrolyte solutions, which were subsequently blanketed with argon.

Results and Discussion

Characterization with Infrared Spectroscopy

The spectrum of the MDS monolayer in the low-frequency region is shown in Figure 2 and confirms the presence of the sulfonate-terminated monolayer. Based on the band assignments for sulfonate salts,[43,44] the strong feature at lower frequency is assigned to the symmetric SO_2 stretching mode and was found to be 1057 cm^{-1}. Several bands are also

present in the 1100-1350 cm^{-1} region, mostly due to the mixture of protonated and deprotonated states of the sulfonate group. This mixing complicates assignment of a feature to the asymmetric SO_2 stretching band. The band at ~1465 cm^{-1} is the CH_2 scissoring mode of polymethylene chain.

Figure 3A shows the spectrum of the MDS monolayer in the C-H stretching region. For comparison, the spectrum of MDS in KBr matrix in the same spectral region is shown in Figure 3B. Band assignments are based on the previous studies.[11] In a KBr matrix, the peak positions of the asymmetric C-H stretching, $\nu_a(CH_2)$, and symmetric C-H stretching, $\nu_s(CH_2)$, modes of MDS (Figure 3B) are 2920 and 2851, respectively. The presence of these bands and those to the SO_3^-, confirms that the adlayer composition is the expected one.

Another interesting feature of the spectra in Figure 3 is the number of bands present in this spectral region. In comparison with the spectrum obtained in KBr matrix, the monolayer spectrum shows an additional band, which was found to be 2960, and a small shoulder on the symmetric C-H stretching band. The occurrence of the 2960 cm^{-1} band, along with the shoulder, is most likely due to the C-H stretching of the CH_2 group adjacent to the sulfonate group of MDS, analogous to the shifts of C-H stretchings of CH_2 group adjacent to an electronegative atom to higher frequencies.[13] The relative intensity of this band, when compared to the 2924 cm^{-1} band is higher, in the monolayer spectrum than it is in the KBr spectrum due to surface selection rules.[45]

The most important feature of the spectra is the position of the C-H stretching modes of methylene groups. It has been well documented that the peak position of the C-H stretching modes of methylene groups are sensitive to the degree of organization of the polymethylene chains of a monolayer.[11] A densely packed *n*-alkanethiol monolayer shows

C-H stretching modes of methylene groups in a crystalline environment, and a shift in peak position of the C-H stretching modes to higher energy is indicative of a liquid-like environment.[11] In the case of the monolayer, the peak positions for the $\nu_a(CH_2)$ and $\nu_s(CH_2)$ modes of MDS (Figure 3A) are noticeably higher those in the KBr matrix. The peak positions for the $\nu_a(CH_2)$ and $\nu_s(CH_2)$ modes of MDS monolayer were determined to be 2924 and 2855, respectively. Compared with the positions observed in KBr, both $\nu_a(CH_2)$ and $\nu_s(CH_2)$ modes of the monolayer show a shift to higher energy, indicating the chains in the adlayer are more disordered than those in KBr. Furthermore, the positions of the C-H stretching modes of the MDS monolayer are not appreciably different from those observed for *n*-octanethiol in its liquid state.[11]

Characterization with X-Ray Photoelectron Spectroscopy

XPS binding energies are another set of diagnostics for determining the composition of monolayers. For sulfur-containing species, the binding energy in the S (2p) region provides insights into the oxidation state of sulfur. Each type of sulfur species will have a doublet arising from spin-orbit coupling ($2p_{3/2}$ and $2p_{1/2}$), with an energy separation of 1.2 eV and intensity ratio of 2:1.[46] Shown in Figure 4 is the XPS spectrum of a MDS monolayer at gold in the S (2p) region, together with the deconvolution profiles derived by using Gaussian line shapes.[47] Two sets of couplets are observed. The one at lower binding energy can be reasonably fit by a doublet, with the S ($2p_{3/2}$) component centered at 162.1 eV and S ($2p_{1/2}$) component centered at 163.3 eV. These binding energies are consistent with those for a gold-bound thiolate species,[41,48,49] indicating that this set of features is attributable to the sulfur head group of the adlayer; the second couplet occurs at a higher binding energy and

can also be fit by a doublet. This doublet is well separated from the thiolate doublet, clearly revealing the presence of a sulfur species in a different oxidation state. The peak positions of the deconvoluted profile has S ($2p_{3/2}$) feature at 168.3 eV, while the S ($2p_{1/2}$) feature is 1.2 eV higher than the S ($2p_{3/2}$) feature. These features are assigned to the sulfonate group of MDS monolayer, based on data for aliphatic sulfonate salts.[46]

Figure 4 also shows that the intensities of these two couplets are significantly different from each other. Integration of the area under each couplet yields a ratio of 1.8:1 for the sulfonate couplet with respect to the thiolate couplet. This difference arises from the difference in escape depth for the photoelectrons ejected from the thiolate sulfur with respect to that for those ejected from the sulfonate sulfur and is consistent with the fact that the thiolate group is located at the substrate-monolayer interface, while the sulfonate group is located at the chain terminus of the monolayer.

Characterization with Reductive Desorption

In addition to the IR and XPS studies, electrochemical reductive desorption was used to estimate the surface concentration of the MDS monolayer. We and others[36-42,50,51] have previously shown that alkanethiolate monolayers at gold undergo cathodic desorption in alkaline electrolytes, and that the charge associated with the one-electron reduction provides a measure of the surface concentration of the monolayer. As shown in Figure 5, the reductive desorption of MDS monolayer occurs at a large negative potential, with the peak potential of the cathodic wave at -959 mV.

The charge under each of the desorption waves, after accounting for surface roughness,[37] translates to surface concentration values of 7.4×10^{-10} mol/cm^2 for the MDS monolayers. The surface roughness factor, the ratio of "actual" surface area to geometric

surface area, of the mica-supported gold used for the present investigation was estimated from the experimentally-determined charge associated with the reductive desorption of 1-decanethiol monolayer by assuming that the *n*-alkanethiol forms a closest-packed monolayer with a coverage of 7.7×10^{-10} mol/cm^2.[37,39] The surface concentration of MDS monolayer is only slightly lower than that of the corresponding *n*-alkanethiol, and we ascribe this difference in surface concentrations of the two films to the greater bulk of the terminal sulfonate group.

In summary, the combined IR, XPS, and reductive desorption characterizations suggest that MDS forms a liquid-like monolayer at gold with a surface concentration slightly less than that of the corresponding *n*-alkanethiol.

Voltammetry

For consistency, the following electrochemical measurements were performed using the same gold electrode, which entailed alternately forming the monolayer assembly after cleaning the surface with Piranha solution. Figure 6 shows representative cyclic voltammograms observed at (A) uncoated and (B) MDS monolayer-coated gold (MDS/Au) electrodes in dopamine and ascorbic acid solutions at pH 2.2. The voltammetric responses of the electrodes in blank electrolyte are also presented. All of the voltammograms shown were recorded after three repetitive cycles.

At the uncoated electrode (Figure 6A), ascorbic acid is clearly a significant interference to the detection of dopamine. At the MDS/Au electrode (Figure 6B), however, the rate for ascorbic acid oxidation is strongly suppressed. The response for dopamine is also affected, as shown by the increase in the separation of the oxidative and reductive peak potentials. The peak current, however, is only marginally affected. More specifically, the

magnitude of the anodic wave at the MDS/Au electrode is ca. 90% of that at the bare electrode, and the peak potential for the oxidation of dopamine at the modified electrode is about 0.1 V positive of that at the bare electrode.

We also found that the decrease in the anodic current for dopamine is small when compared to that observed using electrodes coated with an alkanethiolate monolayer having a chain length comparable to that of MDS. The inset of Figure 6B shows the voltammetric response at a decanethiolate monolayer-coated gold electrode in 1 mM dopamine solution. As is evident, the response of the electrode to dopamine is strongly attenuated by presence of the more densely packed alkanethiol monolayer. The higher current flow at the MDS-coated electrode, compared with that at the decanethiolate-coated electrode, strongly implies that the MDS monolayer is much more permeable to dopamine. The larger flow of oxidative current for dopamine is attributed to the liquid-like methylene phase (i.e., less-densely packed) of the MDS monolayer.

While fairly permeable to dopamine, the MDS monolayer markedly impedes the electrolysis of ascorbic acid. This impermeability is indicated by the significant increase in overpotential required for the oxidation of ascorbic acid (Figure 6). As a result, the interference of ascorbic acid in dopamine detection is suspected to be significantly less pronounced than that at the bare electrode.

We attribute the differences in the permeability to differences in the hydrophilicity of the two compounds. The pK_a values for the loss of the first proton from ascorbic acid and the conjugate acid of dopamine are 4.1 and 8.9 respectively.[52] Dopamine is therefore a positively charged cation at pH 2.2, whereas ~99% of ascorbic acid exists in its neutral form. It appears, however, that the large number of hydroxyl groups renders it more hydrophilic

than the cationic dopamine, which then reduces permeation through the hydrophobic chain structures of the MDS monolayer. MDS monolayers at gold should be more useful in the determination of the cationic dopamine species at higher pHs where ascorbate is negatively charged. It should, however, be noted that, at a higher pH, the application of a high anodic potential may cause a rapid deterioration of the monolayer, due to the oxidation of the underlying gold substrate. For instance, at pH 7, the formation and stripping of a gold oxide layer at the MDS/Au electrode were detected only after a couple of voltammetric cycles whose anodic limits were +0.9 V.

Figure 7 shows the cyclic voltammetric responses at MDS/Au electrode in blank, dopamine, and ascorbic acid solutions at pH 7.0. The anodic limiting potential is set at +0.7 V, which is insufficient to induce any detectable oxidation of the underlying gold. At pH 7.0, the electrochemical reversibility of dopamine is even lower than that at pH 2.2. Though at a higher overpotential, the magnitude of the anodic wave is, however, not substantially affected. These differences are in marked contrast to that of ascorbic acid, which has a current-potential curve indistinguishable from that of the background. These data again demonstrate the effectiveness of the MDS monolayer in suppressing the electrolysis of ascorbic acid. The observed stability of the MDS monolayer at this pH, which is based on the absence of currents due to gold oxidation, together with the selectivity of the monolayer-covered gold electrode for dopamine over ascorbic acid, support the feasibility of coupling amplification the amperometric detection of dopamine with amplification by ascorbic acid at physiological pH values.

From structural description of the MDS monolayer, one can speculate as to the combination of characteristics of the electrode surface which give rise to this behavior. The

negative surface charge would provide an attractive interaction for the positively charge dopamine, whereas the interaction for the negatively charged ascorbate would be repulsive. Furthermore, the disorganized polymethylene chains would allow dopamine to have a plane of closest approach that is located less than 1 nm from the electrode surface giving a reasonable probability that electrons would tunnel from the dopamine to the electrode surface.

The above observations suggest that at a rationally selected electrolysis potential, the contribution of ascorbic acid to the electrochemical response of the electrode for dopamine would be insignificant, because of the ability of the MDS-monolayer to selectively suppress the rate of mass transport of ascorbic acid to the electrode surface. The next section examines the effectiveness of Scheme 2 in lowering the detection limit of dopamine

Amplification via Regeneration of Dopamine

In the presence of ascorbic acid, the electrochemical determination of dopamine will be affected not only by any heterogeneous oxidation of ascorbic acid, but also by the rate of the homogeneous chemical reaction between ascorbic acid and the oxidized form of dopamine. This reaction will act to recycle dopamine back to its reduced state. However, the presence of the MDS monolayer strongly suppresses the heterogeneous oxidation of ascorbic acid at the electrode, reducing any interference with the response for dopamine to background levels (see above).

Presented in Figure 8 are the cyclic voltammograms observed at the MDS/Au electrode in the presence of only ascorbic acid (curve a) and in the presence of both ascorbic acid and dopamine (curves b and c), as detailed in the caption. These data, along with those in Figure 6B, demonstrate the types of signal enhancement that can be observed upon the

effective suppression of the heterogeneous oxidation of ascorbic acid. There are four important observations. First, when dopamine and ascorbic acid concentrations are both 1 mM (Fig. 8B), the oxidation wave is shifted negatively by a few tens of millivolts and the reduction wave is shifted positively by more than 100 mV. Second, at an applied potential corresponding to the peak potential of dopamine oxidation wave, the voltammetric response, for the conversion of 5 mM ascorbic acid (curve a) is close to background levels. Third, in the presence of 1 mM dopamine and 1 mM ascorbic acid (curve b), the anodic peak current is nearly twice that observed in the presence of only 1 mM dopamine (Figure 6B). Fourth, when the concentration of ascorbic acid was raised to 5 mM while the concentration of dopamine was kept constant at 1 mM (curve c), the anodic peak current is even greater (3.3 times), whereas the corresponding cathodic wave has decreased to near-background levels.

All of these results are consistent with the expectations of the amplification processes. For example, the decrease in the reduction wave indicates that enough ascorbic acid is present to completely reduce most of the dopamine-*o*-quinone that is formed during the course of the experiment, and the regenerated dopamine is re-oxidized giving a current that is dependent on the ascorbate concentration.

Conclusions

In conclusion, amplification effects that arise from homogeneous recycling of the dopamine by using MDS-coated electrodes could be effective in determining trace amounts in complex samples such as those encountered in biological environments. To determine analytes such as dopamine in these samples, one must know the expected amplification factor

and the concentration of the sacrificial species and the approximate concentration of the analyte. For many physiological environments, metabolic processes maintain nearly constant concentrations of species such as ascorbic acid, suggesting such quantitation may be possible.

The structural characterizations of MDS monolayers at gold using IR, XPS, and electrochemical reductive desorption have provided evidence that the monolayer has a disordered chain structure, with a surface concentration less than but close to that of 1-decanethiol. The MDS monolayer facilitates the heterogeneous electrochemical oxidation of dopamine while impeding that of ascorbic acid. This effect is most likely attributable to the surface charge of the monolayer and the liquid-like polymethylene phase. As a result, the monolayer is much more selective for the oxidation of dopamine over ascorbic acid. Because of the appreciable selectivity of the MDS monolayer-modified electrode, the signal amplification resulting from the homogeneous chemical reduction of dopamine-*o*-quinone by ascorbic acid can be explored and would be valuable for the low level detection of dopamine by its recycling with ascorbic acid. It can be noted that, at electrodes modified with polymers such as Nafion®, this level of signal amplification may not be achieved in the time scale of a typical electrochemical measurement because of the large thickness of the electrode coating. While the subject of ongoing experiments, the level of amplification achievable at the MDS/Au electrode and the fast response times of monolayer-modified electrodes could give rise to new, highly sensitive detection methods.

Acknowledgements

R. L. M gratefully acknowledges support from Louisiana State University during a sabbatical. G.B.D. acknowledges the Phillips Petroleum Research Fellowship for a year of financial support. The XPS data were acquired by James Anderegg. Other support was provided by the Microanalytical Instrumentation Center of the Institute for Physical Research and Technology at Iowa State University and the U.S Department of Energy.

References

(1) Lunte, S. M.; Lunte, C. E.; Kissinger, P. T. In Laboratory Techniques in Electroanalytical Chemistry; Kissinger, P. T., Heineman, W. R., Eds.; Marcel Dekker: New York, **1996,** pp 813-854.

(2) Wang, J. *Analytical Electrochemistry;* John Wiley & Sons, Inc.: New York, **2000.**

(3) Martin, C. R.; Colby A. Foss, J. In Laboratory Techniques in Electroanalytical Chemistry; Kissinger, P. T., Heineman, W. R., Eds.; Marcel Dekker: New York, **1996,** pp 403-439.

(4) Whitely, L. D.; Martin, C. R. *Anal. Chem.* **1987,** *59,* 1746-1751.

(5) Gerhardt, G.; Adams, R. N. *Anal. Chem.* **1982,** *54,* 2618-2620.

(6) Ulman, A. *Introduction to Thin Organic Films: From Langmuir-Blodgett to Self-Assembly;* Academic Press: Boston, 1991.

(7) Mallouk, T. E. *Interfacial Design and Chemical Sensing, ACS Symposium Series 561;* American Chemical Society: Washington, DC, 1994.

(8) Zhong, C.-J.; Porter, M. D. *Anal. Chem.* **1995,** *67,* 709 A-715 A.

(9) Allara, D. L. *Biosens. Bioelectron.* **1995,** *10,* 771-783.

(10) Mandler, D.; Turyan, I. *Electroanalysis.* **1996,** *8,* 207-213.

(11) Porter, M. D.; Bright, T. B.; Allara, D. L.; Chidsey, C. E. D. *J. Am. Chem. Soc.* **1987,** *109,* 3559-3568.

(12) Bain, C. D.; Evall, J.; Whitesides, G. M. *J. Am. Chem. Soc.* **1989,** *111,* 7155-7164.

(13) Popenoe, D. D.; Deinhammer, R. S.; Porter, M. D. *Langmuir.* **1992,** *8,* 2521-2530.

(14) Everett, W. R.; Fritsch-Faules, I. *Anal. Chim. Acta.* **1995,** *307,* 253-268.

(15) Xu, J.; Li, H.-L. *J. Colloid Interface Sci.* **1995,** *176,* 138-149.

(16) Turyan, I.; Mandler, D. *Isr. J. Chem.* **1997,** *37,* 225-233.

(17) Bain, C. D.; Whitesides, G. M. *Science.* **1988,** *240,* 62-63.

(18) Chailapakul, O.; Crooks, R. M. *Langmuir.* **1993,** *9,* 884-888.

(19) Rubinstein, I.; Steinberg, S.; Tor, Y.; Shanzer, A.; Sagiv, J. *Nature.* **1988,** *332,* 426-429.

(20) Steinberg, S.; Rubinstein, I. *Langmuir.* **1992,** *8,* 1183-1187.

(21) Wang, J.; Wu, H.; Angnes, L. *Anal. Chem.* **1993,** *65,* 1893-1896.

(22) Liu, Z.; Li, J.; Dong, S.; Wang, E. *Anal. Chem.* **1996,** *68,* 2432-2436.

(23) Chen, M.; Li, H. *Electroanalysis.* **1998,** *10,* 477-479.

(24) Takehara, K.; Takemura, H.; Aihara, M.; Yoshimura, M. *J. Electroanal. Chem.* **1996,** *404,* 179-182.

(25) Giz, M. J.; Duong, B.; Tao, N. J. *J. Electroanal. Chem.* **1999,** *465,* 72-79.

(26) Malem, F.; Mandler, D. *Anal. Chem.* **1993,** *65,* 37-41.

(27) Kristensen, E. W.; Kuhr, W. G.; Wightman, R. M. *Anal. Chem.* **1987,** *59,* 1752-1757.

(28) Cahill, P. S.; Walker, Q. D.; Finnegan, J. M.; Mickelson, G. E.; Travis, E. R.; Wightman, R. M. *Anal. Chem.* **1996,** *68,* 3180-3186.

(29) Radford, P. T.; French, M.; Creager, S. E. *Anal. Chem.* **1999,** *71,* 5101-5108.

(30) Dalmia, A.; Liu, C. C.; Savinell, R. F. *J. Electroanal. Chem.* **1997,** *430,* 205-214.

(31) Dayton, M. A.; Ewing, A. G.; Wightman, R. M. *Anal. Chem.* **1980,** *52,* 2392-2396.

(32) Wen, X.-L.; Jia, Y.-H.; Liu, Z.-L. *Talanta.* **1999,** *50,* 1027-1033.

(33) Uchiyama, S.; Itoi, N.; Hasebe, Y. *Electroanalysis.* **1995,** *7,* 731-733.

(34) Hasebe, Y.; Takamori, K.; Uchiyama, S. *Anal. Chim. Acta.* **1993,** *282,* 363-367.

(35) Turyan, I.; Mandler, D. *J. Am. Chem. Soc.* **1998,** *120,* 10733-10742.

(36) Walczak, M. M.; Popenoe, D. D.; Deinhammer, R. S.; Lamp, B. D.; Chung, C.; Porter, M. D. *Langmuir.* **1991,** *7,* 2687-2693.

(37) Widrig, C. A.; Chung, C.; Porter, M. D. *J. Electroanal. Chem.* **1991,** *310,* 335-359.

(38) Weisshaar, D. E.; Walczak, M. M.; Porter, M. D. *Langmuir.* **1993,** *9,* 323-329.

(39) Walczak, M. M.; Alves, C. A.; Lamp, B. D.; Porter, M. D. *J. Electroanal. Chem.* **1995,** *396,* 103-114.

(40) Zhong, C.-J.; Porter, M. D. *J. Electroanal. Chem.* **1997,** *425,* 147-153.

(41) Zhong, C.-J.; Zak, J.; Porter, M. D. *J. Electroanal. Chem.* **1997,** *421,* 9-13.

(42) Lamp, B. D.; Hobara, D.; Porter, M. D.; Niki, K.; Cotton, T. M. *Langmuir.* **1997,** *13,* 736-741.

(43) Colthup, N. B.; Daly, L. H.; Wiberley, S. E. *Introduction to Infrared and Raman Spectroscopy;* 3rd ed. ; Academic Press: New York, 1990.

(44) Lin-Vien, D.; Colthup, N. B.; Fateley, W. G.; Grasselli, J. G. *The Handbook of Infrared and Raman Characteristic Frequencies of Organic Molecules;* Academic Press: Boston, 1991.

(45) Greenler, R. G. *J. Chem. Phys.* **1966,** *44,* 310-355.

(46) Lindberg, B. J.; Hamrin, K.; Johansson, G.; Gelius, U.; Fahlman, A.; Nordling, C.; Siegbahn, K. *Phys. Scr.* **1970,** *1,* 286-298.

(47) Ratner, B. D.; Castner, D. G. In Surface Analysis: the principal techniques; Vickerman, J. C., Ed.; John Wiley & Sons: New York, 1997, pp 43-98.

(48) Zhong, C.-J.; Porter, M. D. *J. Am. Chem. Soc.* **1994,** *116,* 11616-11617.

(49) Laibinis, P. E.; Whitesides, G. M.; Allara, D. L.; Tao, Y.-T.; Parikh, A. N.; Nuzzo, R. G. *J. Am. Chem. Soc.* **1991,** *113,* 7152-7167.

(50) Zhong, C.-J.; Porter, M. D. *Sulfur-gold interactions in organosulfur-based monolayers: implications of the reductive desorption of two-component monolayers.* **1997,** *preprint.*

(51) Niwa, O.; Morita, M.; Tabei, H. *Electroanalysis.* **1994,** *6,* 237-243.

(52) Lide, D. R. *CRC Handbook of Chemistry and Physics;* 81th ed. ; CRC Press: Boca Raton, 2000-2001.

Figure Captions

Scheme 1. The dodecanethiol monolayer on the electrode surface acts as a barrier to the ferrocyanide preventing its heterogeneous oxidation. Hydroxymethyl ferrocene (HMF) permeates the films and is oxidized at the electrode. Subsequently HMF undergoes homogeneous electron transfer with the ferrocyanide present in solution. The detected current is amplified due to the oxidation of the regenerated hydroxymethyl ferrocene.

Scheme 2. The top reaction shows the reversible heterogeneous electrode reaction for dopamine. The bottom reaction shows the subsequent homogenous reactions for dopamine-*o*-quinone and ascorbic acid.

Figure 1. Idealized depiction of the ionized form of a 10-mercaptodecane sulfonate monolayer at a gold electrode.

Figure 2. Infrared spectra in the low-energy region of (A) MDS monolayer at gold measured in reflection-absorption mode and (B) MDS in KBr matrix measured in transmission mode.

Figure 3. Infrared spectra in the high-energy region of (A) MDS monolayer at gold measured in reflection-absorption mode and (B) MDS in KBr matrix measured in transmission mode.

Figure 4. XPS spectra of MDS monolayer at gold in the sulfur 2p region. The thin solid curves represent deconvolution profiles. The regressional fitting of the spectral data is shown as the thick curve, which is also the sum of the deconvolution profiles. The straight lines indicate the peak positions for the $2p_{3/2}$ and $2p_{1/2}$ couplet in the deconvolution profiles.

Figure 5. Voltammogram of the cathodic desorption of a MDS monolayer at gold in aqueous 0.5 M KOH with linear potential sweep at the scan rate of 50 mV/s. Initial potential: -0.2 V. The arrow indicates the initial scan direction.

Figure 6. Cyclic voltammograms at (A) bare gold and (B) MDS/Au electrodes in blank (dotted line), 1 mM ascorbic acid (dashed line), and 1 mM dopamine (solid line) solutions. The voltammogram in the inset was obtained at a 1-decanethiol-modified gold electrode in 1 mM dopamine. Potential scan was initiated at -0.2 V with a scan rate of 100 mV/s. Supporting electrolyte: 0.1 M Na_2SO_4 and 0.05 M phosphate buffer (pH 2.2). The arrow indicates the initial scan direction.

Figure 7. Cyclic voltammograms at the MDS/Au electrode in blank (dotted line), 1 mM ascorbic acid (dashed line), and 1 mM dopamine (solid line) solutions containing 0.1 M Na_2SO_4 and 0.05 M phosphate buffer (pH 7.0). The potential scan was initiated at -0.2 V with a scan rate of 100 mV/s. The arrow indicates the initial scan direction.

Figure 8. Cyclic voltammograms at the MDS/Au electrode in blank (a), 1 mM dopamine and 1 mM ascorbic acid (b), and 1 mM dopamine and 5 mM ascorbic acid (c) solutions containing 0.1 M Na_2SO_4 and 0.05 M phosphate buffer (pH 2.2). Voltammetric scan: 100 mV/s with an initial potential of -0.2 V. The arrow indicates the initial scan direction.

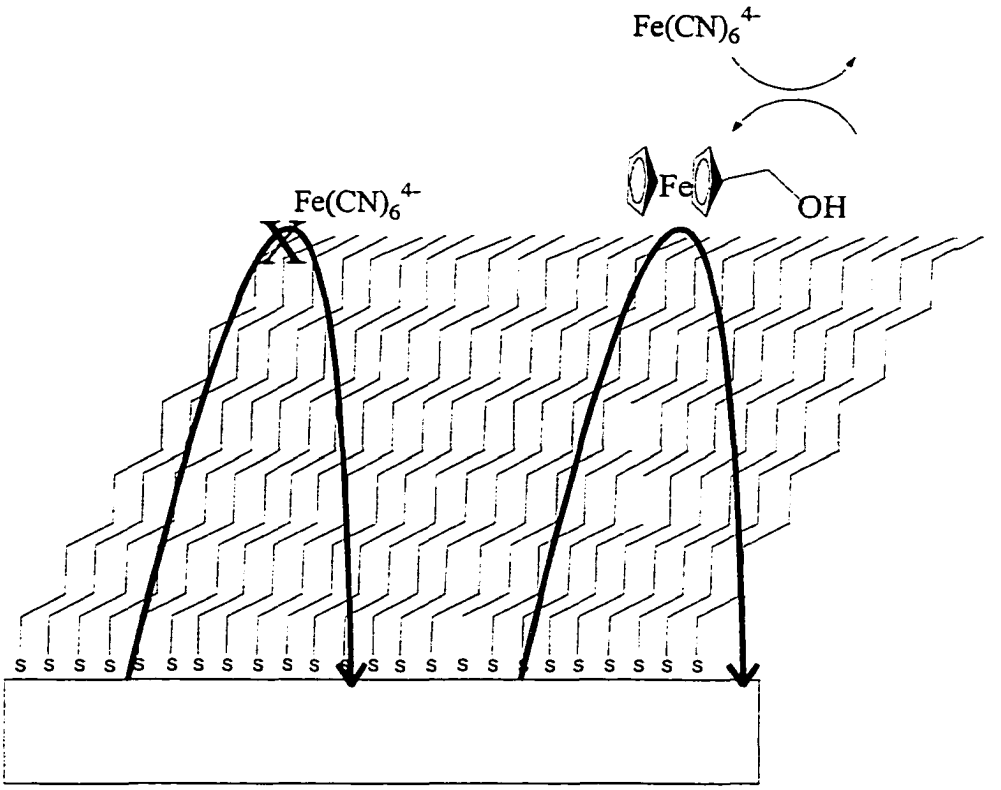

Scheme 1

Adapted from Radford, P. T.; French, M.; Creager, S. E. *Anal. Chem.* **1999,** *71,* 5101-5108.

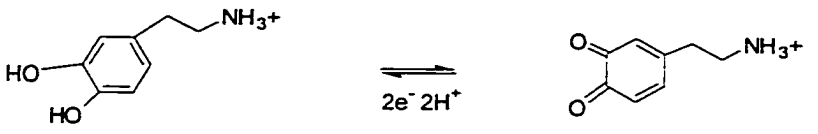

heterogeneous

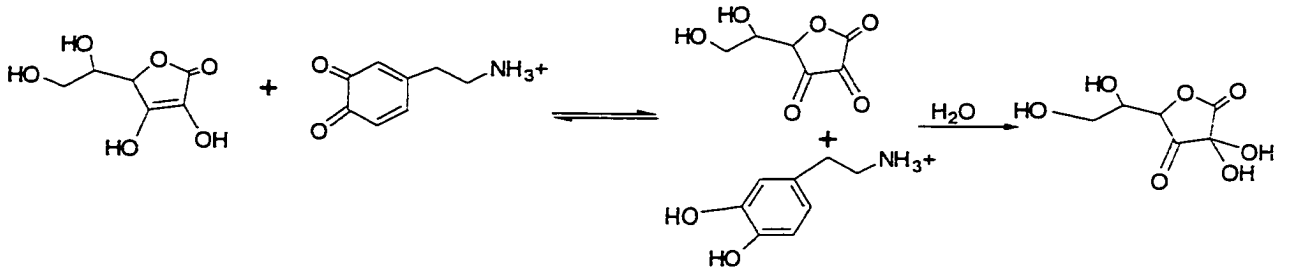

homogeneous

Scheme 2

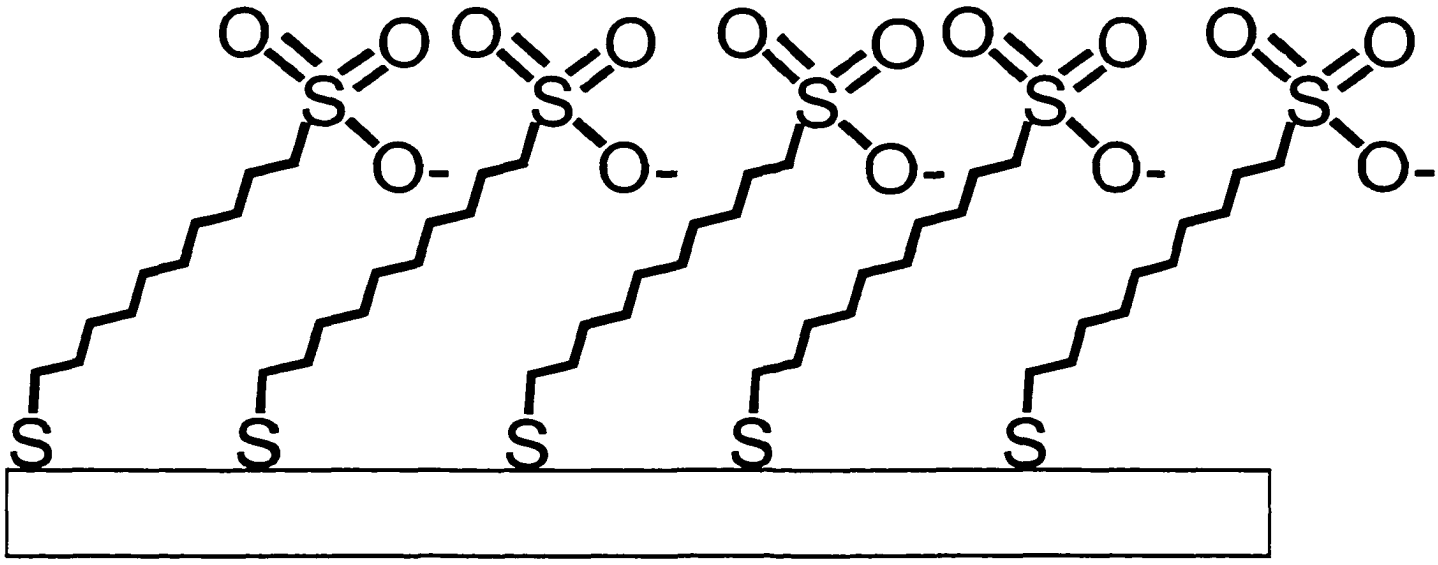

Figure 1

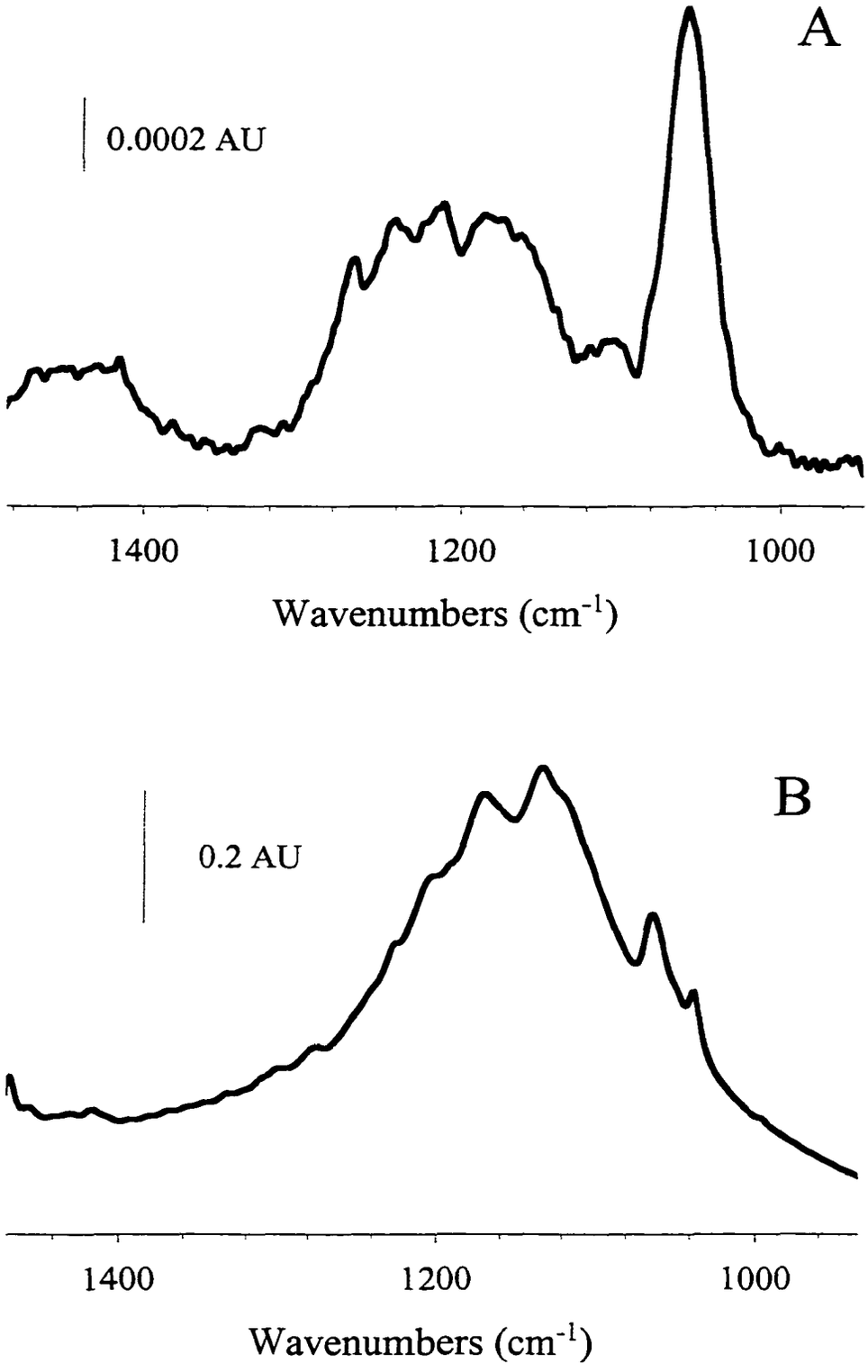
A
0.0002 AU
1400
1200
1000
Wavenumbers (cm-1)
B
0.2 AU
1400
1200
1000
Wavenumbers (cm-1)

Figure 2

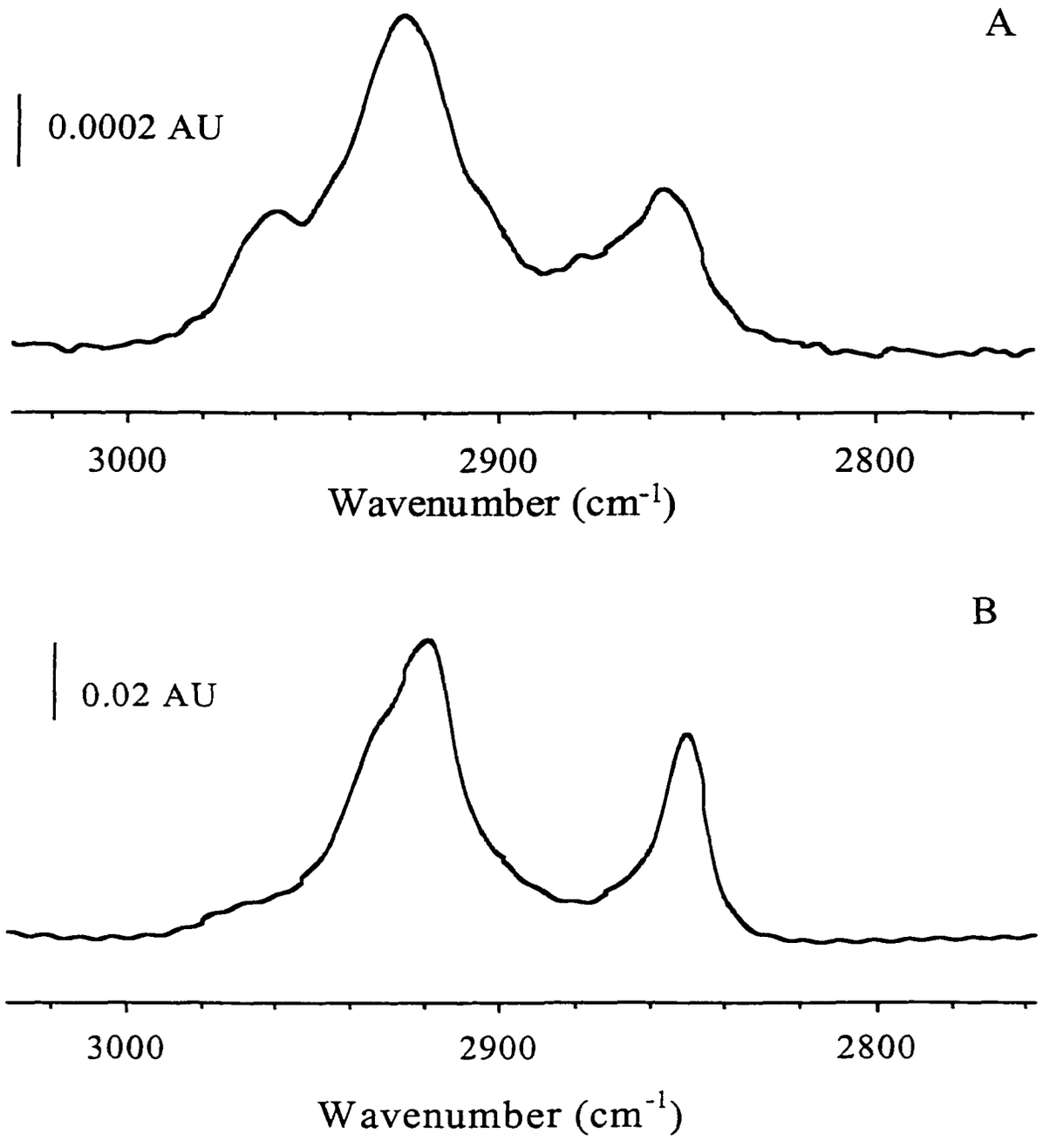
A
0.0002 AU
3000
2900
2800
Wavenumber (cm-1)
B
0.02 AU
3000
2900
2800
Wavenumber (cm-1)

Figure 3

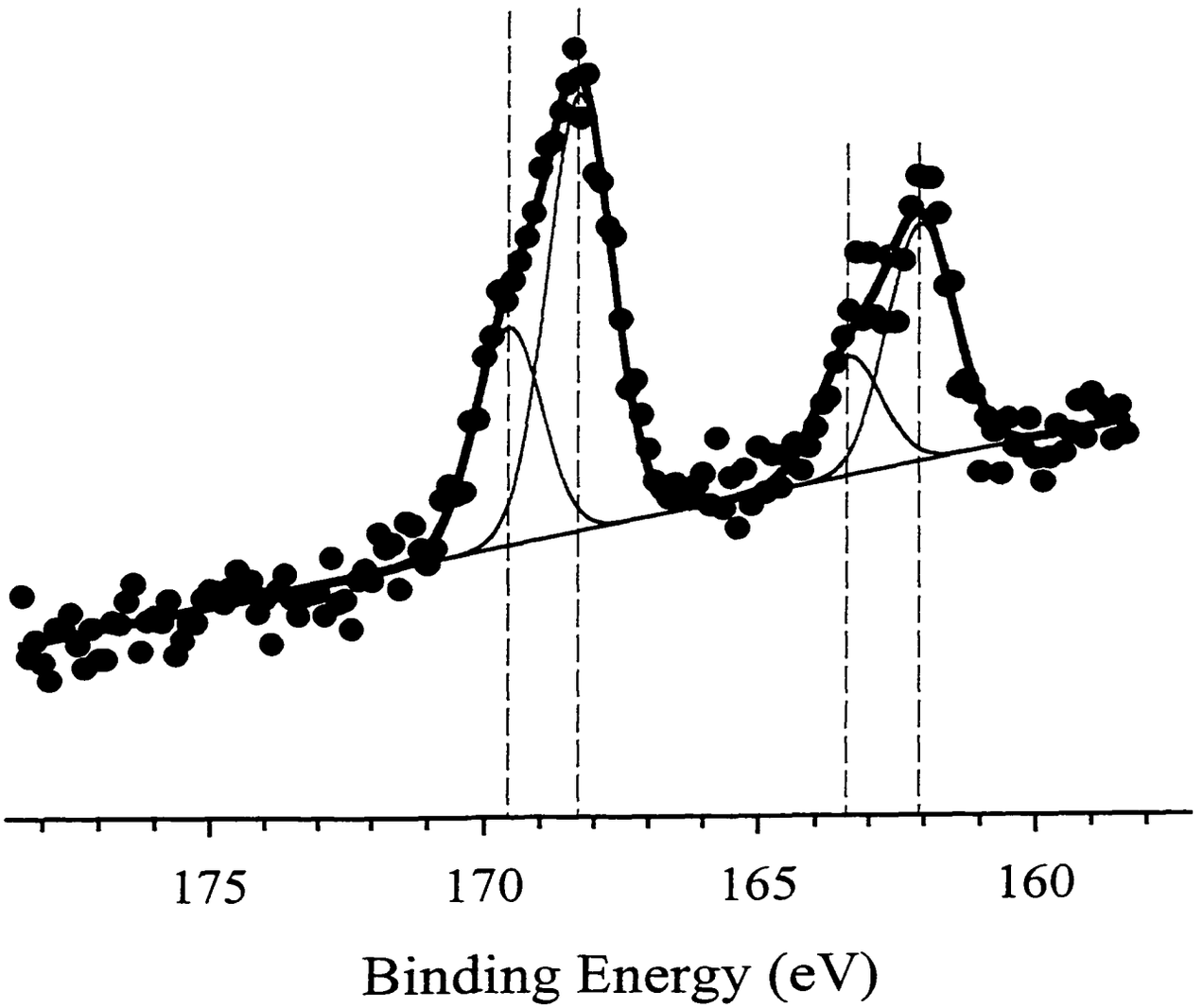

Figure 4

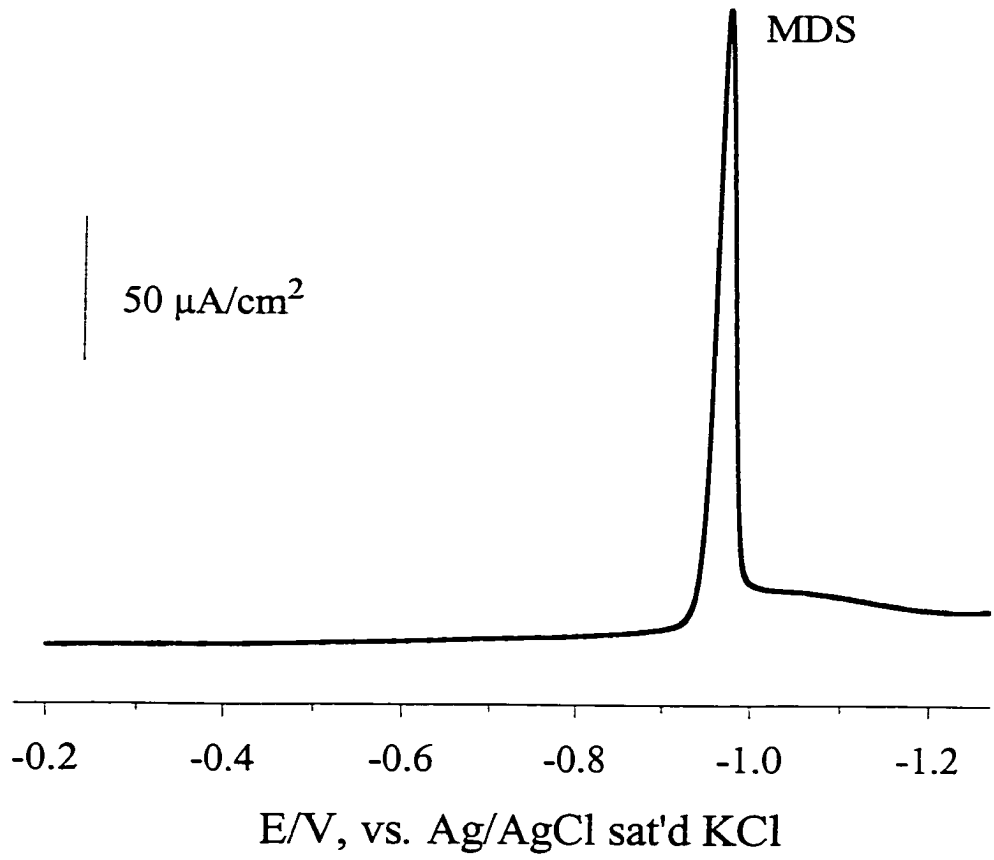

Figure 5

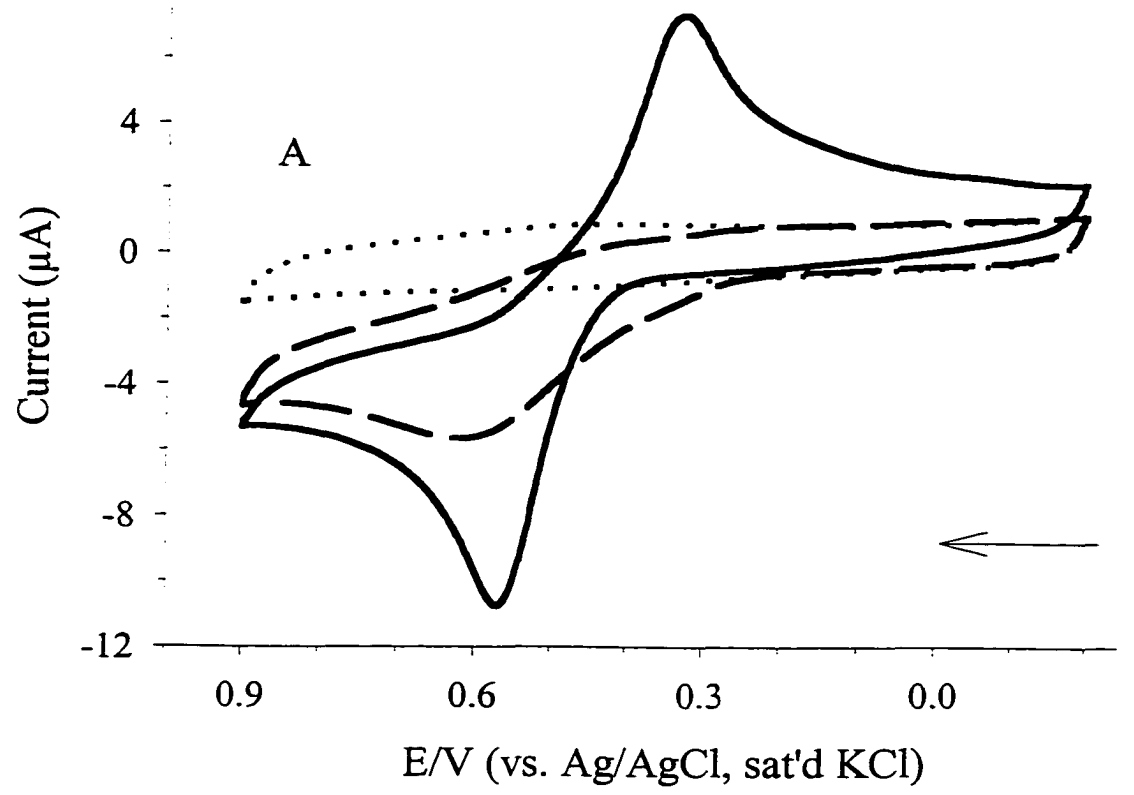
A
4
0
-4
-8
-12
Current (μA)
0.9
0.6
0.3
0.0
E/V (vs. Ag/AgCl, sat'd KCl)

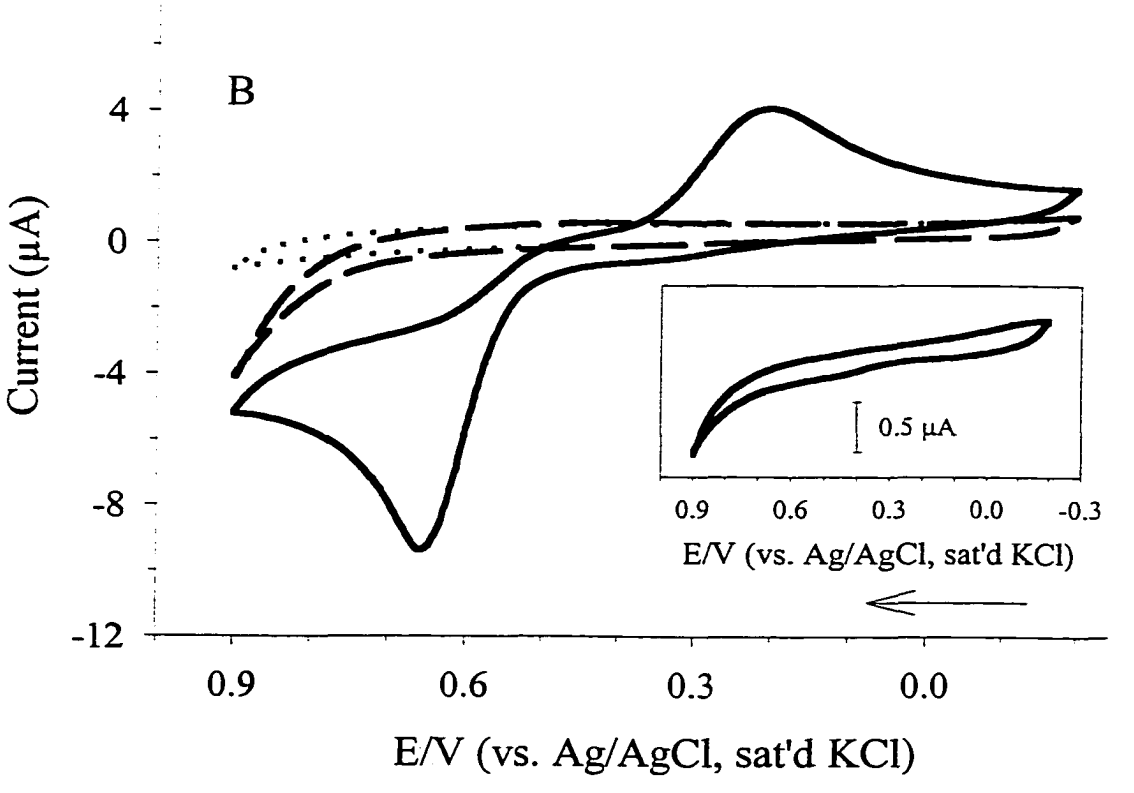
B
4
0
-4
-8
-12
Current (μA)
0.5 μA
0.9
0.6
0.3
0.0
-0.3
E/V (vs. Ag/AgCl, sat'd KCl)
0.9
0.6
0.3
0.0
E/V (vs. Ag/AgCl, sat'd KCl)

Figure 6

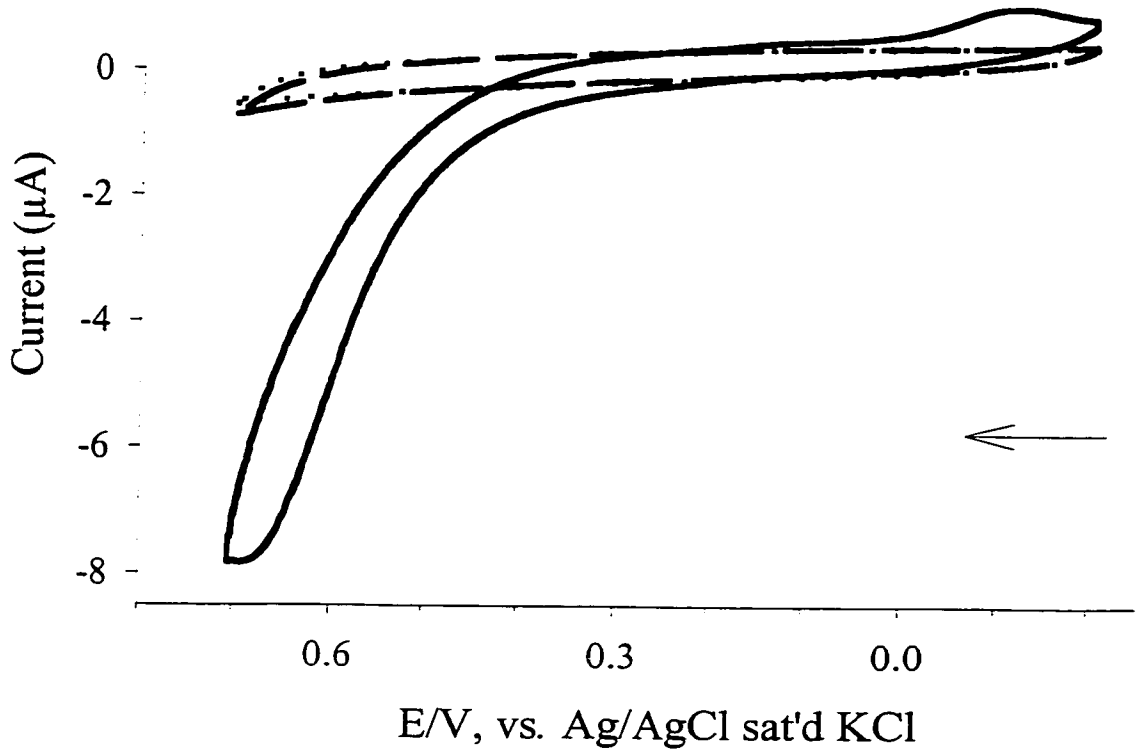

Figure 7

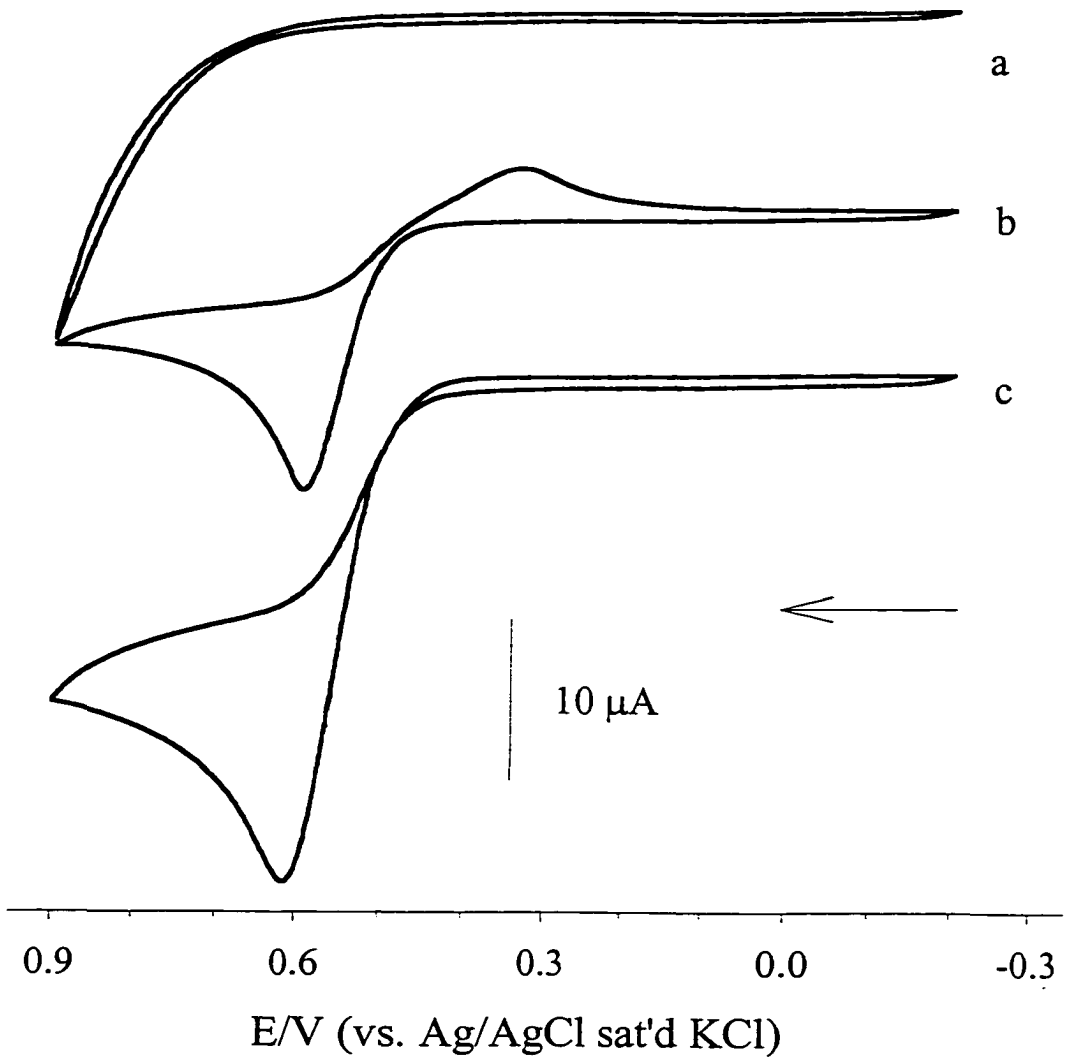

Figure 8

CHAPTER 2. NITRIC OXIDE DETECTION WITH THIOL MONOLAYERS AT GOLD ELECTRODES

A paper to be submitted to the Journal of Electroanalytical Chemistry

G. Brent Dawson, Desiree S. Grubisha, Jennifer A. Harnisch, L. Keith Woo, and Marc D. Porter

Abstract

Differently functionalized thiol monolayers adsorbed at gold were investigated for the voltammetric detection of nitric oxide. Mercaptodecanesulfonate-coated electrodes showed an enhanced selectivity for nitric oxide over the interfering species, nitrite, while providing a detection limit in the low micromolar concentration range. Electrodes coated with a thiolated iron diphenyl etio porphyrin gave no detectable response to nitric oxide and were assumed to block electron transfer or form nitrosyl complexes with low surface coverages. Also, thiolated tetra pyridyl iron porphyrin monolayers were synthesized and utilized to form self-assembled monolayers. While, infrared spectroscopic characterizations confirmed the presence of the monolayer, no detectable response for oxidation or reduction of nitric oxide was recorded.

Introduction

Nitric oxide (NO) is a relatively unreactive radical but it combines with O_2 to form NO_2. While not a physiological irritant, NO has been identified as an active component in intercellular signaling pathways and as a part of the immune response mediated by macrophages.[1] Macrophages destroy bacteria by releasing NO, which presumably attacks

iron-sulfur prosthetic groups in many enzymes.[1] In the endothelial cells surrounding blood vessels, NO binds to the heme group of guanylate cyclase, which activates the production of cyclic guanosine monophosphate (cGMP). cGMP is known to cause dilation of blood vessels, lowering blood pressure.[2]

While many alternative transduction schemes for NO detection have been developed, electrochemical detection has gained the most attention because of its use for *in vivo* applications.[3,4] Arvia and coworkers examined the NO^+/NO redox couple in concentrated sulfuric acid.[5] Using rotated-disc voltammetry at a gold electrode, they reported a reduction potential of +0.739 V vs. the normal hydrogen electrode (NHE). They also found this reaction to be chemically reversible under these conditions. Sedlak and Blurton described a method to simultaneously detect CO, NO, and NO_2 in acidic solutions by applying different oxidation potentials.[6] NO_2 was oxidized at +0.8 V vs NHE, while larger potentials were needed to oxidize NO and CO. To detect NO, a potential of +1.5 V was applied-- a potential where CO was unresponsive.

Additionally, Clark-type oxygen sensing electrodes were modified to detect NO selectively. Shibuki described a technique where two platinum electrodes were placed in one compartment filled with 30 mM NaCl/0.3 mM HCl solution separated from the analyte solution by a chloroprene rubber membrane.[7] When the electrode was poised at +0.9 V vs the saturated calomel electrode (SCE), the amperometric response for nitric oxide was highly selective with detection limits in the low nanomolar range. Unfortunately, these electrodes were insensitive to changes in concentration in the micromolar range because of NO-induced degradation of the polymer membrane.[8]

Bedioui et al. used Nafion® and a nickel porphyrin to induce catalytic activity at an Au electrode.[9] The Nafion® acts to stabilize the nitrosium cation shifting the oxidative potential negatively. These types of sensors give linear responses over four decades of NO concentration and have detection limits below 1 nM in biological environments. Amperometric sensors were also created with platinum and carbon electrodes coated with poly[4,4'-dihydroxybenzophenone] or with Nafion.[10] With detection at +0.8 V vs. Ag/AgCl, detection limits of 35 nM were reached using the platinum electrode coated with 4,4' dihydroxybenzophenone in the presence of interfering species such as ascorbate, dopamine, or potassium nitrite.

Haruyama and coworkers showed that denatured cytochrome *c* immobilized on a pyridine thiol-coated gold electrode could be utilized to detect NO. The NO oxidized the porphyrin prosthetic group of the protein that was subsequently reduced at 0 V vs. Ag/AgCl reference electrode. This method had a linear response of 0.5-4 μM and was free from interference by nitrite.

Fluorescent methods that yield low limits of detection and high sensitivity have also recently been developed. Lippard and coworkers described a fluorescence method for the determination of nitric oxide.[11] In this method, a Co^{2+} ion brings two fluorophore ligands into close proximity through coordination and quenches their fluorescence. However, when NO is present, it replaces the fluorescent ligands at the metal center, and the two fluorophores move apart and no longer quench each other. A detection limit of 50-100 μM was estimated for this technique that showed no detectable response to O_2.

Another report demonstrated a method where diaminofluorescein derivatives were used to detect NO.[12] Upon NO binding, these compounds were converted to the highly

fluorescent triazole. Real time imaging of NO *in vivo* was demonstrated with a detection limit of 5 nM. Kopelman and coworkers described a completely reversible method of NO detection with a ratiometric sensor using cytochrome *c* derivatized with fluorescent molecules.[13] The method could be use to selectively determine NO in the presence of nitrite, nitrate, and oxygen species with a detection limit of 8 μM.

This paper details our efforts in using monolayers to introduce selectivity to the electrochemical detection of NO at gold electrodes under physiological conditions (pH 7.2). First, data from schemes employing sulfonate-terminated thiol monolayers will be described. These systems showed increased selectivity and lower background currents than uncoated electrodes. Thiolated-porphyrin monolayers were synthesized, characterized and examined for catalytic activity toward NO oxidation, but no enhancements in the sensitivity over uncoated electrodes were recorded.

Experimental

Cyclic Voltammetry (CV)

Electrochemical experiments were performed with a model 263 potentiostat/galvanostat (Princeton Applied Research). A conventional three-electrode cell was used with the geometrically exposed area of the working electrode defined by an elastomer o-ring (geometric area of 0.65 cm^2). A platinum coil and $Ag|AgCl|NaCl_{sat}$ electrode were used as the auxiliary and reference electrodes, respectively. All potentials are reported with respect to the $Ag|AgCl|NaCl_{sat}$ electrode. The electrolytes, either the aqueous

0.1 M $NaClO_4$/0.02 M Na_2PO_4 (pH =7.2) or 0.1 M Na_2PO_4 (pH = 6.2), and were deoxygenated with argon just prior to the electrochemical measurements.

Au/Cr/glass working electrodes were prepared by resistive evaporation in an Edwards 306A coating system. Prior to gold deposition, the pre-cleaned glass slides were first primed with 15 nm of chromium at the deposition rate of 0.1 nm/s. Gold was deposited at a rate of 0.3 nm/s to give a thickness of 300 nm. These films were subsequently stored in a dessicator and were used within a month of preparation. All glassware was thoroughly cleaned with piranha solution (1 part 30 % H_2O_2: 3 parts 98 % H_2SO_4) prior to use and rinsed with distilled-deionized water (Millipore). **Caution piranha solution is explosive when in contact with organic compounds and should not be stored.**

Mercaptodecanesulfonic acid was prepared from a standard procedure recently reported by Turyan and Mandler.[14] The monolayer-coated electrodes were prepared by immersing the gold thin film electrode into a 1 mM solution of mercaptodecanesulfonic acid in 0.1 M $HClO_4$. The acidic solvent was used to protonate the precursor and reduces electrostatic repulsion among the endgroups. Prior to use, the electrodes were rinsed with deionized water and dried in a stream of nitrogen.

An electrolyte solution saturated with nitric oxide ([NO] = ~1.8 mM)[9] solution was prepared by first purging 3 mL of the electrolyte with nitrogen and then with nitric oxide (Aldrich) for 5 min. Solutions were prepared daily and stored under a headspace of nitrogen. No nitrogen dioxide was detected visually. During the analysis, microliter aliquots of this solution were removed with a gas-tight syringe and injected into the electrochemical cell while under a blanket of nitrogen.

Infrared Reflection Absorption Spectroscopy (IRRAS)

IR spectra were acquired using a Magna 750 FT-IR spectrometer (Nicolet), equipped with a liquid nitrogen-cooled HgCdTe detector. Monolayer spectra were obtained, under the purge of nitrogen, in an external reflection mode using *p*-polarized light incident at 82° with respect to the surface normal. The spectra are reported as -log(R/R_o), where R is the reflectance of the sample and R_o is the reflectance of the reference, or *n*-octadecanethiol-d_{37} monolayer at gold. For both sample and reference, the reflectance is the average of 512 scans. All spectra were collected at a 2 cm^{-1} resolution and one level of zero filling with Happ-Genzel apodization.

Synthesis of a *meso*{[6-(N-mercaptohexyl pyridyl) *tris*(4-pyridyl) porphyrinato]} iron (Fe (tpyp))

A 1 mL aliquout of 6-mercaptohexanol (Aldrich 95 %) in 15 mL of methylene chloride was reacted with 15 mL of an 1 M phosphorus tribromide (PBr_3 Aldrich) solution in methylene chloride at 0°C under a nitrogen atmosphere. The mixture was stirred overnight and then 15 mL of deionized water (Millipore) was added to quench the remaining PBr_3. The product was extracted 3x with methylene chloride, dried with magnesium sulfate (Fisher) and filtered. The solvent was removed by rotary evaporation and ~100 μL of the yellow oil was dissolved in ethanol. A 1 mL aliquot of this compound was dissolved in a 9:1 chloroform:methanol (Fisher) solution and refluxed with 100 mg of tetra pyridyl porphine (Aldrich) for 12 h. The solvent was removed under reduced pressure and the brown solid was triturated 3 times with diethyl ether (Fisher), suspended in 3 mL of methanol (Fisher) and filtered. A 10 μM solution of this compound in methanol was prepared and Au/Cr/glass

substrates were placed in the solution for 12 h prior to IRRAS analysis. Iron was inserted into the porphyrin by refluxing the monolayer-coated electrodes in a 9:1 chloroform:methanol solution and iron (II) bromide. NMR and IR analysis were consistent with Structure 1.

Synthesis of 5a,15a-bis[o-(6-mercaptohexylamido)phenyl]-etioporphyrin

Preparation of the free-base thiol derivatized etio porphyrins followed modifications of earlier procedures.[15-18] Of paramount importance is the placement of both thiol appendages on the same side of the porphyrin plane. This aspect of the architecture was achieved using the *cis*-amine isomer of 5,15-bis[*o*-aminophenyl]etioporphyrin as the precursor, which was chromatographically separated from its trans-amine isomer. Alkylation of the *cis*-amine isomer with 6-(tritylthio)hexanoyl chloride, followed by removal of the trityl protecting groups with $Hg(OAc)_2$ and H_2S, produced 5a,15a-bis[o-(6-mercaptohexylamido)phenyl]-etioporphyrin. Monolayers were prepared by the immersion of annealed mica-supported gold into 10 μM CH_2Cl_2 solutions of the thiol derivatives for ~12 h. Monolayers were metallated with $FeBr_2$ in tetrahydrofuran and pyridine post assembly. NMR and IR data were consistent with Structure 2.

Results and Discussion

To determine NO selectively under physiological conditions, we chose a voltammetric method involving its oxidation. This method allowed us to exclude the response due to oxygen and other interfering species by carefully controlling the potential. Figure 1 shows the voltammetric scans for an uncoated gold electrode with (solid curve) and

without NO (dashed curve) present. In the absence of NO a current density of 25 $\mu A/cm^2$ is recorded at +0.8 V. This response is attributed to the oxidation of the gold electrode surface. When 15 μL of NO are injected into the cell, the observed current increases to ~40 $\mu A/cm^2$. The mechanism active under these conditions is the one-electron oxidation of NO to the nitrosonium cation (NO^+), which rapidly reacts with water to form nitrous acid and a proton.[19]

When the electrode is coated with a mercaptodecanesulfonic acid (MDS) monolayer, the recorded voltammogram changes in the ways evident in Figure 2. The capacitive charging is greatly decreased, and the oxidation of the electrode surface is dramatically diminished. When 15 μL of the NO saturated (solid curve) electrolyte are injected to the cell, the voltammogram shows the oxidation of the NO at 800 mV giving a current of 35.8 $\mu A/cm^2$. These data show that the mercaptodecanesulfonate monolayer greatly increases the signal to noise (S/N) for the voltammetric detection of NO. This result is most likely due to the suppression of gold oxide formation at the monolayer-coated electrode combined with its low capacitance.[20,21] No attenuation in the current is noticed when the monolayer is present on the surface indicating that the monolayer does not greatly affect the rate of diffusion of NO or the rate of electron transfer from NO to the electrode.

Figure 3 shows the sensitivity of the monolayer-coated electrode to the oxidation of nitric oxide. The plot of concentration versus current density is linear up to a concentration of 10 μM. This sensitivity (5.54 $\mu A\ cm^{-2}\mu M^{-1}$) is similar to that found for an uncoated gold electrode, indicating that the monolayer does not have a notable impact on the detectability. However the MDS film shows excellent selectivity for NO versus NO_2^-. When

voltammograms of a 2 mM $NaNO_2$ solution were acquired, a large attenuation in the current is noticed for the monolayer-coated electrode (Figure 4). In fact, the peak current at the monolayer-coated electrode is approximately half that at the uncoated one (107 $\mu A/cm^2$ and 208 $\mu A/cm^2$ respectively). These initial data indicate the possibility of using spontaneously adsorbed monolayers for the selective determination of nitric oxide in the presence of interfering species such as nitrite.

The role of NO in cellular signaling is strongly tied to its interaction with the heme group of guanylate cyclase causing a conformational change in the enzyme and thereby increasing the rate of production of cyclic guanosine monophosphate.[2] In efforts to use the NO binding characteristics of metal porphyrins in a detection scheme, we investigated the attachment of porphyrin molecules to the surface of gold electrodes through monolayer chemistry.

Based on our previous work with monolayer oxygen sensors,[17] we investigated gold electrodes coated with bis-*meso*-[-*o*-(6mercaptohexylamido)phenyl] tetra-methyl tetra-ethyl porphyrin (DPE) as sensors for NO in solution. This monolayer contains two thiol appendages that are used to anchor it to the gold surface. The monolayer is subsequently metallated by placing it in a tetrahydrofuran solution of a metal salt and pyridine. Figure 5 shows the IRRAS spectrum of the monolayer formed from Fe DPE. The three bands in the 2850-2980 region are due to the methylene units of the porphyrin where the bands at 1713, 1581, and 1519 are due to the amide, pyrrole and phenyl ring, respectively. The large absorbances due to the ring stretching could indicate that the porphyrin is lying more along the normal to the electrode surface. For this to occur, the molecules must have only one thiol appendage attached to the electrode surface.

The two voltammograms in Figure 6 show that the iron porphyrin is present and active towards the catalytic reduction of oxygen in a phosphate buffered saline solution. The top voltammogram shows the reduction of oxygen at a bare gold electrode. The peak in the reduction wave occurs at –0.4 V, with a current of 85 $\mu A/cm^2$. The lower voltammogram shows the reduction of oxygen in an air-saturated solution at a Fe DPE coated electrode. The peak potential has shifted positively by 100 mV and the peak current is ~180 $\mu A/cm^2$. These shifts are due to the porphyrin acting as a mediator in the reduction of dissolved oxygen. Figure 7 shows the voltammogram recorded when 20 μL of a saturated NO solution has been added to the electrolyte. No detectable faradaic processes are recorded in this potential region though one sees a decrease in the capacitive charging current. This lack of an oxidation current could arise from a variety of processes each of which is examined below.

Another approach to form porphyrin monolayers utilized tetra pyridyl porphyrin (tpyp) after reaction with 6-bromohexanethiol. The brominated thiol acts to quaternize the pyridyl group, and brominated silanes have been used to attach pyridyl porphyrins to glass surfaces.[22] After quaternization, the monolayer was metallated by refluxing it in a 90:10 mixture of chloroform:methanol containing $FeBr_2$. Figure 8 shows the IRRAS spectrum of the monolayer formed from this thiolated porphyrin. The bands at 2930 and 2856 are due to the methylene stretching modes while the bands at 1636 and 1593 have been attributed to the quaternized pyridyl porphyrin.[22] Unfortunately, these spectra show large absorbances in the 1100-900 region, which are likely from an impurity possessing P-O bonds.

Cyclic voltammetry again revealed that the porphyrin monolayer did not enhance but actually increased the detection limit of the electrode towards nitric oxide detection. Figure 9 shows the voltammograms for monolayer-coated electrode and for bare gold. The dashed

curve shows the response of a bare gold electrode to a 10 μM solution of nitric oxide in a pH 6.4 phosphate buffer solution. The dotted curve shows the response of the porphyrin monolayer that has been metallated with iron while the solid curve shows the response at a non-metallated porphyrin monolayer. While the current is higher at the metallated porphyrin it is only ~25 % of the response seen for a bare gold electrode

Our work with sulfonate monolayers has shown that these monolayers do not attenuate the oxidation current for NO. The porphyrin monolayers in this study should be less well packed than the aliphatic sulfonate systems and should not present a diffusional barrier to the NO. However, the NO could react with metal center or the porphyrin to form a species that is electro-inactive in the examined potential region. The tendency NO to form stable complexes with porphyrins has been well documented.[23-26] The stability of these complexes could place their redox transformation out of the examined potential range. Future work will examine electrodes by infrared spectroscopy to confirm the presence of NO on the surface and determine the potential dependent stability of the complex. While these reactions block the direct oxidation of NO, a mediated electron transfer could be plausible in other potential regions.

Conclusions

Several attempts to construct monolayer-based electrochemical sensors have been examined. The use of a mercaptodecane sulfonate coated electrode has shown potential in for the determination of nitric oxide in the presence of an interfering species. This technique showed high sensitivity in the micromolar range and was selective against nitrite. Efforts to realize low detection limits for nitric oxide detection with thiolated porphyrins were

unsuccessful, though the quaternization of the tetra-pyridyl porphyrin with a brominated thiol was demonstrated to be a simple method to attach such porphyrins to gold electrodes. The data presented here shows that iron porphyrins do not show catalytic activity for NO oxidation, likely due to the formation of stable Fe-NO complexes. Future efforts will focus on introducing high selectivity with charge monolayers while maintaining fast rates of electron transfer. Specifically, shorter chainlength sulfonates will be utilized increase rates of sensitivity while discrimination against electroactive anions.

Acknowledgements

The 10-mercaptodecane sulfonate was synthesized by Robin L. McCarley. G. B. D. acknowledges the Phillips Petroleum Research Fellowship for year of financial support. Preliminary XPS data were acquired by James Anderegg of Ames Laboratory. Other support was provided by the Microanalytical Instrumentation Center of the Institute for Physical Research and Technology at Iowa State University.

References

(1) Galla, H.-J. *Angew. Chem. , Int. Ed.* **1993,** *32,* 378-380.

(2) Ignarro, L. J. *Angew. Chem. , Int. Ed.* **1999,** *38,* 1882-1892.

(3) Malinski, T.; Mesaros, S.; Tamboulian, P. In Methods in Enzymology; Packer, L., Ed.; Academic Press: San Diego, 1996; Vol. 268, pp 58-69.

(4) Malinski, T.; Taha, Z. *Nature.* **1992,** *358,* 676-8.

(5) Garcia, C. T.; Calandra, A. J.; Arvia, A. J. *Electrochimica Acta.* **1972,** *17,* 2181-2194.

(6) Sedlak, J. M.; Burton, K. F. *J. Electrochem. Soc.* **1976,** *123,* 1476-1478.

(7) Shibuki, K.; Okada, D. *Nature.* **1991,** *349,* 326-8.

(8) Christodoulou, D.; Kudo, S.; Cook, J. A.; Krishna, M. C.; Mills, A.; Grisham, M. B.; Murugesan, R.; Ford, P. C.; Wink, D. A. *Methods in Enzymology.* **1996,** *268,* 69-83.

(9) Bedioui, F.; Trevin, S.; Devynck, J. *J. Electroanal. Chem. Interfacial Electrochem.* **1994,** *377,* 295-298.

(10) Pallini, M.; Curulli, A.; Palleschi, G. *Electroanalysis.* **1998,** *10,* 1010-1016.

(11) Franz, K. J.; Singh, N.; Lippard, S. J. *Angew. Chem. , Int. Ed.* **2000,** *39,* 2120-2122.

(12) Kojima, H.; Nakatsubo, N.; Kikuchi, K.; Kawahara, S.; Kirino, Y.; Nagoshi, H.; Hirata, Y.; Nagano, T. *Anal. Chem.* **1998,** *70,* 2446-2453.

(13) Barker, S. L. R.; Clark, H. A.; Swallen, S. F.; Kopelman, R.; Tsang, A. W.; Swanson, J. A. *Anal. Chem.* **1999,** *71,* 1767-1772.

(14) Turyan, I.; Mandler, D. *J. Am. Chem. Soc.* **1998,** *120,* 10733-10742.

(15) Woo, L. K.; Maurya, M. R.; Jacobson, R. A.; Yang, S.; Ringrose, S. L. *Inorg. Chim. Acta.* **1992,** *193,* 143-7.

(16) Woo, L. K.; Maurya, M. R.; Jacobson, R. A.; Yang, S.; Ringrose, S. L. *Inorg. Chem.* **1992,** *31,* 913-919.

(17) Zak, J.; Yuan, H.; Ho, M.; Woo, L. K.; Porter, M. D. *Langmuir.* **1993,** *9,* 2772-2774.

(18) Yuan, H.; Woo, L. K. *Porphyrins and Phthalocyanines.* **1997,** *1,* 189-200.

(19) Mori, V.; Bertotti, M. *Analyst.* **2000,** *125,* 1629-1632.

(20) Wise, D. L.; Houghton, G. *Chem. Eng. Sci.* **1968,** *23,* 1211-1216.

(21) Vanderkooi, J. M.; Wright, W. W.; Erecinska, M. *Biochim. et Biophys. Acta.* **1994,** *1207,* 249-254.

(22) Li, D.; Swanson, B. I.; Robinson, J. M.; Hoffbauer, M. A. *J. Am. Chem. Soc.* **1993,** *115,* 6975-6981.

(23) Guilard, R.; Lagrange, G.; Tabard, A.; Lancon, D.; Kadish, K. M. *Inorg. Chem.* **1985,** *24,* 3649-56.

(24) Kadish, K. M.; Adamian, V. A.; Caemelbecke, E. V.; Tan, Z.; Tagliatesta, P.; Bianco, P.; Boschi, T.; Yi, G.-B.; Khan, M.; Richter-Addo, G. B. *Inorg. Chem.* **1996,** *35,* 1343-8.

(25) Kadish, K. M.; Ou, Z.; Tan, X.; Boschi, T.; Monti, D.; Fares, V.; Tagliatesta, P. *J. Chem. Soc., Dalton Transactions.* **1999**, 1595-1601.

(26) Richter-Addo, G. B.; Hodge, S. J.; Yi, G.-B.; Khan, M. A.; Ma, T.; Caemelbecke, E. V.; Guo, N.; Kadish, K. M. *Inorg. Chem.* **1996,** *35,* 6530-6538.

Figure Captions

Structure 1. Structure of *meso*{[6-(N-mercaptohexyl pyridyl) *tris*(4-pyridyl) porphyrinato]} iron (Fe (tpyp))

Structure 2. Structure of 5a,15a-bis[o-(6-mercaptohexylamido)phenyl]-etioporphyrin Fe.

Figure 1. Current-potential curves recorded at a bare gold electrode in 0.1 M $NaClO_4$ and 0.02 M Na_2PO_4 (pH 7.2). The dashed curve shows a background scan and the solid curve shows the oxidation of NO after the injection of 15 μL of a electrolyte saturated with NO. The arrow indicates the initial scan direction. Scan rate: 50 mV/s.

Figure 2. Current-potential curves recorded at a MDS monolayer-coated gold electrode in 0.1 M $NaClO_4$ and 0.02 M Na_2PO_4 (pH 7.2). The dashed curve shows a background scan and the solid curve shows the oxidation of NO after the injection of 15 μL of a electrolyte saturated with NO. The arrow indicates the initial scan direction. [NO] = 5.4 μM Scan rate: 50 mV/s.

Figure 3. Calibration curve for the voltammetric detection of NO at a MDS monolayer-coated gold electrolyte. Detection voltage: 0.800 V vs. Ag/AgCl, saturated NaCl.

Figure 4. Current-potential curves recorded at a MDS monolayer-coated gold electrode (solid curve) and bare gold electrode (dashed curve) for 2 mM $NaNO_2$ in 0.1 M $NaClO_4$ and 0.02 M Na_2PO_4 (pH 7.2). The arrow indicates the initial scan direction. Scan rate: 50 mV/s.

Figure 5. IRRAS spectrum for the Fe DPE monolayer at a gold electrode. The negative features are due to the $CD_3(CD)_{17}SH$ reference monolayer.

Figure 6. Current-potential curves recorded in air-saturated electrode [0.1 M Na_2PO_4 (pH 6.2)]. The top curve shows the response at an uncoated gold electrode scan and the bottom curve shows the response at an Fe DPE monolayer-coated electrode. Scan rate: 50 mV/s.

Figure 7. Current-potential curves recorded at a Fe DPE monolayer-coated gold electrode in 0.1 M Na_2PO_4 (pH 6.2). The dashed curve shows a background scan and the solid curve shows the oxidation of NO after the injection of 15 μL of an electrolyte saturated with NO. The arrow indicates the initial scan direction. Scan rate: 50 mV/s.

Figure 8. IRRAS spectrum for the Fe (tpyp) monolayer at a gold electrode. The negative features are due to the $CD_3(CD)_{17}SH$ reference monolayer.

Figure 9. Current-potential curves recorded at a Fe (tpyp) monolayer-coated gold electrode in 0.1 M Na_2PO_4 (pH 6.2). The dashed curve shows a background scan and the solid curve shows the oxidation of NO after the injection of 15 μL of an electrolyte saturated with NO. The arrow indicates the initial scan direction. Scan rate: 50 mV/s.

Structure 1

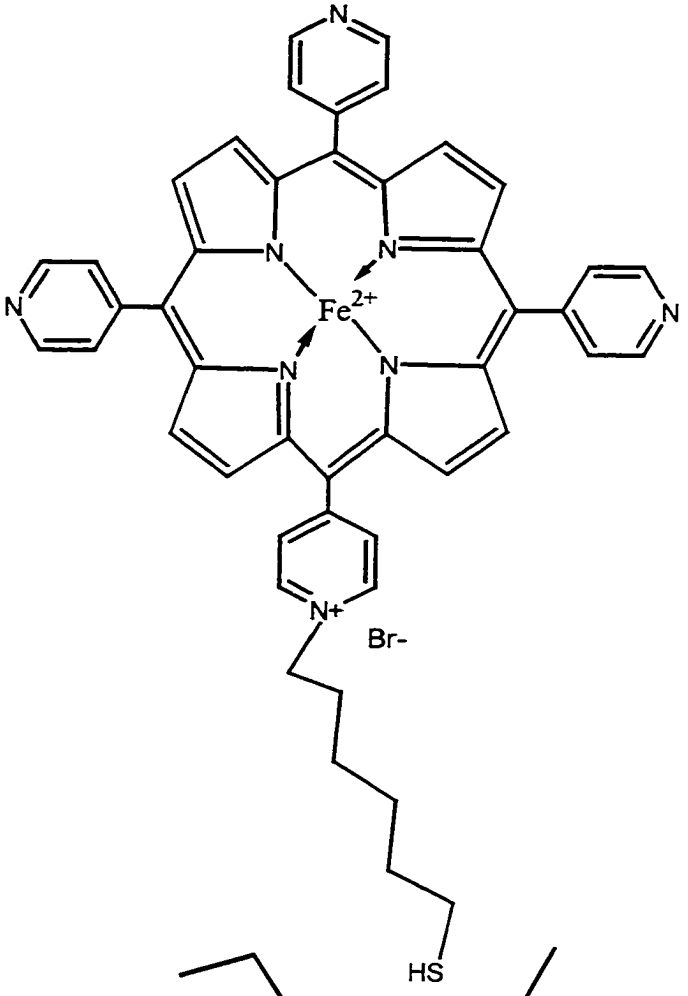

Structure 2

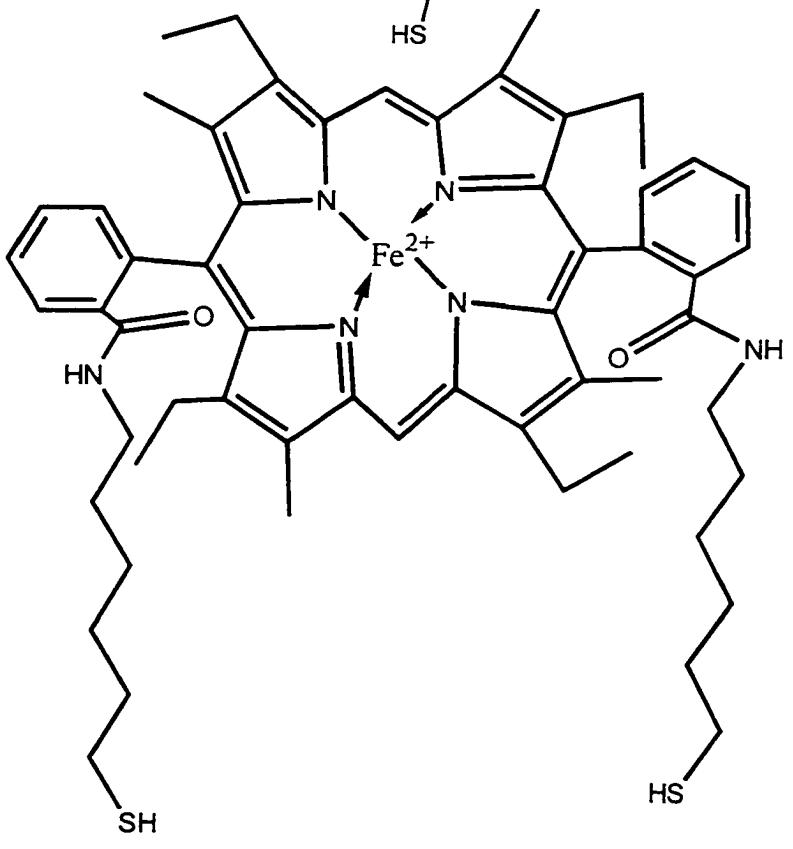

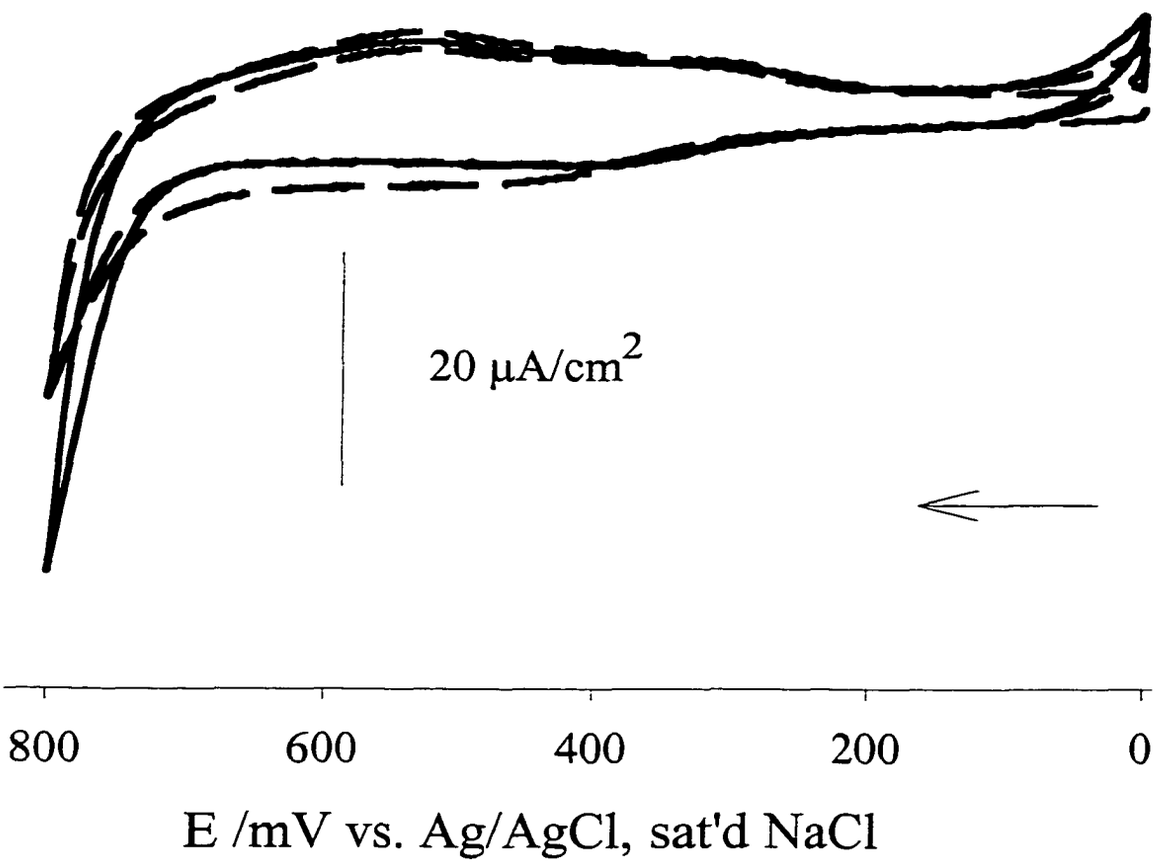

Figure 1

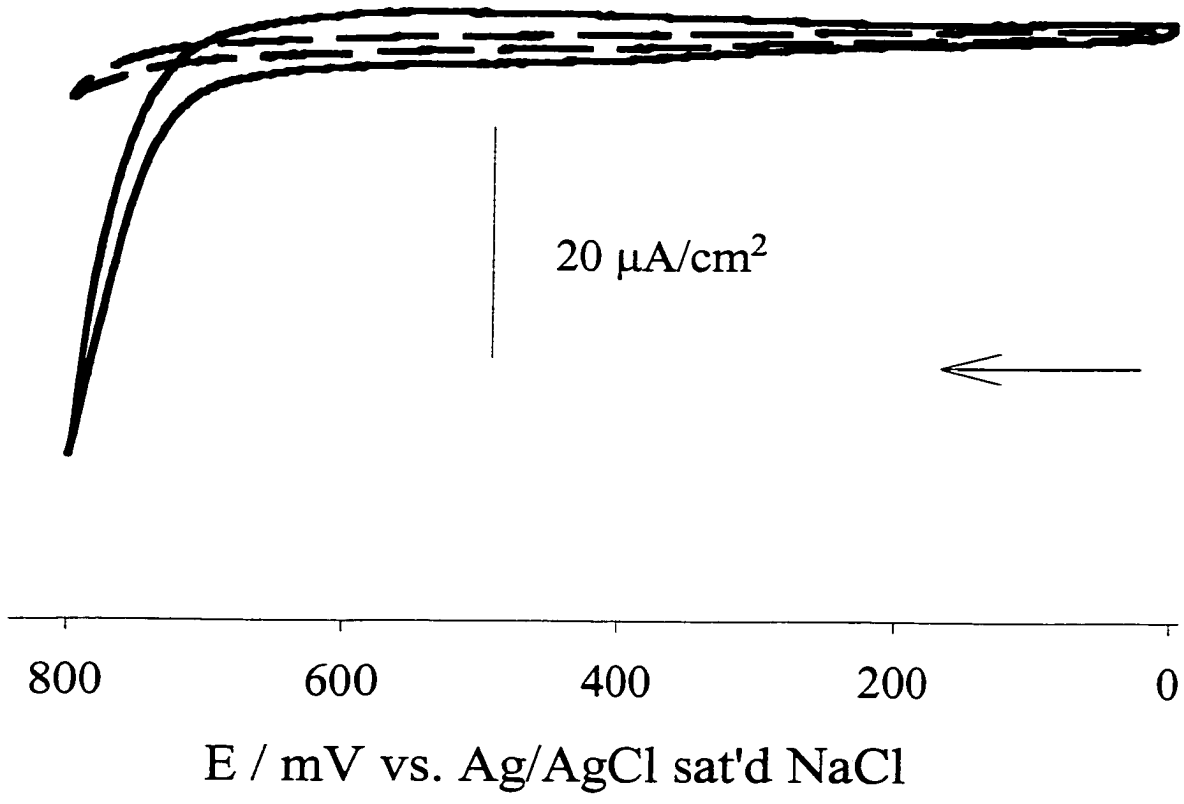

Figure 2

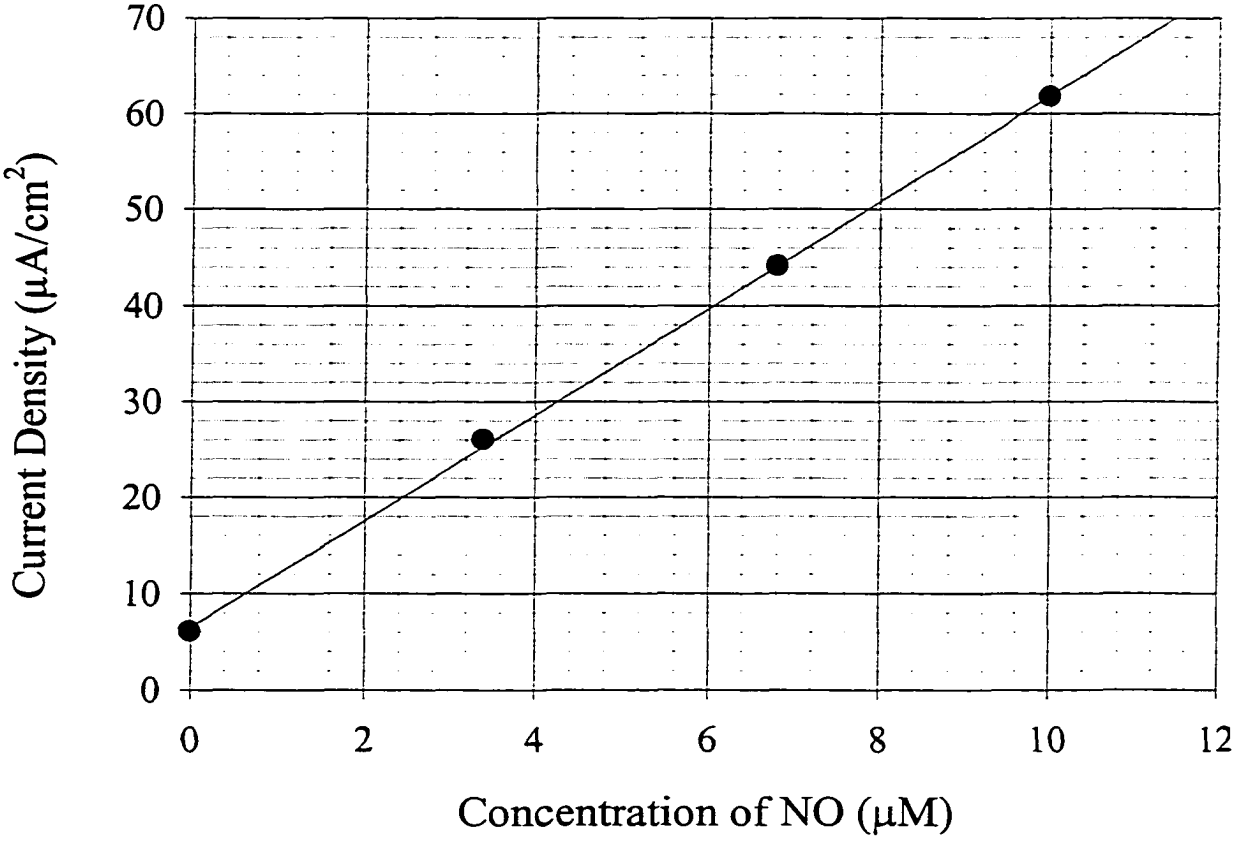
70
60
50
40
30
20
10
0
Current Density (μA/cm²)
0
2
4
6
8
10
12
Concentration of NO (μM)

Figure 3

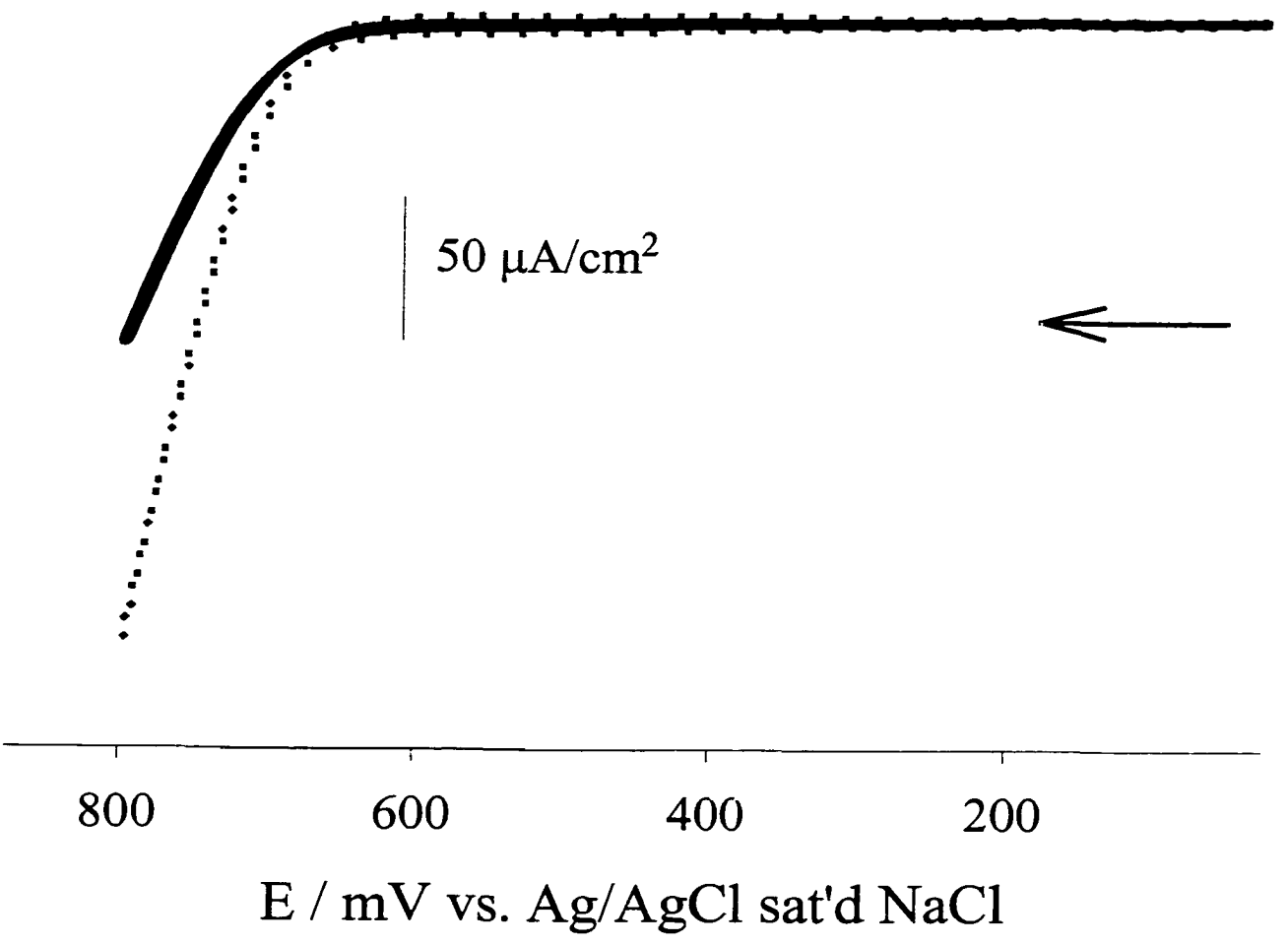

Figure 4

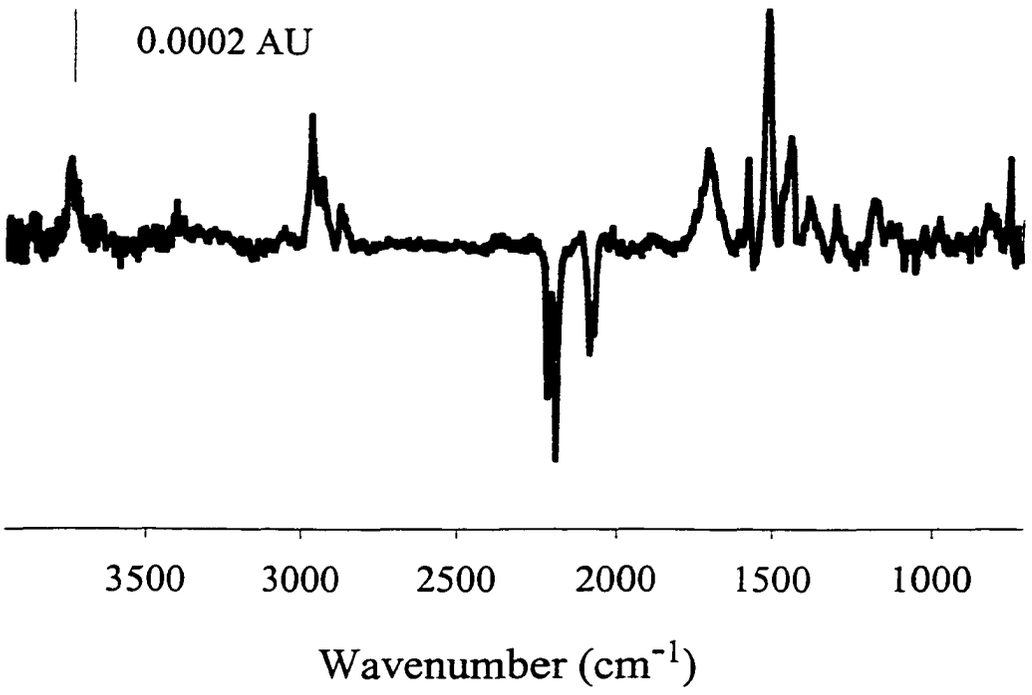

Figure 5

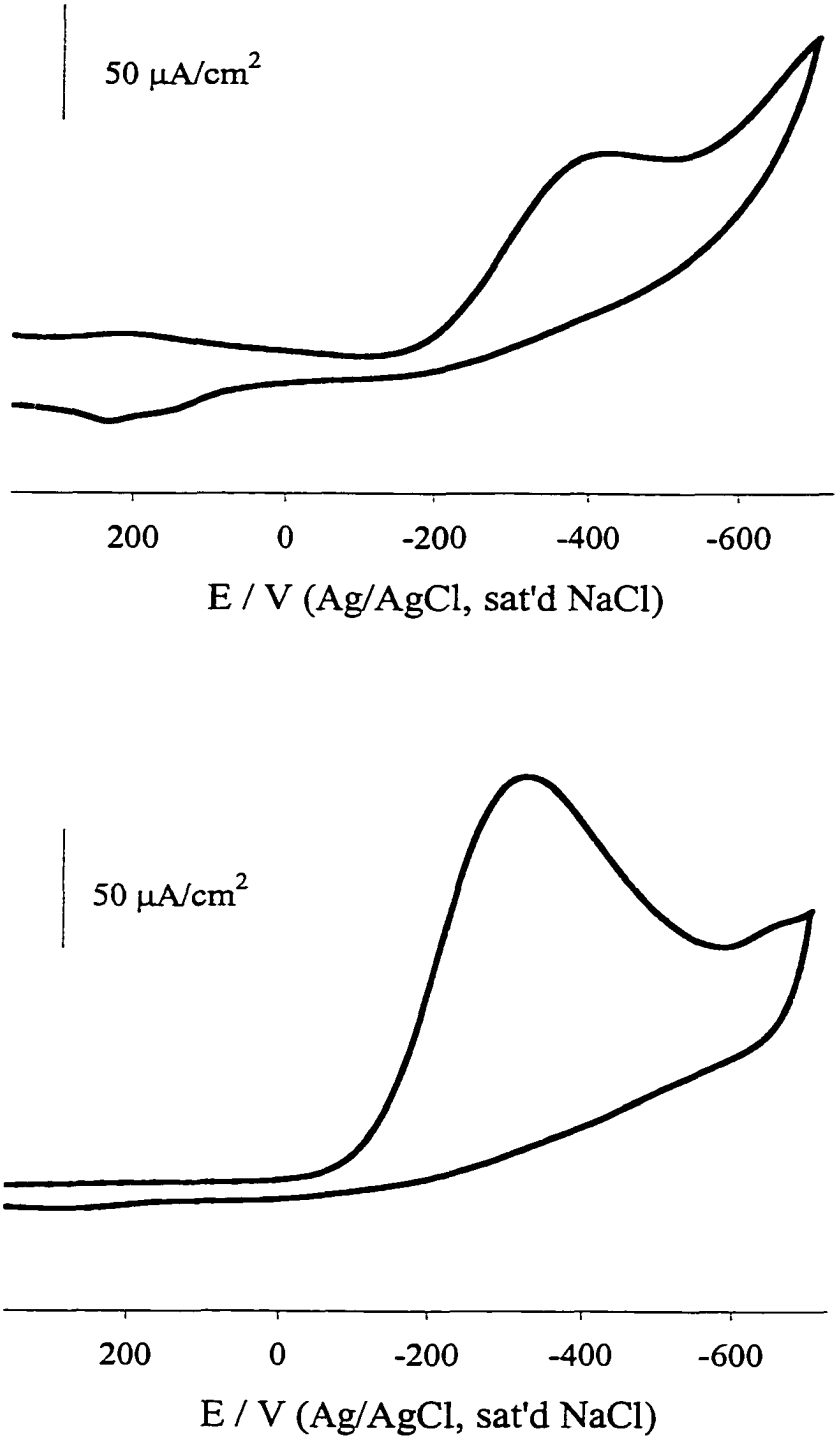
50 μA/cm2
200
0
-200
-400
-600
E / V (Ag/AgCl, sat'd NaCl)
50 μA/cm2
200
0
-200
-400
-600
E / V (Ag/AgCl, sat'd NaCl)

Figure 6

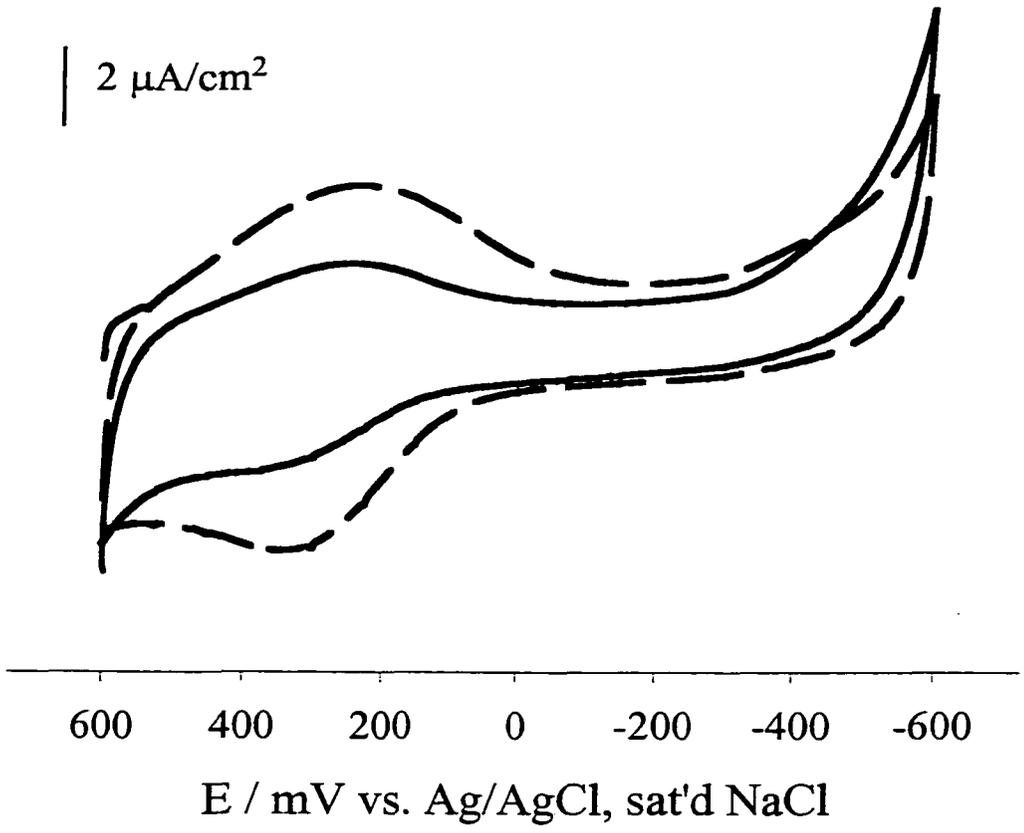

Figure 7

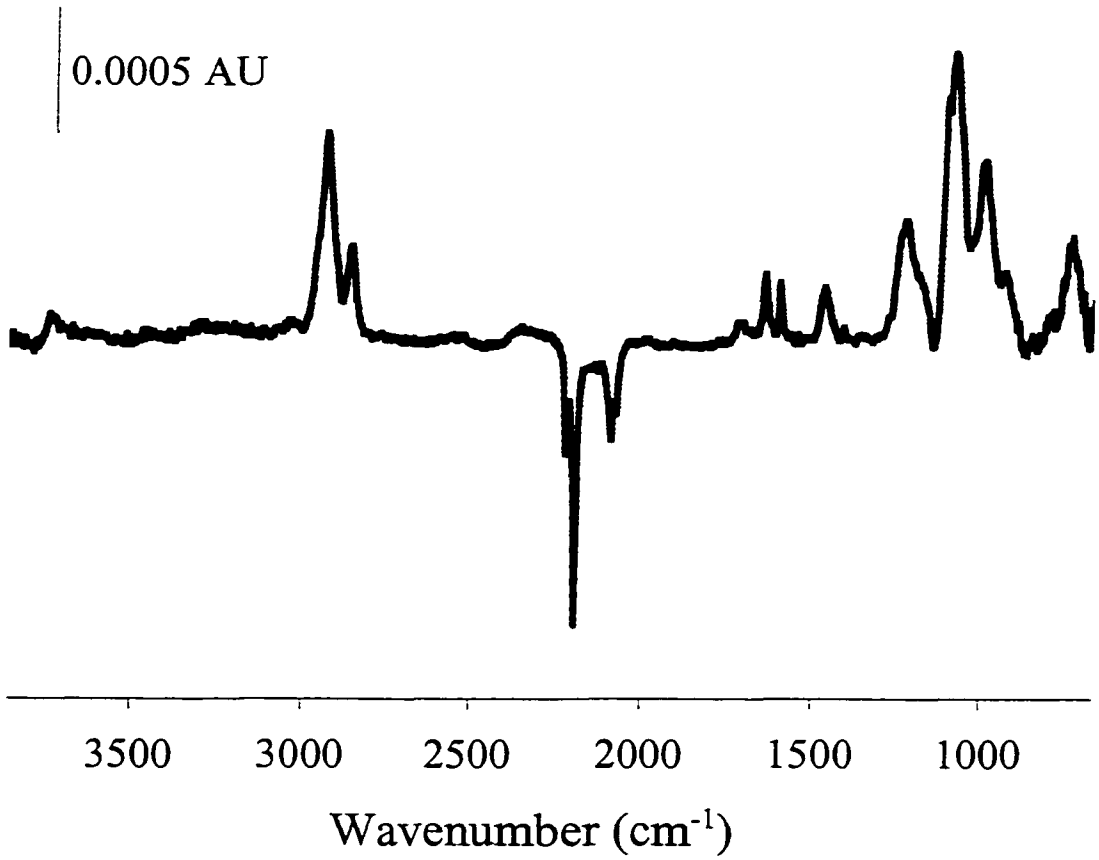

Figure 8

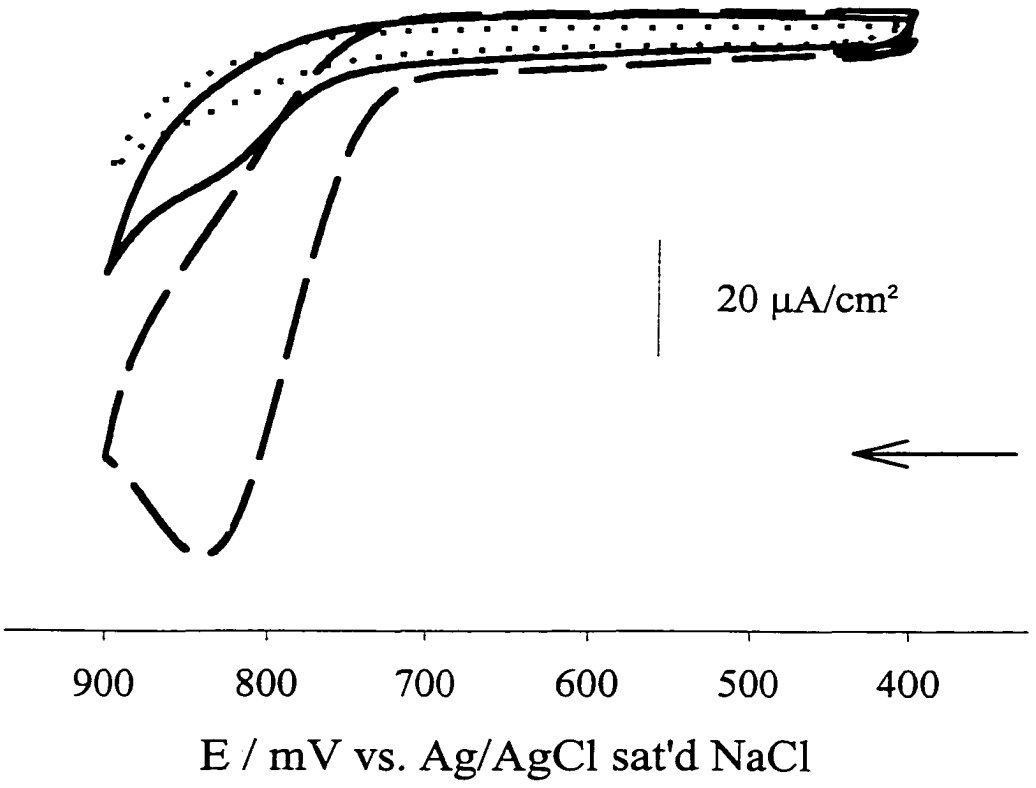

Figure 9

CHAPTER 3. EFFECTS OF SURFACE MORPHOLOGY ON THE FORMATION KINETICS OF ALKANETHIOL MONOLAYER MONITORED BY ELECTROCHEMICAL REDUCTIVE DESORPTION

A paper to be submitted to Langmuir

G. Brent Dawson, Chuanjian Zhong, and Marc D. Porter

Abstract

This paper describes the use of electrochemical reductive desorption (ERD) to monitor the kinetics of butanethiol and octanethiol adsorption at annealed and unannealed polycrystalline gold electrode surfaces. Specifically, the integrated charge under the desorption wave for monolayers formed for various immersion times is used to calculate the rate of increase of the surface concentration. The adsorption process is shown to be slow at micromolar thiol precursor concentrations in ethanol solutions. Differences in the rates of adsorption of different chainlength thiols as well as differences in the rates of adsorption at annealed and unannealed surfaces were examined. Butanethiol was shown to have only a slightly higher initial rate of adsorption than octanethiol, while thiols adsorbing at unannealed surfaces are shown to have faster rates than those adsorbing at annealed surfaces. When the rates of adsorption of thiols at the terrace and step sites on unannealed surfaces were compared, thiol adsorption was shown to be slower at terrace sites. The data were fit to Langmuir adsorption isotherms and a ΔG_{ads} = -9.8 kcal/mol was calculated for the octanethiol system.

Introduction

Spontaneously adsorbed thiolate monolayers at gold ($R(CH_2)_nS$-Au) have been extensively used to examine and control a wide variety of interfacial processes.[1-20] While the general structure of alkanethiolate monolayers has been examined in great detail, many fundamental questions remain concerning the formation process. Techniques such as ellipsometry,[3] infrared reflection adsorption spectroscopy,[21,22] and quartz crystal microgravimetry[23,24] have indicated the multi-step nature of the formation process, but detailing the underlying elements of the mechanism has been more problematic.[16,20,25-31]

In our [15,25] [13,14] [16,18-20] laboratory, the use of electrochemical reductive desorption

$$R(CH_2)_nS\text{-}Au + e^- = R(CH_2)_nS^- + Au \qquad (1)$$

has proven to be an effective tool in the determination of the relative binding strengths and surface concentrations of these monolayers. An intriguing aspect of this previous work is that differences in surface roughness, which can be correlated with differences in the number of step sites on the Au (111) substrate are manifested in the desorption curves for alkanethiolate monolayers. In general two desorption waves are observed: one diagnostic of the presence of the terrace sites on atomically smooth Au (111), and the other indicative of step sites surrounding each terrace. Based on our previous work on single crystal electrodes,[19] we have attributed the less negative wave to desorption from Au (111) terrace sites, and the more negative wave to desorption from the step sites (i. e., a convolution of the many types of coordination sites possible on a stepped Au (111) surface).

Cyclic voltammetry can be utilized to determine surface concentrations (Γ) at and below the monolayer level. Brown and Anson showed that both cyclic voltammetry and differential pulse voltammetry of adsorbed electroactive species can measure surface

coverages as low at 1.2 X 10^{-11} moles/cm^2. In our group, we have utilized linear sweep voltammetry to determine the surface concentration of alkanethiols adsorbed at annealed and unannealed Au surfaces. In this technique, the charge (Q) under the desorption wave for the thiol is integrated and related to Γ through equation 2

$$\Gamma = Q /(nFA) \qquad (2)$$

where n is the electron stochiometry of the reaction, F is taken as 96,486 C / mole e^-, and A is the area of the electrode. The fractional coverage monolayer coverage is then calculated from equation 3

$$\theta = \Gamma / \Gamma_{th} r_f \qquad (3)$$

where Γ_{th} is the theoretical surface concentration for a monolayer of adsorbate and r_f is the roughness factor. The roughness factor is the ratio of the true surface area of the electrode to its geometric area and accounts for the surface imperfections. We have previously determined the roughness factors for annealed and unannealed surfaces by surface voltammetry of adsorbed iodine and scanning tunneling microscopy (STM) to have values of 1.1 ± 0.1 for annealed gold and 1.3 ± 0.3 for the unannealed surfaces.[16,25]

Our electrochemically determined results agree well with helium diffraction data and show that alkanethiols effectively reach limiting coverages (7.5×10^{-10} mol cm^{-2}) within ~5 minutes when using an ethanol solution with a thiol concentration of ~1 mM. In our measurements, the background current flowing due to the change in double layer capacitance caused by the voltage sweep and the monolayer desorption is accounted for by extrapolating a baseline from the current on the curve just prior to desorption to the background current achieved subsequent to desorption. Also, this desorption technique probes specifically the interaction between the gold substrate and the sulfur head group, and the desorption potential

is a measure of the kinetic and thermodynamic driving forces needed to effect electron transfer from the Au to the S with subsequent desorption of the alkanethiolate.

Figure 1a shows a typical electrochemical reductive desorption curve for an octanethiolate monolayer formed at an annealed gold surface. Work in our group and others have shown that such gold surfaces consist of a strong (111) crystallinity with terrace sizes of 100-200 nm.[15,32] The desorption curve shows one wave with a peak position of -0.95 V and a full width at half maximum (FWHM) < 90 mV, indicating attractive interactions between neighboring adsorbates.[33,34] The small oxidative deposition wave located at –0.80 V with a large FWHM is typical of short chainlength thiols (shorter than 10 methylene units). Only a small fraction of the as-formed film is re-deposited due to the relatively high solubility of the desorbed thiolate in the alkaline electrolyte and the modest scan rates (~ 50 mV/s) used in the experiments. Furthermore, the low background current located before the desorption peak is diagnostic of the low capacitance (1 μ F/cm^2) of such monolayer-covered electrodes.

Figure 1b represents the voltammetric wave for the same monolayer from an unannealed surface. Such surfaces have been shown to consist of several different crystallinities ((111), (110), (100)), with the (111) being the predominant crystal face.[32] Several differences are apparent in the curves. First, two waves for the monolayer desorption are seen with one occurring at –0.95 V and a broader wave centered at –1.12 V. Previous work in our group[20,25] has shown this wave, with the less negative desorption potential, to be due to desorption from (111) terrace sites with the wave at the more negative desorption potential to be due to the step sites. The more negative desorption potential for thiolates adsorbed at step sites represents the stronger interactions between the sulfur atoms and the gold surface.

Kinetic information can be obtained with electrochemical reductive desorption (ERD) by monitoring the increase in desorption charge with the increase in monolayer formation time. While alkanethiols form full monolayers relatively quickly at millimolar concentrations, the rate of adsorption shows a decrease as the thiol concentration in the precursor solution is decreased. Measurements in our laboratory have shown that at a thiol concentration of 2 μM (in ethanol) immersion times must be > 60 min before a limiting surface concentration is reached.

Initial studies reported by Bain et al., which utilized ellipsometry, found a two-step mechanism for monolayer formation. Specifically during the first step, octadecanethiol monolayers reached 80-90 % of their limiting thicknesses rapidly, while equilibrium was not reached until 1000 min for a 1 μM solution. At lower concentrations (1 μM), two distinct rates were also noticed, and after 10^4 minutes of adsorption the measured thicknesses and hexadecane contact angles were slightly lower than those measured for monolayers formed in 1 mM solutions. These data show that the ordering process in the systems is slow at concentrations typically used to form monolayers.

Hähner et al. used NEXAFS to show the sluggish nature of chain organization in docosanethiol monolayers and also observed a process with a fast initial step followed by a slow step.[35] Karpovich and Blanchard used quartz crystal microgravimetry to examine adsorption processes of thiols from nonpolar solvents and recorded a fast one-step process of adsorption.[24] They also discussed the validity of the assumptions of the Langmuir isotherm in the adsorption of thiols at polycrystalline Au surfaces and concluded that the variation in the ΔH_{ads} values at the different adsorption sites on the surface was small enough that the sites could be considered equivalent, and the Langmuir model remained valid. Shimazu et al.

utilized QCM techniques to show that the formation of a ferrocenylundecanethiol consisted of a fast adsorption step followed by a slower one.[36] A later QCM study by Pan, Durning, and Turro, using monolayers formed in ethanol at high concentrations (5 mM), found adsorption to consist of two slow steps with the 80% of the total frequency change requiring ~400 min[23]. Truong and Rowntree reported that equilibrium absorbance values obtained by IRRAS were not reached for butanethiolate monolayers formed in a 5 μM solution in methanol until 15 h of adsorption.[22] Ellis and coworkers reported the relatively fast increase in surface coverage as followed by IRRAS when the monolayer was allowed to organize under ultrahigh vacuum conditions before measurements were taken.[21] Finally, Peterlinz and Georgiadis proposed a three-step adsorption mechanism based on their surface plasmon resonance spectroscopy studies where the first step is the most rapid and the third step is the slowest. The intermediate step was found to zero order overall, and it was postulated that thiols were moving from a physisorbed state of a domain boundary of adsorbed thiolate.[21]

An electrochemical kinetic study was performed by Forouzan, Bard, and Mirkin and used scanning electrochemical microscopy, cyclic voltammetry, and chronoamperometry to follow the decrease in the rate of electron transfer through the monolayer upon exposing the Au surface to thiol.[21] Their results showed that greater than 90% of the surface was covered after remaining in the 5 mM formation solution for 5 minutes and that surface defects had radii < 0.5 μm. Furthermore they found that electron transfer had been completely blocked after 50 min of monolayer formation.

Of the aforementioned techniques, only the QCM studies monitor uniquely the increase in surface coverage uncomplicated by chain reorganization. Furthermore, while most of these studies used polycrystalline gold substrates, none were able to separately

interrogate the adsorption processes occurring at the different crystal faces. The thiolates at different adsorption sites will likely have different kinetic and thermodynamic driving forces for adsorption of thiolates. The following reductive desorption data will show how these sites can be interrogated separately.

This paper presents electrochemical data that represent the rate of monolayer formation through electrochemical reductive desorption and the effect of surface crystallinity and roughness on the kinetics of the Au-S bond formation process for both shorter and longer chain length thiols. Specifically the rates of monolayer formation at a predominantly Au (111) surface will be compared to those at surfaces with step sites of higher coordination (e. g. (110) and (100)) by evaluating the growth of the integrated charge for the desorption waves of monolayers formed under increasing immersion times.

Experimental

The gold films (300 nm thickness) were evaporated on thoroughly cleaned glass slides or freshly cleaved mica in a cryopumped E306A Edwards Coating System. The glass slides were first primed with a 15 nm chromium adhesion layer. Subsequent to evaporation, the films on the mica sheets were annealed at atmospheric pressure in a muffle furnace at 300 °C for 5 hours; this process yielded a surface composed of large (100 to 200 nm^2), atomically smooth Au (111) crystallites.[25] The roughness factor of these substrates, given as the ratio of adsorbed iodine to the exposed geometric surface area of the electrode, is 1.1 ± 0.1. The roughness factor for the Au/glass substrate was found to be 1.3 ± 0.3 nm.[25] Monolayers were prepared by immersing gold substrates in ethanolic solutions of 2 μM, 20 μM and 1 mM alkanethiol (Aldrich) concentrations under ambient conditions for times varying from 0.083

min to 540 min. No steps were taken to pre-clean these surfaces for two reasons—to mimic commonly used procedures and to maintain the surface roughness of the "as-prepared" films. The monolayer-coated samples were rinsed with ethanol and dried under a stream of high purity argon just prior to electrochemical experiments.

Electrochemical experiments were performed with either a CV-27 potentiostat (Bioanalytical Systems) or a model 263 potentiostat/galvanostat (Princeton Applied Research). A conventional three-electrode cell was used with the geometrically exposed area of the working electrode defined by an elastomer o-ring (geometric area of 0.65 cm^2). A platinum coil and $Ag|AgCl|KCl_{sat}$ electrode were used as the auxiliary and reference electrodes respectively. All potentials are reported with respect to the $Ag|AgCl|KCl_{sat}$ electrode. The electrolyte used in all experiments was 0.5 M KOH and was deoxygenated with argon before the electrochemical measurements. Measurements were performed within 15 minutes of removing the Au electrode from the thiol formation solution. All glassware was thoroughly cleaned with piranha solution (1 part 30 % H_2O_2: 3 parts 98 % H_2SO_4) prior to use and rinsed with distilled-deionized water. **Caution piranha solution is explosive when in contact with organic compounds and should not be stored.**

Results and Discussion

Kinetics of Adsorption

The change in the surface concentration of the adlayer was monitored as a function of immersion time using ethanolic thiol solutions at low concentrations (i.e., 2 and 20 μM) by ERD. At these concentrations, the growth of the adlayer does not reach detectable limiting surface concentrations until formation times reach 20 minutes. At higher concentrations (i.e.,

1 mM), the limit is reached in ~ 1 min. We note that physisorbed and possibly weakly chemisorbed species are clearly present prior to immersion in the thiol-containing solution, and that the temporal evolution of the adlayer formation is affected by the competitive displacement of these contaminants. Nevertheless, the change in integrated desorption charge is indicative of the change in the amount of thiolate chemisorbed to the gold surface.

Figure 2 shows the evolution of the desorption curves for octanethiolate monolayers formed from a 20 μM ethanolic solution at annealed substrates. Each scan shows one prominent desorption wave that is attributed to desorption from the Au (111) terraces of the annealed gold substrate. As the immersion time of the gold substrates increases (moving from bottom to top in the figure) the integrated area under the desorption wave increases from 34.0 $\mu C/cm^2$ to 88.8 $\mu C/cm^2$. These values of charge translate to 2.9 X 10^{-10} and 7.7 X 10^{-10} mol/cm^{-2}, respectively. We believe this increase in charge to be mostly faradaic in nature and due to the increase in surface thiolate concentration. Also the peak potential (E_p) for the desorption wave shifts from –955 mV for the 5 min immersion time to –990 mV for the 60 min immersion time. This potential shift, which is indicative of increased monolayer stability, can be attributed to an increase in the cohesive interactions between neighboring adsorbates with increased immersion times.

A notable difference is seen in the immersion time needed for the limiting surface concentration for monolayers formed in 2 μM and those formed 20 μM thiol solutions. Figure 3 compares the increase in desorption charge resulting from these two cases. Each data point represents the average of eight measurements with the uncertainty being about the size of the data point (±5 %). This figure shows that the maximum desorption charge is reached within 10 min for the monolayers formed in the 20 μM solution whereas the

maximum desorption charged is not reached for monolayers formed in 2 μM solutions until 60 min. Unlike studies involving monolayers formed from hexane,[24] we find that 2 μM is sufficient enough thiol concentration in ethanol to form a monolayer with a surface coverage that is 90% of that of a monolayer formed from a 1mM thiol precursor solution.

Figure 4 shows a similar increase in coverage for the butanethiolate and octanethiolate monolayers at unannealed surfaces. While there is a small difference in the equilibrium surface coverage of the two systems, this difference is within the margin of error of the measurement. Based on parameters developed from the fit to the Langmuir adsorption isotherm, the initial increase of coverage versus time of the octanethiolate monolayer is only ~1.4 times slower than that of the butanethiolate monolayer. We attribute the small difference in adsorption rates to a variety of factors, including the higher diffusion coefficient of butanethiol and the number of sites covered by a disorganized layer of each thiol on the surface; both factors would have an effect on the overall adsorption rates.

Surface Roughness Effects

Other interesting characteristics of these systems are evident when the adsorption at the two different substrates is compared. Figure 5 shows the plot of surface coverage versus immersion time for octanethiolate monolayers formed at annealed (•) and unannealed (♦) substrates. These data show that the monolayers formed at unannealed substrates reach their limiting surface coverage more rapidly than monolayers formed at annealed substrates. Specifically the monolayers at the unannealed surface have reached their limiting coverages after 30 min whereas the monolayers at the annealed surface require an immersion time > 60 min. Our previous work has shown that an additional wave for thiolate desorption is seen at more negative potentials indicating that the substrate and adsorbate interaction is stronger at

step sites. This stronger interaction agrees well with theories, which invoke the presence of dangling bonds at stepped surfaces[37] due to the absence of nearest neighbors. Furthermore the apparent difference in rates is likely due to the difference in chemisorption activation energy for the different sites.

Figure 6 shows the evolution of the reductive desorption voltammograms as a function of immersion time for an unannealed surface. The first measurable desorption wave appears after the substrate was immersed for 5 min in a 2 μM solution of octanethiol in ethanol. This wave is ~ 200 mV more negative than the one that has been attributed to desorption from terrace sites on an annealed surface. After an immersion time of 30 min, two waves are apparent, the least negative of which we attribute to desorption from terrace sites and the more negative of which we attribute to desorption from step sites.

One attribute of assessing adsorption kinetics with reductive desorption is the ability to separate rates for processes occurring at different adsorption sites. By integrating the areas under the separate desorption waves for unannealed systems, one can interrogate the monolayer formation process for the terraces sites and the step sites separately. Additionally, the integrated charge for the first peak rises from a value of 10.0 $\mu C/cm^2$ after 20 min of immersion to a value of 45.6 $\mu C/cm^2$ after 540 min of immersion. However, the charge under the second wave has reached a value of 32.1 $\mu C/cm^2$ after 20 min of immersion and reaches a value of 45.0 $\mu C/cm^2$ only after 60 min of immersion. The change in the integrated area with time for the less negative desorption peak (desorption from (111) terraces) indicates the rate of monolayer formation at these sites. Figure 7 shows the difference in the rates of adsorption at the two different sites for octanethiolate monolayers formed in a 2 μM

thiol solution. The rate of adsorption at the step sites (◆) is faster than the adsorption at the terrace sites (●). For example, the surface concentration at the step sites reaches its limiting value in 30 min whereas the limiting surface concentration at the terrace sites is not reached until 60 min. When these plots are fit to Langmuir isotherms, the initial rate of adsorption at the step sites is ~7 times faster than that at terrace sites. These findings indicate that there are at least two different rates of adsorption for the thiolate monolayer on polycrystalline surfaces, and that the overall rate is a combination of rates from each site.

Several characteristics are noticeable in these two figures. First, the desorption wave from step sites appears and reaches a limiting value before the one for desorption from terrace sites. Second, the peak for desorption from terraces shifts to more negative potentials with increased immersion time. We attribute this shift to an increase in cohesive interactions between neighboring adsorbates. Third, even after full coverage is reached, the fractional coverages at the two different adsorption sites continue to change. Specifically, the increase of surface coverage at the terrace sites is partially due to a loss of surface coverage at the step sites. Atoms at step sites have been shown to undergo diffusion and combination with terraces. This dynamic nature of the surface has been observed with STM[38,39] by a variety of groups and is attributed to the substrate-induced annealing of the surface.

The ability to separate the events at each adsorption site allows one to identify the molecular basis for the kinetics. Specifically, the difference in the rates of film formation seen at the different adsorption sites is much larger than the difference in the rates of film formation seen for the different length chains. Apparently, the difference in the rates of diffusion has a smaller effect on the rate of film formation than does the nature of the adsorption site. The different adsorption sites likely have significantly different activation

energies for adsorption that give rise to a large difference in the rates of adsorption. Furthermore, the larger stability at the step sites translates to a larger activation energy for desorption of the adsorbate, which on the one hand, argues that these unannealed surfaces would be more ideal for sensor applications involving monolayer films.

Free Energy of Adsorption

The distributions of adsorption sites for the annealed and unannealed surfaces are quite different. The annealed surface has been shown to be primarily composed of (111) terrace sites, with the unannealed surface having 50% of its surface covered by (111) terrace sites. The large surface concentration of step sites, which thermodynamically offers greater stability to the adsorbate, would increase the rate of adsorption only if Au-S bond formation were the rate determining step, yet would not influence the rate if the process were controlled by the rate of diffusion of the thiol to the surface. Therefore the difference in rates of adsorption for the different sites, with adsorption occurring first at the thermodynamically more favorable site suggests that Au-S bond formation is the rate-determining step (at least in the early stages of formation).

With increased immersion time, the concentration on the electrode surface increases. This increased surface concentration is reflected in the integrated charge under the desorption wave. The long times for complete monolayer formation at both concentrations is due to the fact that the concentration of the precursor at the surface affects the rate of Au-S bond formation. By fitting the increase in surface coverage over time to a Langmuir isotherm, one can determine the ΔG_{ads}. This process is explained in the following paragraphs.

The apparent fraction of step sites on these polycrystalline surfaces (~0.5) and the theoretical difference in binding strengths at the different sites questions the rigid

applicability of the Langmuir isotherm to this system. Also the high surface concentrations present at extended immersion times would give rise to adsorbates increasing the rate of adsorption of nearest neighbors due to attractive interactions. In fact, other isotherms such as the Frumkin and Temkin types could possibly give a better fit to the data, yet we have chosen to use the Langmuir isotherm as a simplistic first approximation of the mechanism. Future work will focus on the application of a more advanced treatment utilizing a mixed Temkin and Frumkin isotherm.

From the Langmuir isotherm, the increase in surface coverage with time is given by

$$\frac{d\theta}{dt} = k_a(1-\theta)C - k_d\theta \qquad (4)$$

where k_a and k_d are the rate constants for adsorption and desorption, respectively, C is the concentration of the thiol in the bulk solution, and 1-θ then equals the fractional coverage of adlayer. Integration of (4) yields

$$\theta(t) = \frac{C}{C+(k_d/k_a)}[1-\exp(-(k_aC+k_d)t)] \qquad (5)$$

When is set C / C + (k_a/k_d) equal to a and $k_aC + k_d$ to b then equation (5) is simplified to the standard form of a two parameter exponential rise to a maximum.

$$\theta(t) = a[1-\exp(-bt)] \qquad (6)$$

The equilibrium constant (K_{eq}) can be calculated from

$$K_{eq} = k_a / k_d \qquad (7)$$

and the free energy of adsorption (ΔG_{ads}) from

$$\Delta G_{ads} = -RT \ln K_{eq} \qquad (8)$$

When surface coverage vs. immersion time is plotted for the octanethiol monolayers formed from a 2 μM system at unannealed gold, a ΔG_{ads} of –9.8 kcal/mol is calculated. Karpovich and Blanchard calculated a value of –4.4 kcal/mol for the adsorption from hexane.[24] We feel that this small difference in the values is readily explained by the difference in the entropic contributions to the adsorption process from the two solvents. The similarity of these results using different analytical techniques and solvents indicates that the same process, Au-S bond formation, is being monitored.

Conclusions

Electrochemical reductive desorption has been shown to be a viable method to monitor the kinetics of alkanethiol adsorption at polycrystalline Au surfaces. Integration of the desorption charge can be related to the amount of adsorbate chemisorbed to the Au surface while not being affected by the reorganization of the alkyl chains. It was shown that short chain alkyl thiols adsorb only slightly faster than longer chain ones and that the rates of adsorption at the different sites could be separately monitored due to the 200 mV separation of the desorption waves. Specifically, thiols were found to have lower rates of adsorption at the (111) terrace sites than at the step sites, while little difference in adsorption rates were recorded for different chainlength thiols. We conclude that Au-S bond formation is the rate-determining step in the monolayer formation process. Ongoing work is examining the role of temperature and end group identity in the rates of film formation.

Acknowledgements

The authors gratefully acknowledge James Anderegg of the Ames Laboratory for supplementary x-ray photoelectron spectroscopic data and helpful discussion. This work was supported by the Office of Basic Energy Research, Chemical Sciences Division of the US Department of Energy. Ames Laboratory is operated for the US Department of Energy by Iowa State University under Contract No. W-7405-eng-82.

References

(1) Zhong, C.-J.; Porter, M. D. *Anal. Chem.* **1995,** *67,* 709A-15A.

(2) Porter, M. D.; Bright, T. B.; Allara, D. L.; Chidsey, C. E. D. *J. Am. Chem. Soc.* **1987,** *109,* 3559-68.

(3) Bain, C. D.; Troughton, E. B.; Tao, Y.-T.; Evall, J.; Whitesides, G. M.; Nuzzo, R. G. *J. Am. Chem. Soc.* **1989,** *111,* 321-335.

(4) Bain, C. D.; Evall, J.; Whitesides, G. M. *J. Am. Chem. Soc.* **1989,** *111,* 7155-7164.

(5) Bain, C. D.; Whitesides, G. M. *J. Am. Chem. Soc.* **1989,** *111,* 7164-7175.

(6) Dubois, L. H.; Zegarski, B. R.; Nuzzo, R. G. *J. Am. Chem. Soc.* **1990,** *112,* 570-579.

(7) Dubois, L. H.; Nuzzo, R. G. *Ann. Rev. Phys. Chem.* **1992,** *43,* 437-63.

(8) Laibinis, P. E.; Whitesides, G. M.; Allara, D. L.; Tao, Y.-T.; Parikh, A. N.; Nuzzo, R. G. *J. Am. Chem. Soc.* **1991,** *113,* 7152-7167.

(9) Nuzzo, R. G.; Zegarski, B. R.; Dubois, L. H. *J. Am. Chem. Soc.* **1987,** *109,* 733-740.

(10) Nuzzo, R. G.; Dubois, L. H.; Allara, D. L. *J. Am. Chem. Soc.* **1990,** *112,* 558-569.

(11) Nuzzo, R. G.; Korenic, E. M.; Dubois, L. H. *J. Chem. Phys.* **1990,** *93,* 767-773.

(12) Strong, L.; Whitesides, G. M. *Langmuir.* **1988,** *4,* 546-558.

(13) Weisshaar, D. E.; Lamp, B. D.; Porter, M. D. *J. Am. Chem. Soc.* **1992,** *114,* 5860-2.

(14) Weisshaar, D. E.; Walczak, M. M.; Porter, M. D. *Langmuir.* **1993,** *9,* 323-9.

(15) Widrig, C. A.; Chung, C.; Porter, M. D. *J. Electroanal. Chem. Interfacial Electrochem.* **1991,** *310,* 335-59.

(16) Wong, S.-S.; Porter, M. D. *J. Electroanal. Chem.* **2000,** *485,* 135-143.

(17) Zak, J.; Yuan, H.; Ho, M.; Woo, L. K.; Porter, M. D. *Langmuir.* **1993,** *9,* 2772-4.

(18) Zhong, C.-J.; Porter, M. D. *J. Electroanal. Chem.* **1997,** *425,* 147-153.

(19) Zhong, C.-J.; Zak, J.; Porter, M. D. *J. Electroanal. Chem.* **1997,** *421,* 9-13.

(20) Zhong, C.-J.; Woods, N. T.; Dawson, G. B.; Porter, M. D. *Electrochem. Commun.* **1999,** *1,* 17-21.

(21) Bensebaa, F.; Voicu, R.; Huron, L.; Ellis, T. H. *Langmuir.* **1997,** *13,* 5335-5340.

(22) Truong, K. D.; Rowntree, P. A. *Prog. Surf. Sci.* **1995,** *50,* 207-216.

(23) Pan, W.; Durning, C. J.; Turro, N. J. *Langmuir.* **1996,** *12,* 4469-4473.

(24) Karpovich, D. S.; Blanchard, G. J. *Langmuir.* **1994,** *10,* 3315-3322.

(25) Walczak, M. M.; Alves, C. A.; Lamp, B. D.; Porter, M. D. *J. Electroanal. Chem.* **1995,** *396,* 103-14.

(26) Hatchett, D. W.; Stevenson, K. J.; Lacy, W. B.; Harris, J. M.; White, H. S. *J. Am. Chem. Soc.* **1997,** *119,* 6596-6606.

(27) Hatchett, D. W.; Uibel, R. H.; Stevenson, K. J.; Harris, J. M.; White, H. S. *J. Am. Chem. Soc.* **1998,** *120,* 1062-1069.

(28) Yang, D.-F.; Wilde, C. P.; Morin, M. *Langmuir.* **1997,** *13,* 243-249.

(29) Yang, D.-F.; Al-Maznai, H.; Morin, M. *Journal of Physical Chemistry B.* **1997,** *101,* 1158-1166.

(30) Poirier, G. E.; Tarlov, M. J.; Rushmeier, H. E. *Langmuir.* **1994,** *10,* 3383-3386.

(31) Bryant, M. A.; Pemberton, J. E. *J. Am. Chem. Soc.* **1991,** *113,* 8284-8293.

(32) Hallmark, V. M.; Chiang, S.; Rabolt, J. F.; Swalen, J. D.; Wilson, R. J. *Physical Review Letters.* **1987,** *59,* 2879-2882.

(33) Brown, A. P.; Anson, F. C. *Anal. Chem.* **1977,** *49,* 1589-1595.

(34) Laviron, E. *J. Electroanal. Chem. Interfacial Electrochem.* **1974,** *52,* 395-402.

(35) Hahner, G.; Woll, C.; Buck, M.; Grunze, M. *Langmuir.* **1993,** *9,* 1955-1958.

(36) Shimazu, K.; Yagi, I.; Sato, Y.; Uosaki, K. *Langmuir.* **1992,** *8,* 1385-1387.

(37) Prutton, M. *Surface physics;* 2 ed. ; Oxford University Press: New York, 1982.

(38) McCarley, R. L.; Dunaway, D. J.; Willicut, R. J. *Langmuir.* **1993,** *9,* 2775-2777.

(39) Stranick, S. J.; Parikh, A. N.; Allara, D. L.; Weiss, P. S. *J. Phys. Chem.* **1994,** *98,* 11136-11142.

Figure Captions

Figure 1. Current-potential curves for the reductive desorption of monolayers formed from octanethiol at (A) annealed Au/mica and (B) unannealed Au/Cr/glass. Electrolyte: 0.5 M KOH. Scanrate: 50 mV s^{-1}.

Figure 2. Series of current-potential curves for the reductive desorption of monolayer formed with various immersion times at annealed gold. Precursor solution: 2 μM octanethiol in ethanol. The arrow indicates the initial scan direction. Electrolyte: 0.5 M KOH. Scanrate: 50 mV s^{-1}.

Figure 3. Graph of integrated charge density versus electrode immersion time for the reductive desorption current-potential curves for octanethiol monolayers formed at unannealed gold. The concentration of the thiol precursor was either 2 μM (•) or 20 μM (♦). Electrolyte: 0.5 M KOH. Scanrate: 50 mV s^{-1}.

Figure 4. Graph of fractional coverage versus electrode immersion time for monolayers formed at unannealed gold electrodes from 2 μM (•) or 20 μM (♦) octanethiol solutions.

Figure 5. Graph of fractional coverage versus electrode immersion for octanethiol monolayers formed from 2 μM octanethiol solutions at annealed (•) and unannealed (♦) electrode surfaces respectively.

Figure 6. Series of current-potential curves for the reductive desorption of monolayer formed with various immersion times at unannealed gold. Precursor solution: 2 μM octanethiol in ethanol. The arrow indicates the initial scan direction. Electrolyte: 0.5 M KOH. Scanrate: 50 mV s^{-1}.

Figure 7. Graph of partial fractional coverage versus electrode immersion time for monolayers formed at unannealed gold electrodes for terrace (•) and step sites (♦).

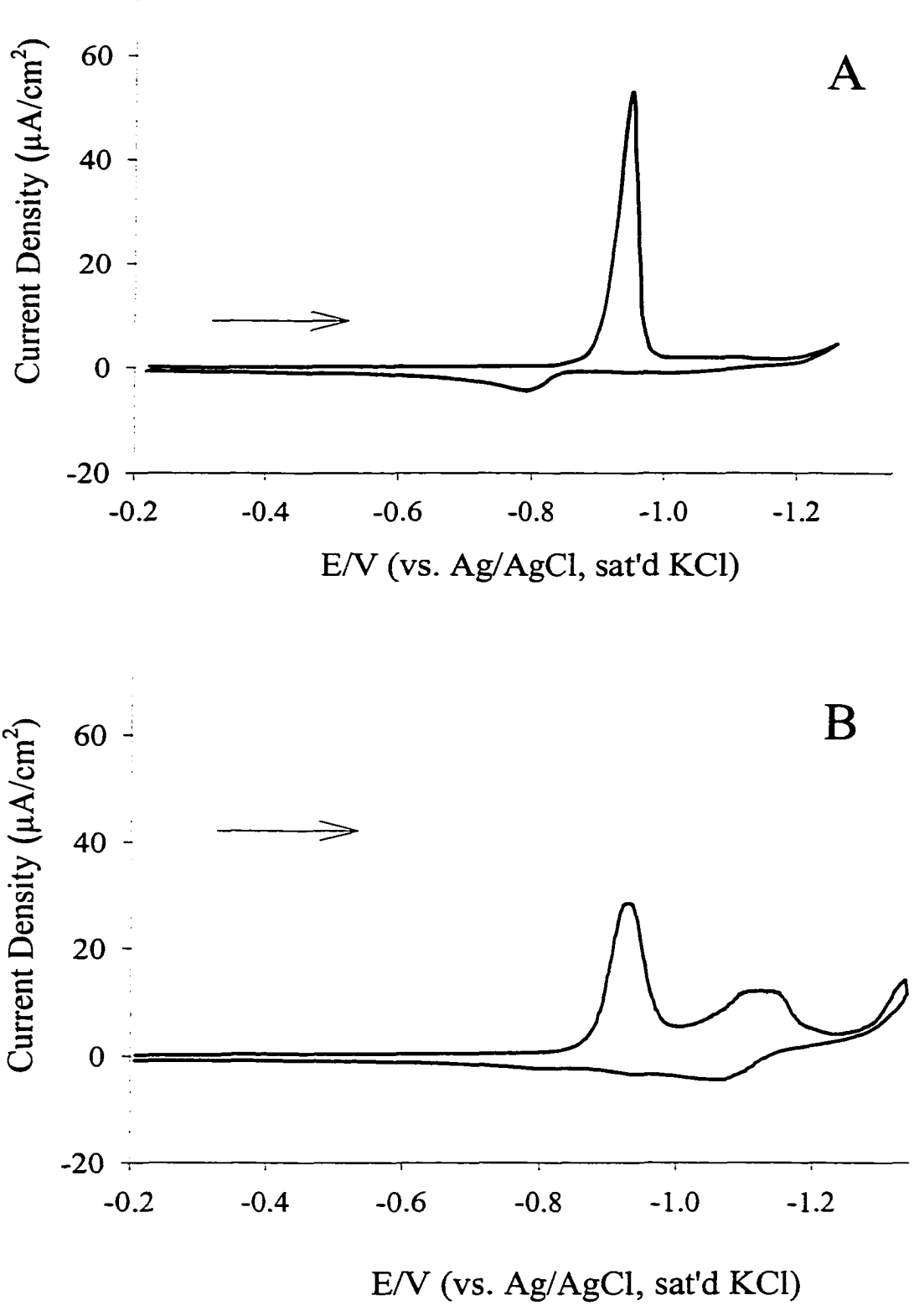
A
Current Density (μA/cm²)
60
40
20
0
-20
-0.2
-0.4
-0.6
-0.8
-1.0
-1.2
E/V (vs. Ag/AgCl, sat'd KCl)
B
Current Density (μA/cm²)
60
40
20
0
-20
-0.2
-0.4
-0.6
-0.8
-1.0
-1.2
E/V (vs. Ag/AgCl, sat'd KCl)

Figure 1

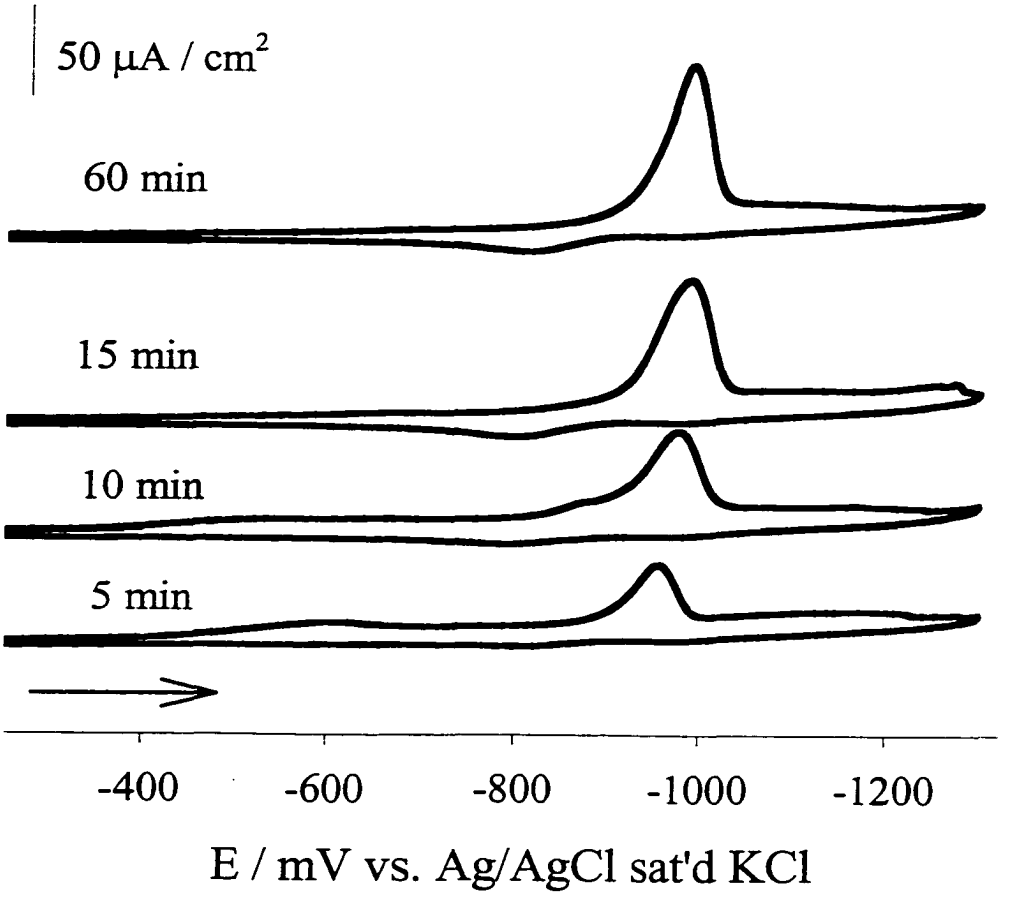
50 μA / cm2
60 min
15 min
10 min
5 min
-400
-600
-800
-1000
-1200
E / mV vs. Ag/AgCl sat'd KCl

Figure 2

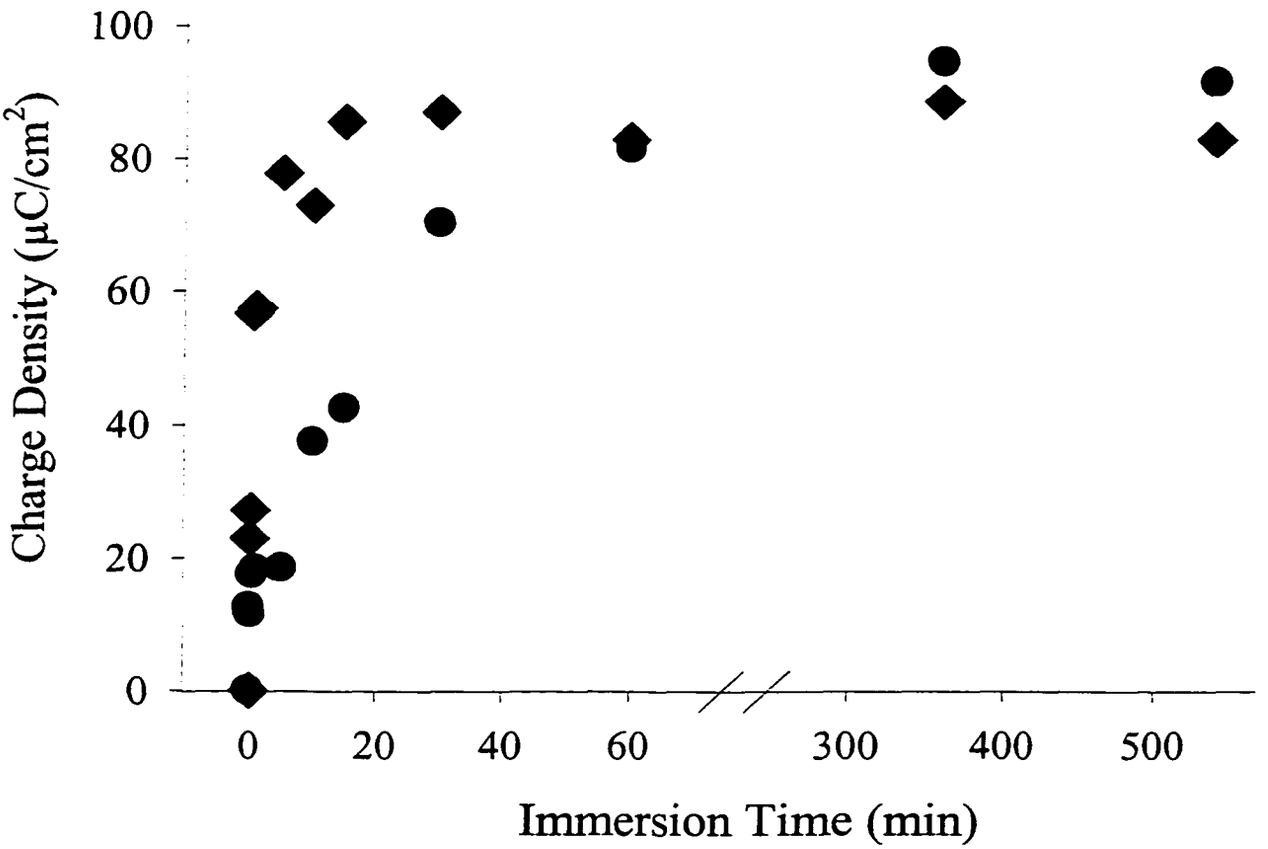
100
80
60
40
20
0
Charge Density (μC/cm²)
0
20
40
60
300
400
500
Immersion Time (min)

Figure 3

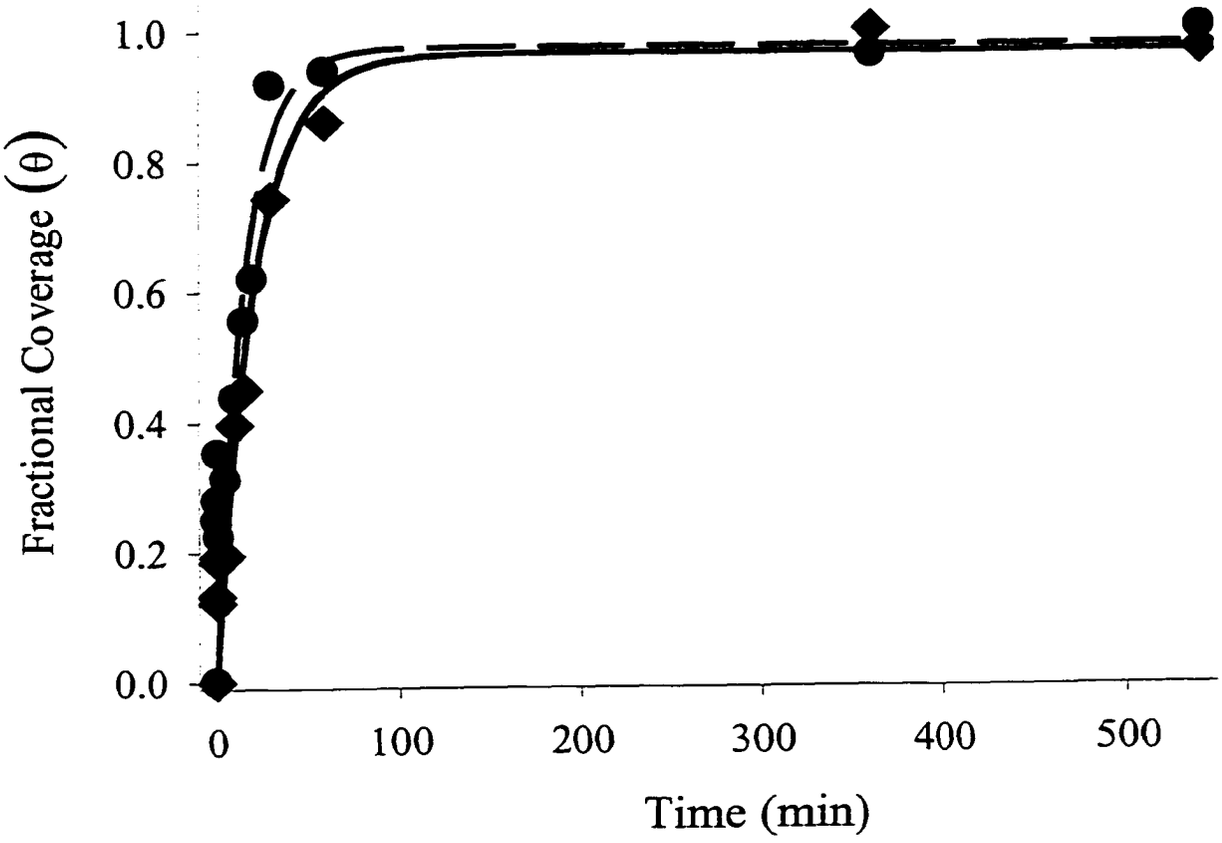
Fractional Coverage (θ)
1.0
0.8
0.6
0.4
0.2
0.0
0
100
200
300
400
500
Time (min)

Figure 4

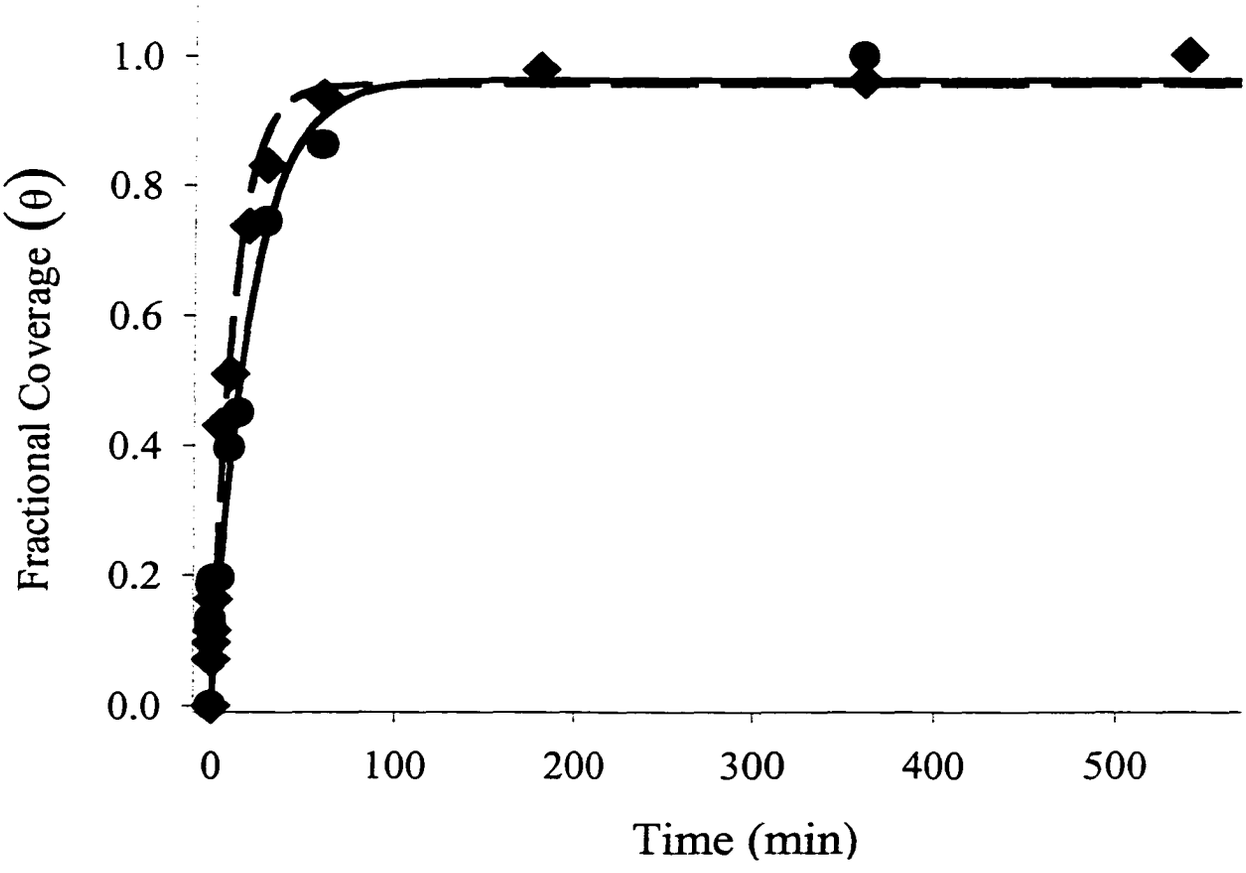
Fractional Coverage (θ)
1.0
0.8
0.6
0.4
0.2
0.0
0
100
200
300
400
500
Time (min)

Figure 5

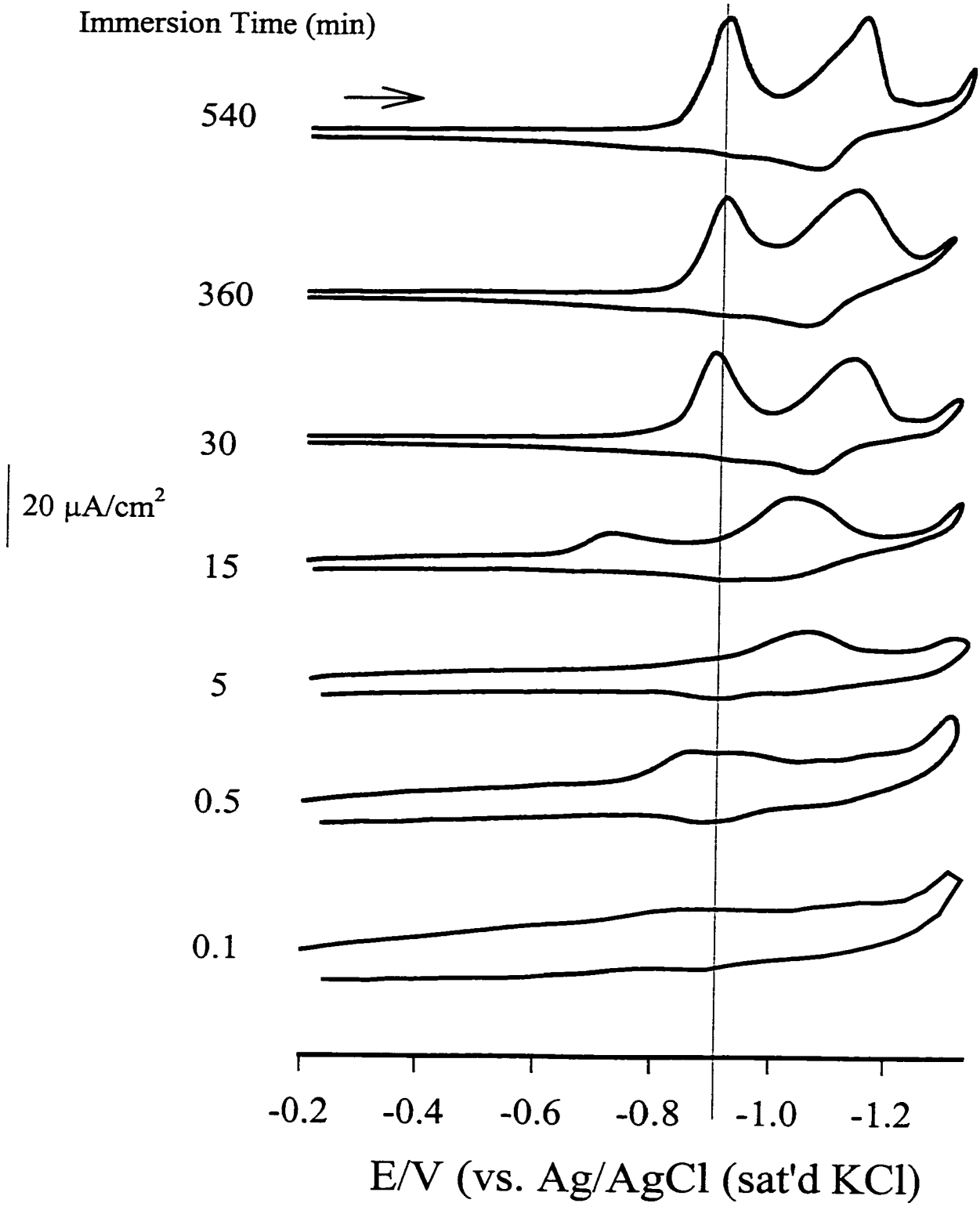
Immersion Time (min)
540
360
30
15
5
0.5
0.1
20 μA/cm²
-0.2
-0.4
-0.6
-0.8
-1.0
-1.2
E/V (vs. Ag/AgCl (sat'd KCl)

Figure 6

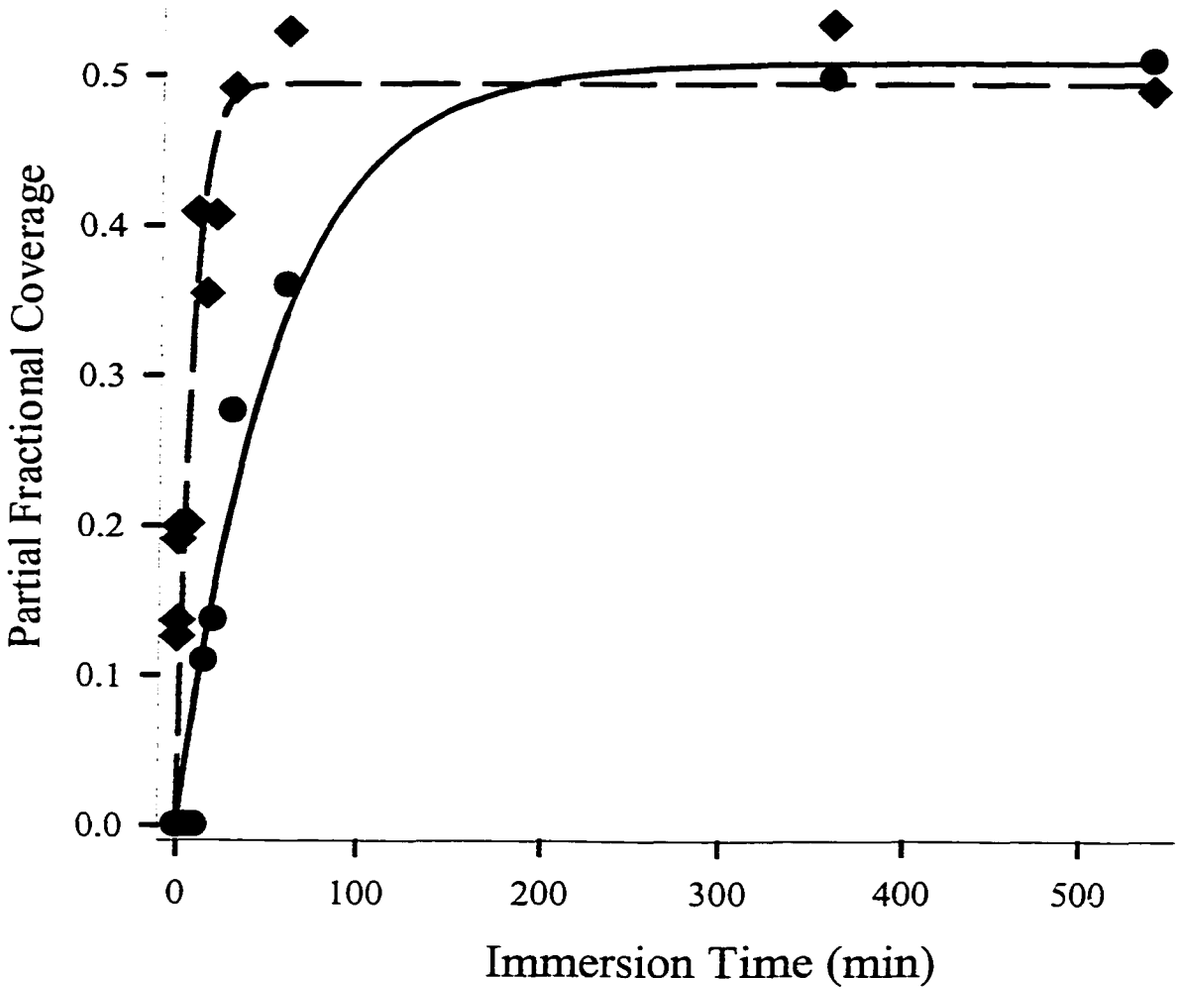
Partial Fractional Coverage
0.0
0.1
0.2
0.3
0.4
0.5
0
100
200
300
400
500
Immersion Time (min)

Figure 7

CHAPTER 4. RE-EXAMINTION OF THE ELECTROCHEMICAL REDUCTIVE DESORPTION PROCESS AT ANNEALED GOLD SUBSTRATES: EVIDENCE FROM BUTANETHIOLATE MONOLAYERS

A paper to be submitted to *Electrochemical Communications*

G. Brent Dawson and Marc D. Porter

Abstract

The proposed mechanism for reductive desorption is re-examined in light of new data from butanethiolate monolayers. These monolayer films are shown to give a variety of peak shapes under similar conditions. The voltammetric data show a broad single peak, a single peak with a shoulder, or a split peak. These differences in fine structure are attributed to heterogeneity in substrate terrace size that gives rise to heterogeneity of thiolate domain sizes and not to a mechanism involving micelle formation. The implications of this finding for comparisons of differently prepared surface are also discussed.

Introduction

Electrochemical desorption/deposition techniques have become invaluable as approaches for determining and controlling surface coverage,[1-3] spatial patterning,[4,5] and otherwise manipulating monolayers formed on gold from alkanethiols.[6] In an effort to more fully understand and better utilize the process, much work has been performed to carefully monitor the changes at the interface during reductive desorption. Having acquired these data, many groups have speculated on the mechanism of the reduction and removal of the thiolate

from the surface.[7-22] While most researchers agree that the reductive desorption process is accurately described by equation 1, two studies have questioned the value of the electron transfer stochiometry based on their investigations in nonaqueous environments.[15]

$$X(CH_2)_nS\text{-}Au + e^- \Leftrightarrow X(CH_2)_nS^- + Au \qquad (1)$$

The discrepancies between these studies and those of Porter and coworkers [2,7,11,13] can be attributed to the differences in conditions under which the monolayers were formed and desorbed, and one of the inherent complications in accurately accounting for the change in double layer charging currents.

Other work has found that the shape and position of the voltammetric curves for reductive desorption are highly sensitive to substrate crystallinity[8] as well as the length of the methylene chain (n),[2,9,21,22] and the identity of the endgroup (X).[4,23-26] Specifically, micro-heterogeneity in adsorption sites on unannealed gold gives rise to two desorption waves separated by a potential of ~200 mV.[8] The less negative wave, which coincides with that seen for desorption from an Au (111) single crystal,[10] is ascribed to desorption from Au (111) terraces. The more negative wave, in contrast, is attributed to desorption from sites with a higher degree of coordination than that of the three-fold hollow site. On annealed Au surfaces which are strongly (111) terraced, only one desorption wave was reported for thiols with $n<11$, while a splitting of the desorption wave was recorded for thiols with $n>11$.[9] The small voltage difference in the components of the wave at annealed surfaces led the authors to speculate that presence of this fine structure (i.e., waves with components that are not baseline resolved) was due to the existence of both large and small domains of the adlayer on the surface. Thiolates that are part of large domains would be more difficult to desorb due to the impermeability of the domain to solvated cations. This hypothesis was supported by data

for the desorption of thiols from surfaces with greater homogeneity in terrace size that gave one desorption peak for thiols with n>11.[12]

Recently, Morin and coworkers have speculated a different cause of the fine structure seen in the desorption curves of long chain alkanethiols. Their subtractively normalized interfacial Fourier transform infrared spectroscopy (SNIFTIRS) data, taken at different potentials over the desorption window, showed a biphasic decrease in the asymmetric methylene stretch of the monolayer during monolayer desorption that was the reverse of that expected for the charge passed at these potentials.[21] According to these data, a majority of the molecules in the monolayer are reduced and then undergo a reorientation at more negative potentials. The process is reversed when the potential scan is reversed, and the thiolates return to their original orientation and are subsequently oxidatively deposited. These authors used the data to rule out the possibility that the shape of the voltammograms was caused by differences in domain sizes or the presence of multiple adsorption sites, proposing a model that involved the formation and electro-spreading of micelles. In a related study on single crystal Ag (111) electrodes, the fine structure was reported for short chain length thiols and was not attributed micelle formation but rather to desorption from two different surface sites.[27]

The data presented in this paper show that a range of fine structure is frequently recorded in the reductive desorption of butanethiolate monolayers at annealed gold. This fine structure is again attributed to differences in domain size of the adlayer on the (111) terraces. These domains are stabilized by inter-adsorbate interactions among the thiolate chains. Often this small stabilizing effect has been neglected, leading researchers to assume that short chain length precursors form only partial monolayers. However, our earlier work in

using reductive desorption to determine surface coverage has found little difference in the surface concentrations of short and long chain length adsorbates.[7,9]

Experimental

All substrates were prepared by evaporation of 300 nm of gold were evaporated onto freshly cleaved mica sheets in a cryopumped E306A Edwards Coating System. The substrates were then annealed at atmospheric pressure in a muffle furnace at 300 °C for 5 hours; this process yielded a surface composed of large diameter (100 to 200 nm), atomically smooth Au (111) crystallites.[8] The roughness factor of these substrates, given as the ratio of active surface area, as determined by electrochemistry of adsorbed iodine molecules, to the exposed geometric surface area of the electrode, is 1.1 ± 0.1.[8] The substrates were stored in a dessicator when not immediately coated with a thiolate monolayer. Monolayers were formed by immersing the gold substrates in either 1 mM or 2 μM ethanolic solutions of butanethiol (Aldrich) for 12 h. The monolayer-coated samples were the emersed from the ethanol solution, rinsed, and dried under a stream of high purity argon.

Electrochemical experiments were performed with a model 263 potentiostat/galvanostat (Princeton Applied Research). A conventional three-electrode cell was used, with the geometric area of the working electrode exposed to electrolytic solution defined by an elastomer o-ring (geometric area of 0.65 cm^2). A platinum coil and $Ag|AgCl|KCl_{sat}$ electrode were used as the auxiliary and reference electrodes, respectively. All potentials are reported with respect to the $Ag|AgCl|KCl_{sat}$ electrode. The electrolyte used was aqueous 0.5 M KOH, which was deoxygenated with argon before commencing the electrochemical experiments. All of the electrochemical experiments were performed within

15 minutes of removing the Au electrode from the thiol formation solution. All glassware was thoroughly cleaned with piranha solution (1 part 30 % H_2O_2: 3 parts 98 % H_2SO_4) prior to use and then extensively rinsed with distilled-deionized water. **Caution piranha solution is explosive and reacts violently when in contact with organic compounds and should be neutralized immediately after use.**

Results and Discussion

The voltammograms shown in Figures 1-3 were acquired using the same aqueous electrolyte, cell, and counter and reference electrodes. The only difference was the annealed Au/mica working electrode. A well-defined fine structure is recorded in the first scan of Figure 1. The voltammogram shows two well separated waves: one at –803 mV and the other at –879 mV. While the overlap of the peaks complicates an effective deconvolution for the charge integration, the approximate area located under the first wave gives a charge of 57 $\mu C/cm^2$ while the area under the second wave yields a charge of 31 $\mu C/cm^2$. The small peak located at –1020 mV has been noticed in other reports and is generally attributed to polysulfur impurities (e.g., octameric sulfur).[28-30] Two waves are evident on the oxidative scan, one at –980 mV and the other at –660 mV. The former is attributed to the deposition of polysulfur species, and the latter is ascribed to the oxidative redeposition of butanethiolate. The small charge under the oxidative deposition wave, 19.7 $\mu C/cm^2$, is indicative of the high solubility and rate of mass transport of the desorbed thiolate in the 0.5 M KOH electrolyte.[7] The desorbed molecules are solubilized and diffuse away from the surface before the potential returns to a point where redeposition occurs.

The second cathodic scan, shown by the dotted line, in Figure 1 is markedly different than the first cathodic scan. Only one desorption wave is evident. It has a cathodic current maximum at –750 mV and a charge of 42 $\mu C/cm^2$. These differences indicate that desorption of the redeposited layer is more facile than that of the as-formed layer and that the reformed layer has a surface concentration much lower (~50%) than the original film. In order for the layer to be removed from the surface, cations must permeate the film, and the interactions among the hydrocarbon chains will impede this process. Therefore, the shift to a more positive desorption potential reflects an increased permeability of the redeposited layer due to a lower coverage and a lower degree of order.

The voltammogram in Figure 2 shows a peak with intermediate fine structure for desorption triggered in the first scan. The predominant peak is located at –825 mV and has a shoulder at –862 mV. The curve has an oxidative deposition peak with a charge of ~20 $\mu C/cm^2$ and a peak position of –677.2 mV.

A voltammetric curve with a different shape for a butanethiolate monolayer at an annealed gold substrate of is shown in Figure 3. This figure displays the voltammogram that is typically observed with a peak located at –841.5 mV and a charge of 73.7 $\mu C/cm^2$, which has a full width at half maximum (FWHM) of 70 mV.

The previous paragraphs reported the difference in the features of each voltammogram, but several noteworthy similarities also exists. Specifically, none of the FWHMs for the desorption of the as-formed layer is larger than 90 mV, the value reported for the absence of adsorbate interactions, indicating that attractive interactions exist among the hydrocarbon chains in each of the examples.[31,32] Also the small capacitive envelope, indicates that the films are rather impermeable to electrolyte.

While a well-defined fine structure in the desorption peaks was recorded in only 20% of the voltammograms, other desorption experiments on butanethiolate monolayers adsorbed at gold gave un-split peaks or peaks with shoulders. The causes of this heterogeneity in fine structure could be many. First, the two separate peaks could be due to different adsorption sites on the annealed gold surface. However, scanning tunneling microscopy (STM) data have shown these surfaces to be strongly (111) terraced, with a low occurrence of step sites.[30,33] Furthermore, voltammetry performed at unannealed surfaces shows waves that are separated by 200 mV, much larger than is seen here.[8] While adsorption at bridge sites and on-top sites of the (111) surface is possible, many theoretical calculations have predicted the three-fold hollow site as the thermodynamically stable site for thiol adsorption.[34,35]

Second, the fine structure could be due to the formation and electro-spreading of micelles. However, short chain amphiphiles typically have quite large (>1M) critical micellar concentrations (cmc)[36] that are likely not reached under the conditions of the experiment. Finally, due to the relatively high solubility of short chain thiolates in basic solutions, as evidenced by the fact that less than half of the film is redeposited, we conclude that micelles of butanethiolates are not formed upon desorption of the film.

Third, the fine structure could be caused by the heterogeneity of the domain size that is the result of heterogeneity in terrace width of the substrate. By measuring the full width at half maximum (FWHM), one concludes that attractive interactions are present on the surface.[32] These attractive interactions are on the order of 5 to 10 kJ mol^{-1}, slightly weaker than a hydrogen bond.[37] These data, combined with the reduced rate of electron transfer to solution-phase redox probes and the low capacitance of these films,[38] allows one to infer that the magnitude of these interactions is significant. More evidence for this conclusion is seen

in the desorption of a butanethiolate monolayer formed from a solution with a low precursor concentration. Under this condition, the monolayer reaches only ~70 % of its limiting concentration, and a single desorption peak is recorded at –790 mV. This result is shown in Figure 4. The less negative desorption potential shows that a disordered monolayer is formed and the absence of peak splitting indicates that a micro-heterogeneity is present in the adlayer structure.

Also, the similarities in the shapes of these desorption curves with those of under potentially deposited (UPD) metal monolayer justifies the use of similar explanations to the cause of the fine structure. Hamelin attributed the fine structure in desorption curves for Pb monolayers from Au to the differences in domain size.[39,40] UPD metal monolayers and self-assembled thiol monolayers are analogous systems, and the fine structure present in their voltammetric desorption curves should arise from a similar source—heterogeneity in terrace width of the underlying substrate.

We envision the following mechanism for butanethiol monolayer formation at annealed gold surfaces. Initial adsorption takes place at random sites on the terraces, and growth at these nucleation sites defines the registry of the domain. While some terraces are as large as 150 nm, many are smaller and similar in size to the domains. On the small terraces, the domains would increase in size until they reached a step edge. On the large terraces, several nucleation sites would be formed with domains growing together as the limiting surface concentration is reached. These processes would create small domains on the narrow terraces and large domains on the larger terraces.

Though these interactions increase with increasing n, these forces influence domain formation for short and long chain adsorbates. These forces induce the formation of domains

whose size is determined by the width of the terrace on which they initially form. Domains will grow until they reach a step edge or another domain. While terraces with small diameters will limit the size of some domains, the number of nucleation sites on large terrace will determine domain size on larger terraces.

The reductive desorption curve can be thought of as a number density plot of domain size. The domain size increases with the magnitude of the desorption potential, and the current at give potential is proportional to the number of domains of a given size. Thiolates in smaller domains desorb at less negative potentials followed by the desorption of thiolates in larger domains at more negative potentials. Therefore, the two narrow peaks of Figure 1 are indicative of two local maxima in domain size that are well separated. Figure 3 represents a distinct homogeneity in domain size, whereas Figure 2 represents a surface an intermediate level of homogeneity. These data that arise from similarly prepared substrates argue against the comparison of desorption data obtained on vastly differently substrates (e.g., single crystal Au and annealed Au on mica). Direct comparisons can only be made from data from similar substrates.

Conclusions

A variety of peak shapes in the reductive desorption of butanethiolate has been recorded. This variety has been attributed to heterogeneity in domain size stemming from heterogeneity in terrace width on the annealed gold surface. ERD has been shown to be highly sensitive to the adlayer structure. The data gained in such studies has given insights into the roles that adsorbate-adsorbate interactions and substrate morphology play monolayer formation.

Acknowledgements

The authors gratefully acknowledge James Anderegg of the Ames Laboratory for acquiring supplementary X-ray photoelectron spectroscopic data and Duane Weisshaar for helpful discussion. This work was supported by the Office of Basic Energy Research, Chemical Sciences Division of the US Department of Energy. Ames Laboratory is operated for the US Department of Energy by Iowa State University under Contract No. W-7405-eng-82.

References

(1) Zhong, C.-J.; Porter, M. D. *Sulfur-gold interactions in organosulfur-based monolayers: implications of the reductive desorption of two-component monolayers.* **1997,** *preprint.*

(2) Walczak, M. M.; Popenoe, D. D.; Deinhammer, R. S.; Lamp, B. D.; Chung, C.; Porter, M. D. *Langmuir.* **1991,** *7,* 2687-2693.

(3) Weisshaar, D. E.; Lamp, B. D.; Porter, M. D. *J. Am. Chem. Soc.* **1992,** *114,* 5860-5862.

(4) Nishizawa, M.; Sunagawa, T.; Yoneyama, H. *J. Electroanal. Chem.* **1997,** *436,* 213-218.

(5) Ohtani, M.; Sunagawa, T.; Kuwabata, S.; Yoneyama, H. *J. Electroanal. Chem.* **1997,** *429,* 75-80.

(6) Gorman, C. B.; Biebuyck, H. A.; Whitesides, G. M. *Langmuir.* **1995,** *11,* 2242-2246.

(7) Widrig, C. A.; Chung, C.; Porter, M. D. *J. Electroanal. Chem.* **1991,** *310,* 335-359.

(8) Walczak, M. M.; Alves, C. A.; Lamp, B. D.; Porter, M. D. *J. Electroanal. Chem.* **1995,** *396,* 103-114.

(9) Zhong, C.-J.; Porter, M. D. *J. Electroanal. Chem.* **1997,** *425,* 147-153.

(10) Zhong, C.-J.; Zak, J.; Porter, M. D. *J. Electroanal. Chem.* **1997,** *421,* 9-13.

(11) Zhong, C.-J. *Voltammetric simulations of electrochemical reductive desorption (ERD) of self-assembled monolayers at gold electrodes.* **1993,** *preprint.*

(12) Wong, S.-S.; Porter, M. D. *J. Electroanal. Chem.* **2000,** *485,* 135-143.

(13) Zhong, C.-J.; Porter, M. D. *J. Am. Chem. Soc.* **1994,** *116,* 11616-11617.

(14) Krysinski, P.; Chamberlain II, R. V.; Majda, M. *Langmuir.* **1994,** *10,* 4286-4294.

(15) Schneider, T. W.; Buttry, D. A. *J. Am. Chem. Soc.* **1993,** *115,* 12391-12397.

(16) Yang, D.-F.; Wilde, C. P.; Morin, M. *Langmuir.* **1996,** *12,* 6570-6577.

(17) Yang, D.-F.; Wilde, C. P.; Morin, M. *Langmuir.* **1997,** *13,* 243-249.

(18) Yang, D.-F.; Al-Maznai, H.; Morin, M. *J. Phys. Chem. B.* **1997,** *101,* 1158-1166.

(19) Yang, D.-F.; Morin, M. *J. Electroanal. Chem.* **1997,** *429,* 1-5.

(20) Yang, D.-F.; Morin, M. *J. Electroanal. Chem.* **1998,** *441,* 173-181.

(21) Byloos, M.; Al-Maznai, H.; Morin, M. *J. Phys. Chem. B.* **1999,** *103,* 6554-6561.

(22) Vinokurov, I. A.; Morin, M.; Kankare, J. *J. Phys. Chem. B.* **2000,** *104,* 5790-5796.

(23) Wiesshaar, D. E.; Walczak, M. M.; Porter, M. D. *Langmuir.* **1993,** *9,* 323-329.

(24) Sato, Y.; Mizutani, F. *Electroanalysis.* **1998,** *10,* 633-637.

(25) Hobara, D.; Ota, M.; Imabayashi, S.-i.; Niki, K.; Kakiuchi, T. *J. Electroanal. Chem.* **1998,** *444,* 113-119.

(26) Imabayashi, S.-i.; Hobara, D.; Kakiuchi, T.; Knoll, W. *Langmuir.* **1997,** *13,* 4502-4504.

(27) Mohtat, N.; Byloos, M.; Soucy, M.; Morin, S.; Morin, M. *J. Electroanal. Chem.* **2000,** *484,* 120-130.

(28) Weisshaar, D. E.; Walczak, M. M.; Porter, M. D. *Langmuir.* **1993,** *9,* 323-329.

(29) Gao, X.; Zhang, Y.; Weaver, M. J. *J. Phys. Chem.* **1992,** *96,* 4156-4159.

(30) Widrig, C. A.; Alves, C. A.; Porter, M. D. *J. Am. Chem. Soc.* **1991,** *113,* 2805-2810.

(31) Laviron, E. *J. Electroanal. Chem. Interfacial Electrochem.* **1974,** *52,* 395-402.

(32) Brown, A. P.; Anson, F. C. *Anal. Chem.* **1977,** *49,* 1589-1595.

(33) Hallmark, V. M.; Chiang, S.; Rabolt, J. F.; Swalen, J. D.; Wilson, R. J. *Phys. Rev. Lett.* **1987,** *59,* 2879-2882.

(34) Yourdshahyan, Y.; Zhang, H. K.; Rappe, A. M. *Los Alamos National Laboratory Preprint Archives Condensed Matter.* **2000.**

(35) Sellers, H.; Ulman, A.; Shnidman, Y.; Eilers, J. E. *J. Am. Chem. Soc.* **1993,** *115,* 9389-9401.

(36) Schid, H. G.; Tirrell, D. A. *Langmuir.* **1991,** *7,* 665-671.

(37) Stryer, L. *Biochemistry;* 3 ed. ; W. H. Freeman and Company: New York, 1988.

(38) Porter, M. D.; Bright, T. B.; Allara, D. L.; Chidsey, C. E. D. *J. Am. Chem. Soc.* **1987,** *109,* 3559-3568.

(39) Hamelin, A.; Lipkowski, J. *J. Electroanal. Chem. Interfacial Electrochem.* **1984,** *171,* 317-30.

(40) Hamelin, A. *J. Electroanal. Chem. Interfacial Electrochem.* **1984,** *165,* 167-80.

Figure Captions

Figure 1. Voltammetric curves for the reductive desorption of butanethiolate chemisorbed on annealed Au/mica showing a well-defined fine structure in the first cathodic scan. Concentration of precursor solution: 1 mM. Electrolyte: 0.5 M KOH. Scan rate: 50 mV/s. First Scan (——). Second Scan (— -).

Figure 2. Voltammetric curves for the reductive desorption of butanethiolate chemisorbed on annealed Au/mica showing a intermediate fine structure. Concentration of precursor solution: 1 mM. Electrolyte: 0.5 M KOH. Scan rate: 50 mV/s. First Scan (——). Second Scan (— -).

Figure 3. Voltammetric curves for the reductive desorption of butanethiolate monolayers chemisorbed on annealed Au/mica devoid of any fine structure. Concentration of precursor solution: 1 mM. Electrolyte: 0.5 M KOH. Scan rate: 50 mV/s. First Scan (—). Second Scan (— -).

Figure 4. Voltammetric curves for the reductive desorption of butanethiolate monolayers chemisorbed on annealed Au/mica devoid of any fine structure. Concentration of precursor solution: 2 μM. Electrolyte: 0.5 M KOH. Scan rate: 50 mV/s. First Scan (—). Second Scan (— -).

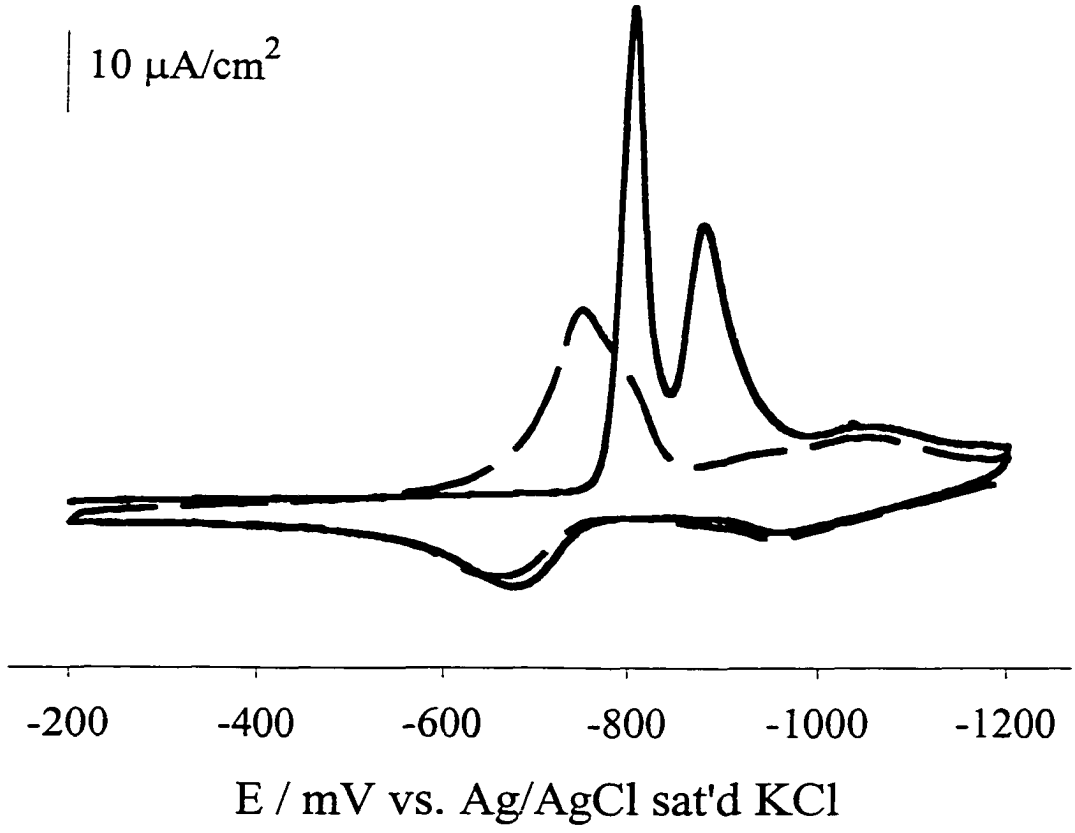

Figure 1

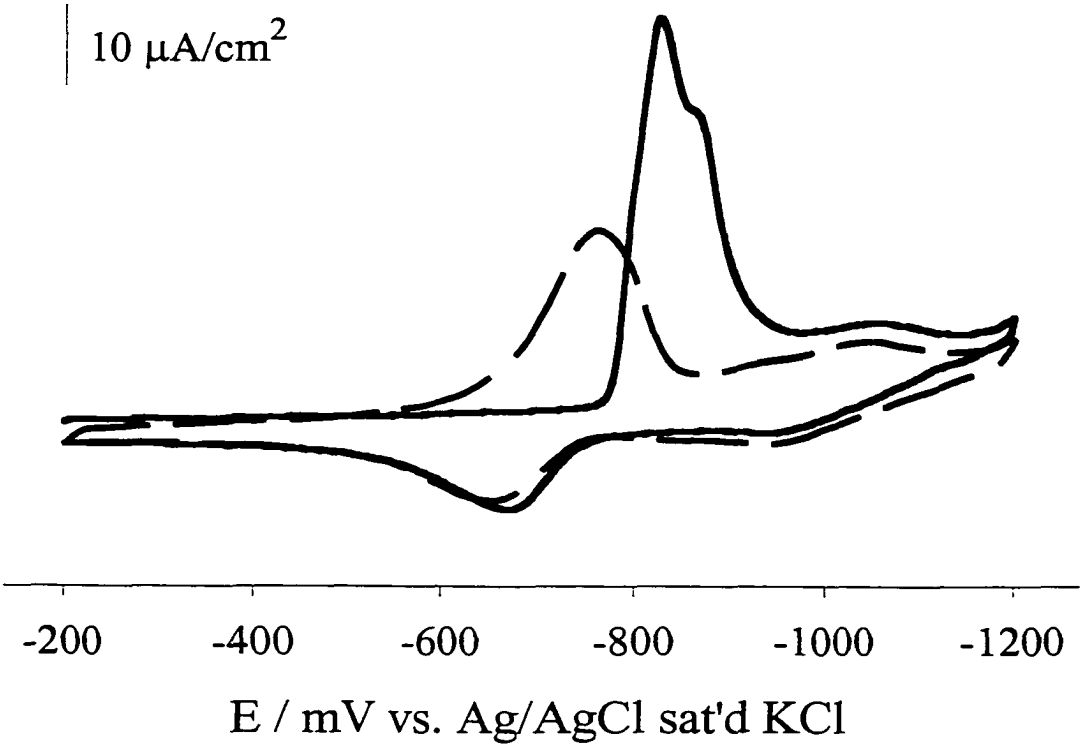

Figure 2

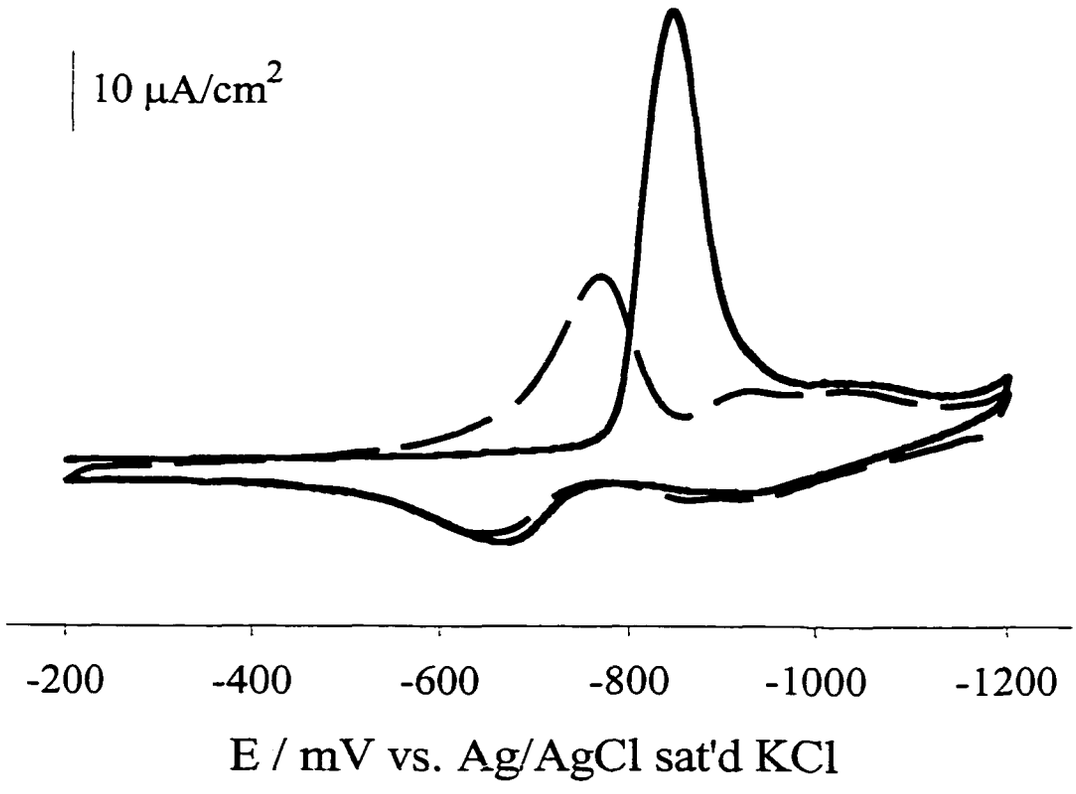

Figure 3

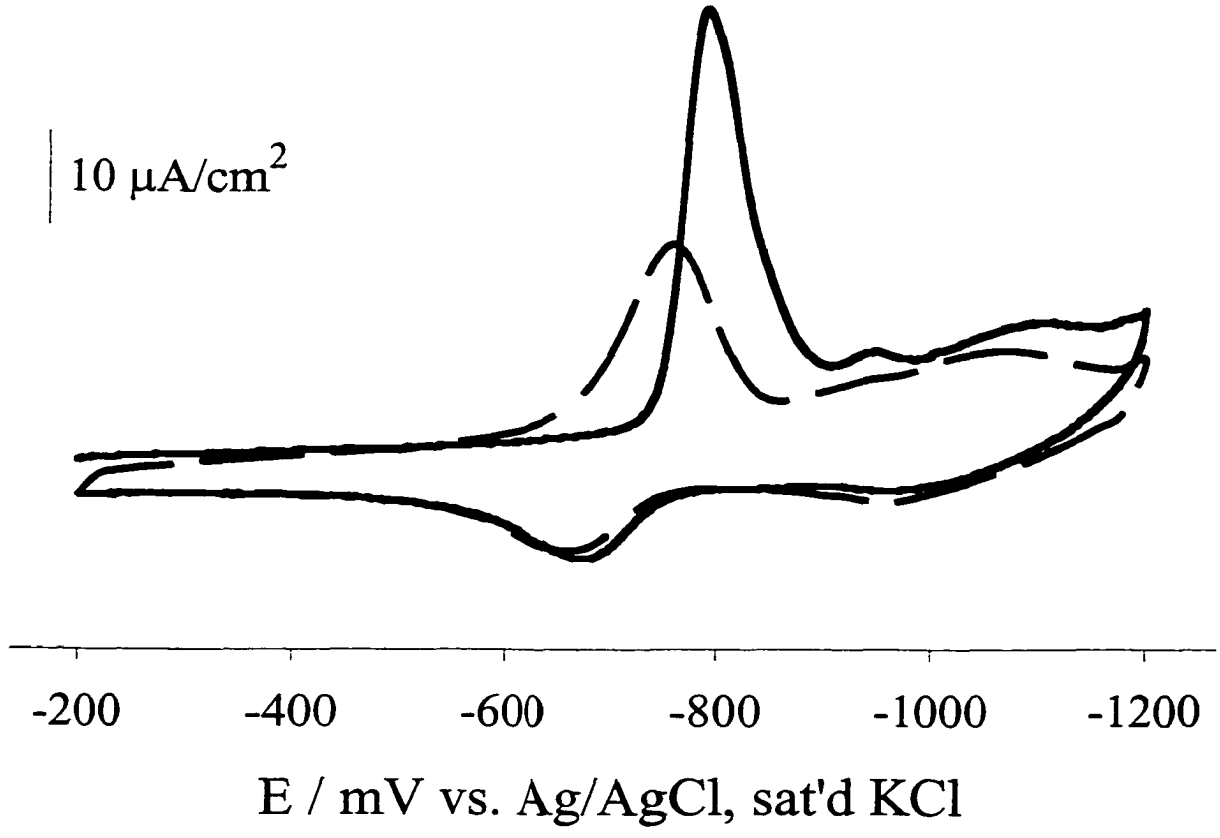

Figure 4

CHAPTER 5. PROBING THE FATE OF THE SULFHYDRYL PROTON DURING MONOLAYER FORMATION WITH THIN LAYER SPECTROSCOPY

A paper to be submitted to *Langmuir*

G. Brent Dawson, Chuanjian Zhong, Neal J. Simmons, and Marc D. Porter

Abstract

A novel approach to determine the hydrogen-containing product of thiolate monolayer formation is described. This work utilized a long optical path length thin layer spectro-electrochemical cell, with a large surface area to volume ratio, to monitor the proton concentration in an aqueous solution of a indicating dye and a monolayer precursor. A calibration curve was constructed using buffered solutions, and the measured absorbance change was converted to a pH change. While protons were detected, the measured pH was only 16% of that expected if one proton were released for each thiolate chemisorbed to the gold surface. The implications of these results are discussed in light of other recent findings.

Introduction

While an extensive amount of information on the structure, formation, and interfacial properties of thiolate monolayers has been developed over the past years, several important fundamental questions still remain.[1-4] One of the most asked of these questions is the fate of the sulfhydryl proton upon monolayer formation. Many laboratories, including our own, have proposed that monolayer formation formally follows equation 1.

$$RSH + Au = RSAu + \frac{1}{2}H_2 \qquad (1)$$

This reaction implies that the thiol precursor undergoes homolytic bond cleavage to produce a hydrogen radical, which could adsorb onto the gold surface, react with solvent molecules, or combine with another radical to form diatomic hydrogen. Other laboratories have speculated that the thiol undergoes heterolytic bond cleavage, producing a thiolate and a proton as shown in equation 2.[5-8] In this mechanism, the gold surface would acquire a negative charge due to the coordinate covalent bond formed between the thiolate and the gold.

$$RSH + Au = RS - Au + H^+ + e^-(Au) \qquad (2)$$

This report describes the use of thin layer spectroscopy to determine the extent of pH changes in a small volume caused by the release of protons during monolayer formation. In this format, a gold electrode forms one wall of a thin layer spectrochemical cell. The cell is filled with a pH indicating dye and an alkanethiol, and the absorbance spectrum is measured. The high surface area of the electrode and the small volume of the cell utilized in these experiments enables the detection of protons originating from the surface reaction. The experiments demonstrate that the amount of protons generated is only a small fraction of that expected suggesting that while protons are formed during the adsorption process, it is probable that more than one hydrogen-containing species is produced.

Experimental

Reagents

Potassium ferricyanide (Fisher), sodium perchlorate (Aldrich), sodium hydroxide (Aldrich), methanol (Fisher HPLC grade), propanethiol 99%(Aldrich), chlorophenol red

(Aldrich, sodium salt), citric acid (Fisher) and sodium phosphate, dibasic (Fisher) were all used as received. The propanethiol was used within a month of opening. Solutions were prepared using deionized water (Millipore).

Electrode Preparation

Glass microscope slides were cut into sections that were 0.99 cm wide and 3.5 cm long in order to fit in the thin-layer cell. These sections were cleaned by sonication in a dilute Micro (Cole-Parmer) solution, rinsed with deionized water and methanol, dried under a stream of ultrahigh-purity argon (Air Products), and loaded into a vacuum deposition chamber. The electrodes were then prepared by vacuum depositing a 15 nm adhesive layer of chromium at 0.1 nm/s, followed by a 300 nm layer of gold (99.99%) at 0.3 nm/s onto cut glass slides, using an Edwards E306A coating system. During the resistive evaporation process, the pressure in the deposition chamber never increased above a value of ~8 X 10^{-6} Torr.

Instrumentation

Electrochemical data were collected with a CV-27 potentiostat (Bioanalytical Systems) and X-Y recorder (Houston Instruments). A Pt coil served as the auxiliary electrode, and all potentials are reported against a Ag|AgCl|saturated NaCl electrode. Due to space limitations within the cuvette-based cell, the diameter of each electrode was constructed to be ~4mm. A bulk cell was used for the electrochemical reductive desorption (ERD) using a platinum coil as the counter electrode and the propanethiolate-coated gold slide as the working electrode. The optical data were collected with a Hewlett-Packard

8452A diode array spectrophotometer. All electrochemical and spectroscopic measurements were carried out under a blanket of argon.

Cell Fabrication

The cell insert was constructed at the Iowa State University Chemistry Machine Shop from a single piece of a poly (methylmethacrylate) (PMMA) and was patterned after a previously published design.[9] The cell insert had a length of 41.30 mm, a width of 10.00 mm, and thickness of 4.06 mm measured at the vertical center. Two thickness spacers located above the back plate, with dimensions of 3.86 mm x 2.18 mm, were separated by a gap of ~ 2 mm. Another spacer was located at the horizontal center of the bottom of the insert and had dimensions of 3.20 mm x 0.94 mm and was raised above the insert surface by 0.10 μm to create the solution cavity. The insert had another raised portion with dimensions of 3.22 mm x 1.65 mm x 4.92 mm that supported the electrode. The cell insert was placed in a PMMA cuvette (Fisher), and the electrode was placed on top of the insert and allowed to rest on the foot and thickness spacers. A mask was applied to the cuvette with a fine tipped pen to ensure that all of the detected light had passed through the thin-layer cavity parallel to the electrode surface.

Volume Determination

The volume of the cavity was determined by thin-layer cyclic voltammetry with 0.690 mM potassium ferricyanide/0.5 M sodium perchlorate solution and a scan rate of 2 mV/s. The charge required to fully electrolyze the probe was determined by integration of the area under the cathodic wave, after accounting for double layer charging current. The volume, V, was found using the following equation:

$$V = \frac{Q}{nFC} \tag{3}$$

where Q is the Faradaic charge passed in the experiment, n is the number of moles needed to reduce 1 mole of ferricyanide, F is Faraday's constant (96,486 C/mole e^-) and C is the concentration of ferricyanide.[10] The experiment was performed in triplicate and the average volume was used. Based on these results, V equals 22.8 (±1.0) μL. The geometric area of the electrode was 2.47 cm^2.

Figure 1 shows the cell insert used for the spectroscopic measurements. The spacers at the top and bottom create a thin layer cavity that is 100 (±4.0) μm in thickness. The spring presses the electrode against the body when it is placed in the PMMA cuvette. The light beam from the spectrophotometer passes parallel to the electrode and probes the solution in the thin layer cavity. After a small volume of solution is placed in the cuvette, capillary action forces it from the bottom of the cuvette to top of the cavity.

Results and Discussion

Figure 2 shows the structure of the chlorophenol red dye and the proposed mechanism for the measurement. If protons are generated in the chemisorption process, they should convert the dye to its acidic form giving an increase in the absorption at 438 nm. If the thiol undergoes homolytic bond cleavage, the atomic hydrogen produced would not give rise to pH decrease. Based on results of cyclic voltammetry, the dye is assumed not to undergo any redox reactions under the conditions used for monolayer formation.[11]

Assuming that the reaction proceeds as shown in equation (2), an appreciable pH change will be produced in the cell. If full monolayer coverage is reached, then 7.6 x 10^{-10}

moles of protons will be produced per cm^2 of the electrode surface. The surface roughness of the unannealed surface will give an additional factor of 1.3[12] because of differences in geometric and actual surface areas.

$$7.6x10^{-10} mol * cm^{-2}(1.3) * (2.47 cm^2) = 2.4x10^{-9} \text{ mol } H^+ \text{ produced}$$

When a dye concentration of 53.5 μM is used in a 22.4 μL cell, this amount of protons would combine with the basic dye (1.20×10^{-9} moles) and the water to give a final pH of 4.26.

Figure 3 shows the visible absorption spectrum for a chlorophenol red solution at pH 4.00 and pH 8.00. At pH 4.00, the absorption maximum appears at 438 nm with a calculated molar absorptivity (ϵ_{438}) of 9.4×10^3 mol cm^{-3}. At pH 8.00 the absorption maximum is at 575 nm, with a molar absorptivity (ϵ_{576}) of 2.4×10^4 mol cm^{-3}. Both of these values agree well with those provided by the manufacturer. Due to its high molar absorptivity at 575 nm and its large shift in absorption maximum with changes in pH, chlorophenol red is well suited for such measurements.

To calibrate the thin layer cell for pH measurements, the absorbance at 575 nm was measured at 6 points over the transition range of the chlorophenol red dye. Figure 4 shows the logarithm of the absorbance response at several pH values. Over the pH range 4.5- 6.5 a linear relationship between the logarithm of the absorbance value and the pH is recorded. The linear regression gave a slope of 0.6 ± 0.3 and an intercept of 3.9 ± 1.5. Also, when a known volume of 10 mM $HClO_4$ was added to an unbuffered dye solution, the measured change in absorbance equaled the expected change ($\pm$ 5%).

Figure 5 shows the visible absorption spectrum taken in the thin layer cell prior to and after monolayer formation. Curve A shows the absorbance spectrum of the blank, an

aqueous solution of chlorophenol red. The absorption at 575 nm dominates the spectrum and is indicative of the dye in its basic form. Curve B shows absorbance of a solution of 53.5 μM chlorophenol red and 5 mM propanethiol. The presence of absorption bands at 438 nm and 576 nm, due to the absorption by both the acidic and basic forms of the dye, indicate that a drop in pH has occurred. The calculated pH of the solution in the cavity without propanethiol present was 5.64 while with propanethiol present it was 5.13. The change in absorbance correlates to a 0.51 unit change in pH. From Figure 4, we calculate that 2.6 X10^{-10} moles of dye were converted to the acidic form giving 3.7 x 10^{-10} moles total of H^+ generated. Since the pH of propanethiol is 11,[13] the contribution of protons from acid hydrolysis would be ~3 orders of magnitude lower than that from monolayer formation. The measured value of generated protons is 16% ± 5% of that expected for the formation of a full monolayer. The lower than expected pH change could arise from one of two situations. Either a full monolayer is not formed or one proton is not produced for every thiol precursor that adsorbs to the surface. The data presented in the next few paragraph rule out the former.

Infrared reflection absorption spectroscopic (IRRAS) characterizations were performed on the gold electrodes to measure the surface concentration of the adsorbed thiolate molecules. Figure 4 shows the IRRAS spectrum of a gold electrode, which was emersed from an aqueous solution of 5 mM propanethiol and 53.5 μM chlorophenol red after 10 min. Three weak bands are present which were not present in a sample prepared in a solution containing only chlorophenol red. The bands correlate to the stretching modes of the methyl and methylene units and agree well with data obtained for a monolayer of butanethiol.[14]

Electrochemical reductive desorption has been shown to be an effective technique in the determination of surface coverage of an adsorbed species.[15] In this technique, the charge (Q) under the desorption wave for the thiol is integrated and related to the surface coverage (Γ) through equation 3,

$$\Gamma = Q / nFA \tag{4}$$

where n is the electron stochiometry of the reaction, F is taken as 96,486 C / mole e^-, and A is the area of the electrode.[16] The fractional coverage monolayer coverage is then calculated from equation 3,

$$\theta = \Gamma / \Gamma_{th} r_f \tag{5}$$

where Γ_{th} is the theoretical coverage for a monolayer of adsorbate and r_f is the roughness factor. The roughness factor is the ratio of the active surface area of the electrode to its geometric area and accounts for the surface defects. We have previously determined the roughness factors for annealed and unannealed surfaces by surface voltammetry of adsorbed iodine and scanning tunneling microscopy (STM) to have values of 1.1 ± 0.1 for annealed gold and 1.3 ± 0.3 for the unannealed surfaces.[12,17] The ERD data of a sample of annealed gold on mica sample placed for 10 minutes in a aqueous solution of 5 mM propanethiol and 53.5 μM chlorophenol red is shown in Figure 5. One large wave is present at a potential of -0.8 V vs. Ag/AgCl with an integrated charge of 84.0 $\mu C/cm^2$. The small wave located at ~-1100 mV is representative of the desorption of propanethiol from step sites. The potentials agree well with previously published results[18] for propanethiol while the charge is indicative of a monolayer coverage of 0.88.

These data show that while a full monolayer has mostly formed, the stochiometry of equation 2 does not hold, and many possible mechanisms exist that could give rise to a

detected proton: adsorbed thiolate stochiometry that is less than one. First, the protons could be reduced at the electrode to form diatomic hydrogen. Recent open circuit potential measurements support such a conclusion,[19] though the most likely oxidant (O_2) has been removed from solution. Second, the protons could adsorb to the gold surface and not diffuse into the solution. The adsorbed protons would not interact with the dye and would go undetected. Third, two or more mechanisms could be active in monolayer formation leading to the adsorption of the thiol precursor forming atomic hydrogen as well as protons. The next few paragraphs will discuss the feasibility and implications of each mechanism.

The initial products of homolytic bond cleavage are a hydrogen atom and a thiyl radical. The thiyl radical would form a covalent bond with the gold retaining its original charge. The hydrogen atom could adsorb to the gold surface, absorb into the bulk, react with another hydrogen atom to form diatomic hydrogen, or react with a solvent to form a more stable radical.

While the homolytic bond strength of S-H bond is relatively high (~87 kcal/mol),[20] the energy needed to break this bond could be released in bond formation, or the adsorption or absorption of atomic hydrogen onto or into the Au. The reported bond strengths for the Au-S and H-H bonds are also relatively high (40 and 104 kcal/mol respectively). Therefore monolayer formation with the production of molecular hydrogen is thermodynamically favored by 5 kcal/mol.[21] While the absorption of hydrogen into Au has been reported,[22] its heat of solution is only 2.1 kcal/mol. From a thermodynamic point of view, H_2 formation is more probable than the absorption of atomic H into the Au substrate.

From a kinetics view, one realizes that the hydrogen atoms must encounter one another to react. Equation 6[23] gives the relationship between the second order rate constant (k_a) and the interaction radius of two species (R_{12}).

$$k_a = 4\pi N_A(D_1+D_2)R_{12}f \qquad (6)$$

Using a diffusion coefficient (D) of 5 X 10^{-9} m^2s^{-1} for each hydrogen atom and 1 for the electrostatic factor (f) and 6.02214 X 10^{23} for N_A, one finds that the hydrogen atoms must be within 1.6 Å to react. If the hydrogen atoms are generated at the adsorption site then their minimum separation distance would be 5 Å and calculating the time needed for this RMS displacement for both hydrogen atoms gives one finds 2.9 ps. The k_a for the reaction of the hydrogen atom with ethanol is 3 orders of magnitude smaller (2.6 X 10^7 $M^{-1}s^{-1}$)[24] than that for the radical elimination reaction, indicating that a hydrogen atom must undergo a significantly larger number of collisions with the solvent before a reaction would occur. Taken together, radical self elimination is more probable than the reaction of H with the solvent.

With heterolytic cleavage of the S-H bond, a thiolate anion and a proton are produced. The thiolate forms a coordinate covalent bond with the gold giving the electrode surface an excess negative charge. The electron could undergo reactions with any oxidants (e.g. oxygen or disulfide) present to remove the excess charge from the surface. Several groups have reported negative shifts in the open circuit potential upon thiol adsorption. Paik and coworkers measured the negative shift in open circuit potentials with monolayer formation and contrasted it to the positive shift when disulfides were used as precursors.[6-8] Porter and coworkers also described the negative shift in potential upon monolayer formation that was mitigated by the presence of oxygen.[25] Earlier, this group had reported the presence

of hydrogen peroxide production during the formation of monolayers on finely divided gold powders in the presence of oxygen.[18] These experimental data indicate that heterolytic bond cleavage is active and such a mechanism generates protons.

This body of work leads to several conclusions. When thiolate monolayers on gold surfaces are prepared in aqueous or ethanolic solution, protons are produced. Whether these protons are long lived or undergo reactions with oxidants present has not been determined. While there is no electrochemical data to support H_2 formation, it has not been ruled out, and is a kinetically and thermodynamically feasible product.

Conclusions

The use of thin layer spectroscopy has proven useful in our work to determine the identity the hydrogen-containing product of monolayer formation. This work has shown that protons are released during monolayer formation. However, the amount of protons detected is much less than the amount expected for the formation of a full monolayer. A thorough review of the relevant literature indicates that subsequent reduction reactions or an alternate reaction mechanisms generating H_2 could explain this discrepancy.

Acknowledgements

The authors gratefully acknowledge Dick Egger of the Iowa State University Chemistry Machine Shop for fabrication the plexiglass cell insert. This work was supported by the Office of Basic Energy Research, Chemical Sciences Division of the US Department

of Energy. Ames Laboratory is operated for the US Department of Energy by Iowa State University under Contract No. W-7405-eng-82.

References

(1) Ulman, A. *Chem. Rev.* **1996,** *96,* 1533-1554.

(2) Dubois, L. H.; Nuzzo, R. G. *Annu. Rev. Phys. Chem.* **1992,** *43,* 437-463.

(3) Allara, D. L. *Biosens. Bioelectron.* **1995,** *10,* 771-783.

(4) Zhong, C.-J.; Porter, M. D. *Anal. Chem.* **1995,** *67,* 709 A-715 A.

(5) Krysinski, P.; Chamberlain II, R. V.; Majda, M. *Langmuir.* **1994,** *10,* 4286-4294.

(6) Eu, S.; Paik, W.-k. *Chem. Lett.* **1998,** *5,* 405-406.

(7) Eu, S.; Paik, W.-k. *Mol. Cryst. Liq. Cryst. Sci. Technol., Sect. A.* **1999,** *337,* 49-52.

(8) Paik, W.-k.; Eu, S.; Lee, K.; Chon, S.; Kim, M. *Langmuir.* **2000,** *16,* 10198-10205.

(9) Simmons, N. J.; Porter, M. D. *Anal. Chem.* **1997,** *69,* 2866-2869.

(10) Hubbard, A. T.; Anson, F. C. In Electroanalytical Chemistry: A Series of Advances; Bard, A. J., Ed.; Marcel Dekker: New York, 1970; Vol. 4, pp 129-214.

(11) Simmons, N. J. *Unpublished results.* **1992.**

(12) Walczak, M. M.; Alves, C. A.; Lamp, B. D.; Porter, M. D. *J. Electroanal. Chem.* **1995,** *396,* 103-114.

(13) Oae, S. *Organic sulfur chemistry;* CRC Press: Boca Raton, FL, 1991.

(14) Porter, M. D.; Bright, T. B.; Allara, D. L.; Chidsey, C. E. D. *J. Am. Chem. Soc.* **1987,** *109,* 3559-3568.

(15) Walczak, M. M.; Popenoe, D. D.; Deinhammer, R. S.; Lamp, B. D.; Chung, C.; Porter, M. D. *Langmuir.* **1991,** *7,* 2687-2693.

(16) Bard, A. J.; Faulkner, L. R. *Electrochemical Methods;* Wiley: New York, 1980.

(17) Wong, S.-S.; Porter, M. D. *J. Electroanal. Chem.* **2000,** *485,* 135-143.

(18) Widrig, C. A.; Chung, C.; Porter, M. D. *J. Electroanal. Chem.* **1991,** *310,* 335-359.

(19) Zhong, C.-J.; Brush, R. C.; Anderegg, J.; Porter, M. D. *Langmuir.* **1999,** *15,* 518-525.

(20) Zhong, C.-J.; Porter, M. D. *J. Am. Chem. Soc.* **1994,** *116,* 11616-11617.

(21) Schessler, H. M.; Karpovich, D. S.; Blanchard, G. J. *J. Am. Chem. Soc.* **1996,** *118,* 9645-9651.

(22) Stobinski, L.; Dus, R. *Appl. Surf. Sci.* **1992,** *62,* 77-82.

(23) Alberty, R. A.; Silbey, R. J. In Physical Chemistry; John Wiley & Sons Inc.: New York, 1992, pp 710-748.

(24) Neta, P. *Chem. Rev.* **1972,** *72,* 533-543.

(25) Zhong, C.-J.; Woods, N. T.; Dawson, G. B.; Porter, M. D. *Electrochem. Commun.* **1999,** *1,* 17-21.

Figure Captions

Figure 1. Thin-layer spectroelectrochemical cell insert with electrode and spring. The thickness spacers at the top and bottom of the insert create a cavity with a thickness of 100 μm. When placed in a cuvette, the electrode rests against the foot and the thickness spacers.

Figure 2. Reaction scheme of propanethiol with a gold surface in the presence of chlorophenol red. The chlorophenol dye accepts the proton released from the thiol during monolayer formation converting the dye to its acidic form, which has an absorption maximum at 438 nm.

Figure 3. Visible absorption spectra of the chlorophenol red dye at pH 4.00 (—) and pH 8.00 (•■). The solid curve shows the spectrum of the dye at pH 4.00 with its absorption maximum at 438 nm while the dotted curve shows the spectrum of the dye at pH 8.00 with an absorption maximum at 575 nm.

Figure 4. Plot of the log of absorbance at 575 nm for the chlorophenol red dye versus buffer pH. A linear increase in signal is seen with a slope of 0.601 and a intercept of -3.92.

Figure 5. Thin layer visible absorption spectra of chlorophenol red in the presence (—) and absence (•■) of propanethiol. The spectra were acquired under a blanket of argon in the same cell using the same electrode.

Figure 6. IRRAS spectra of the gold surfaces exposed to either chlorophenol red (•■) or a mixture of chlorophenol red and propanethiol (—).

Figure 7. Voltammetric curve for the reductive desorption of a propanethiol monolayer formed in the presence of chlorophenol red. The data were acquired with a scan rate of 50 mV/s and the annealed gold electrode was immersed for 2 minutes in a 5 mM propanethiol, 53.5 μM chlorophenol red aqueous solution.

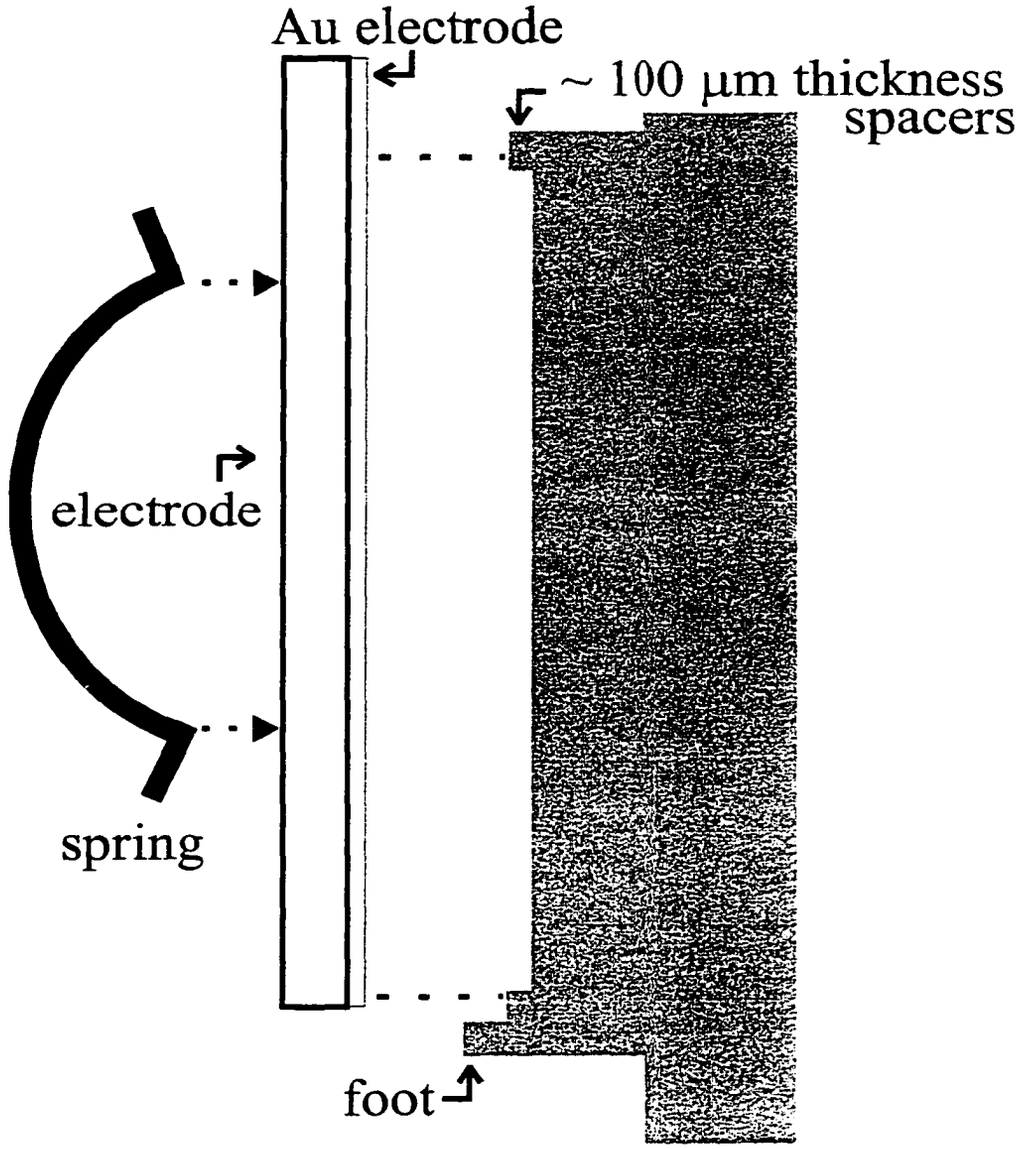
Au electrode
~ 100 μm thickness
spacers
electrode
spring
foot

Figure 1

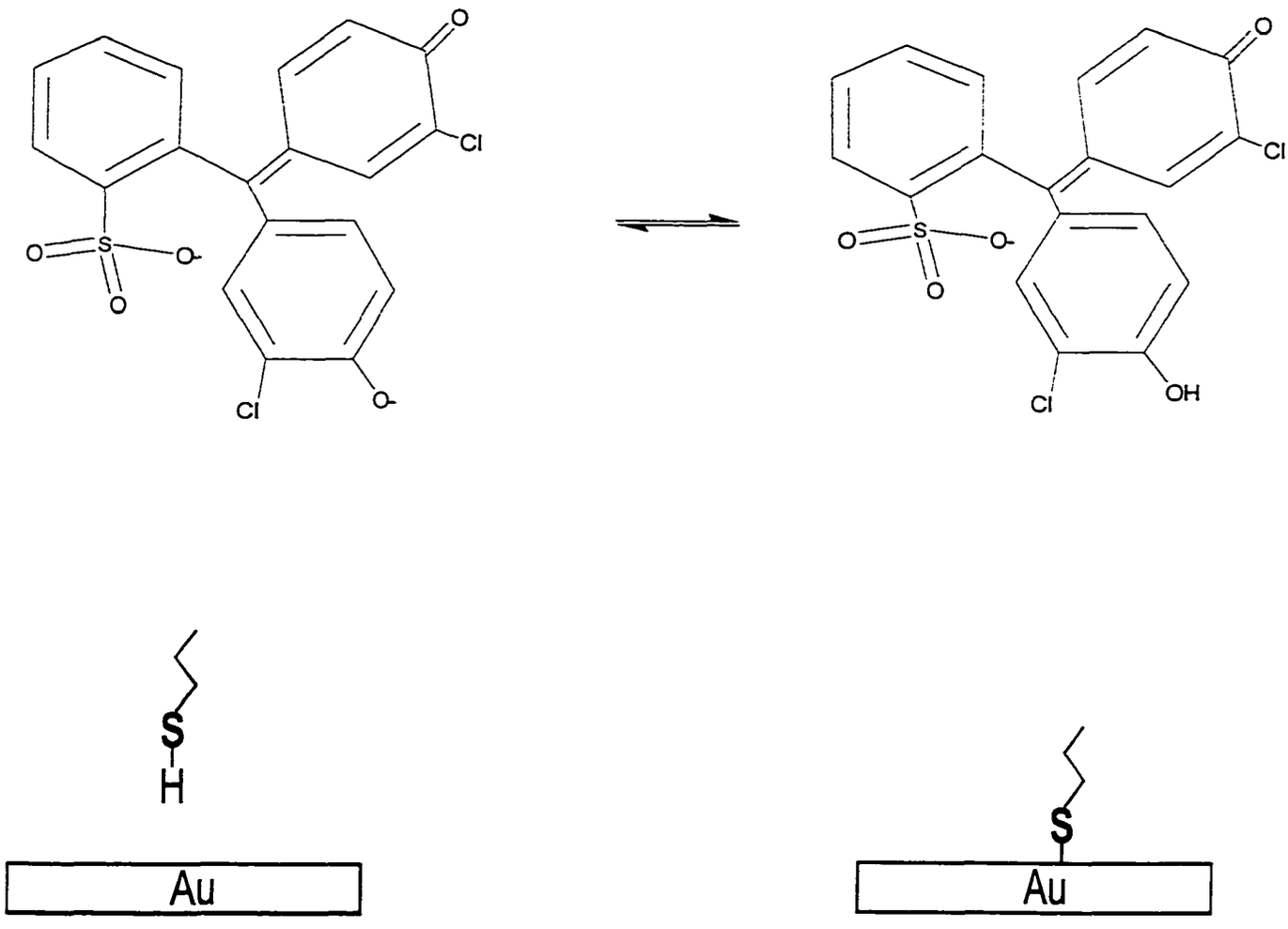

Figure 2

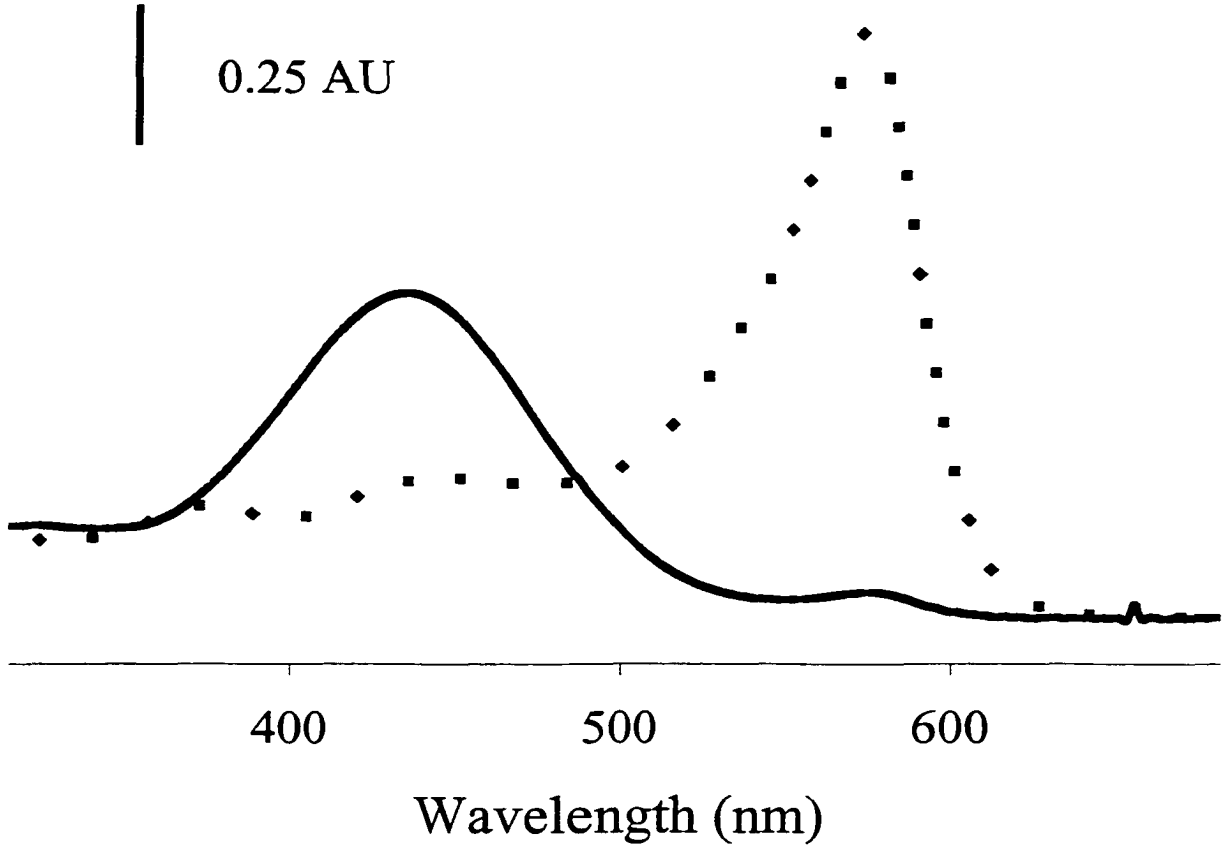

Figure 3

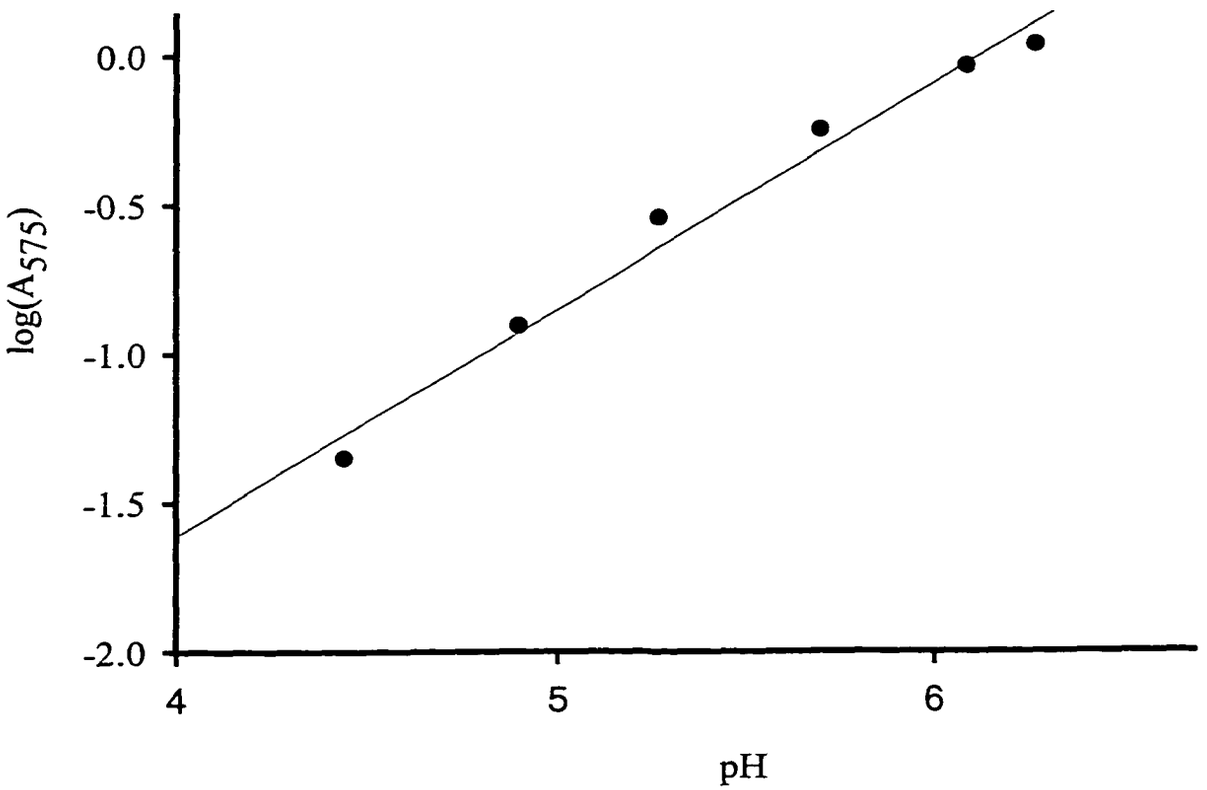

Figure 4

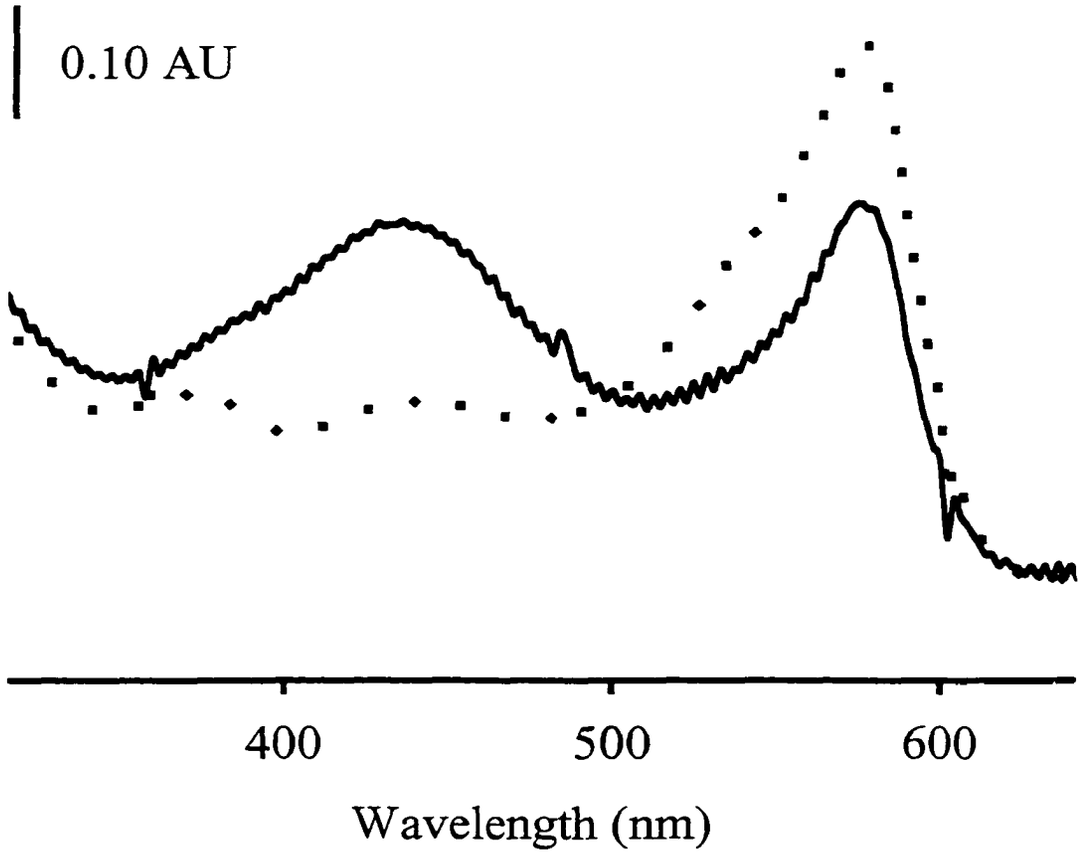

Figure 5

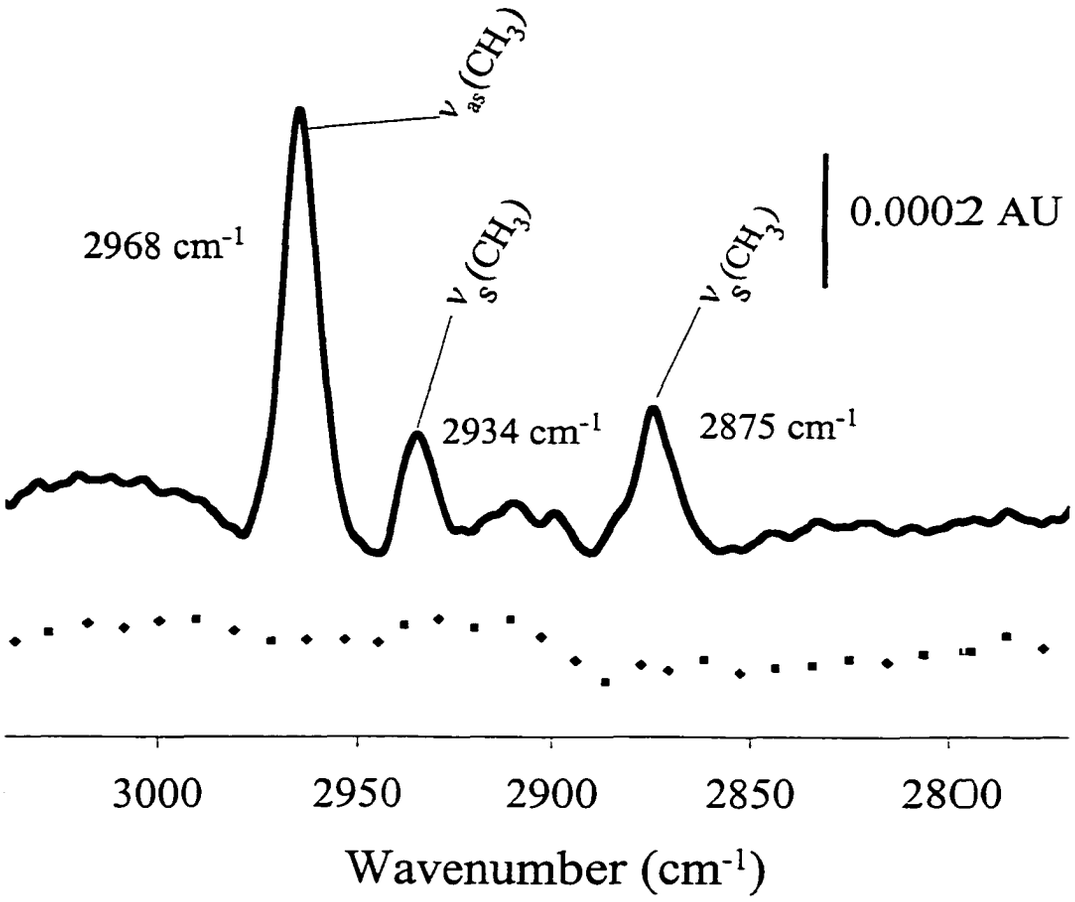
$\nu_{as}(CH_3)$
2968 cm^{-1}
$\nu_s(CH_3)$
$\nu_s(CH_3)$
0.0002 AU
2934 cm^{-1}
2875 cm^{-1}
3000
2950
2900
2850
2800
Wavenumber (cm^{-1})

Figure 6

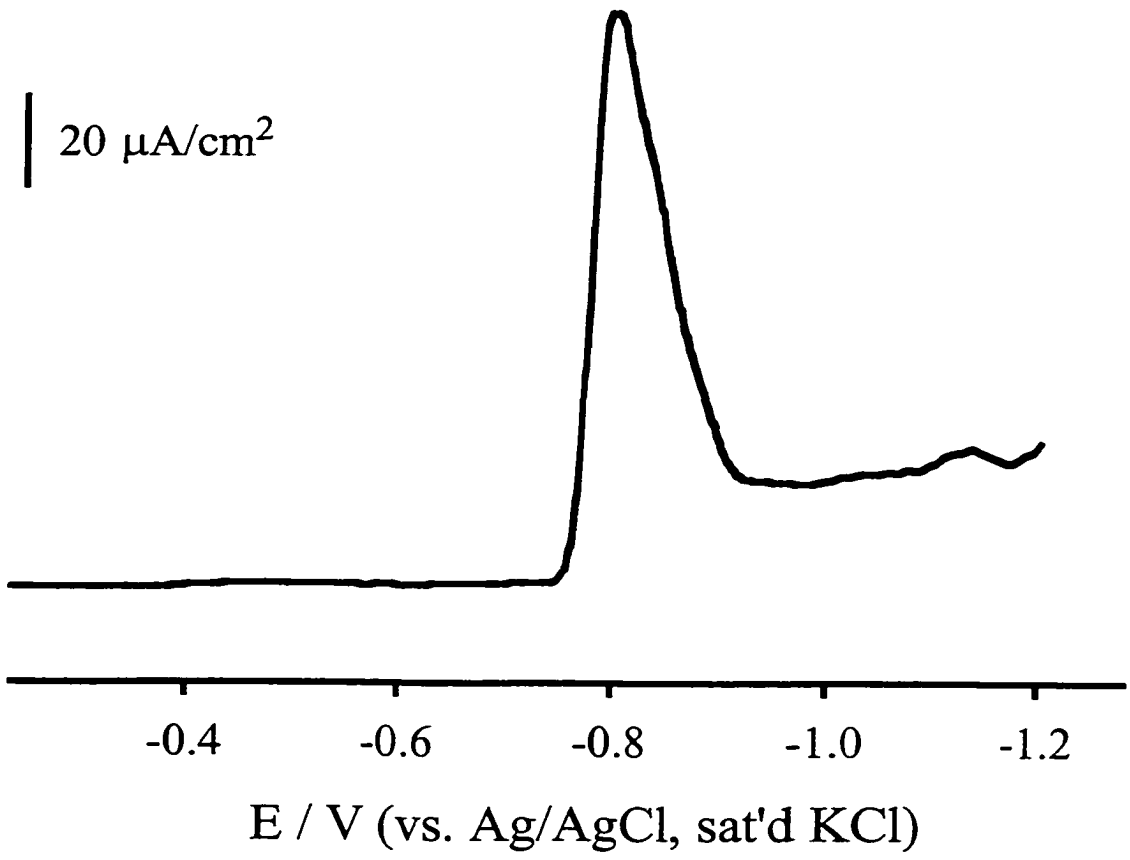

Figure 7

GENERAL CONCLUSIONS AND FUTURE WORK

This dissertation has described several significant characteristics and applications of thiol monolayers chemisorbed at gold electrodes. Several key pieces of information gained from electrochemical and spectroscopic techniques, that advance our fundamental understanding of the individual steps of monolayer formation, have been developed.

The most significant finding is the fate of the sulfhydryl hydrogen. The work involving thin-layer spectroscopy has shown that this hydrogen is released as a proton that causes a decrease in the pH of the formation solution. While the production of atomic or molecular hydrogen was not ruled out, protons were confirmed as an initial product accounting for the build-up of charge on the electrode surface reported in our previous work that reported a build up of negative charge on the electrode surface due to the heterolytic cleavage of the S-H bond.

Data from electrochemical reductive desorption has shown that thiols adsorb faster at step sites than at terrace sites. Other data indicated that the number of methylene units had little effect on the rate of formation leading one to conclude that the slow step in the adsorption mechanism is Au-S bond formation. Interestingly, when a rugged, high throughput analytical technique is needed, this faster rate of monolayer formation at stepped surfaces combined with the higher monolayer stability at such electrodes would them more ideal than annealed surfaces for sensor applications.

While this dissertation reported initial studies of analytical applications of such films, much work remains. Thorough characterization of functionalized thiol monolayers with unique characteristics should continue, giving a firm foundation for the development of

electrochemical and optical sensors. Also, emphasis should be placed on the design and formation of heterogeneously and homogeneously mixed monolayers for affinity and enzyme based electrochemical sensors. This fundamental work will allow for the optimization of the selectivity of electrochemical sensors for the determination of oligonucleotides, pathogenic antigens, and toxic transition metal cations. Moreover, the inherent sensitivity of monolayer-based enzyme electrodes will be raised to new levels due to the development of electrode surfaces, which better mimic physiological environments. Expanding applications to areas such as chip-scale chromatography, molecular electronics, and biomaterials will advance the understanding of monolayer technology while fostering growth into new fields. Furthermore, the use of monolayer technology as platforms to study interfacial chemistry at the molecular level will increase in importance as research in nanotechnology accelerates in the present decade.

Over the past eighteen years, monolayer technology has moved from infancy to adolescence and is poised to assume a significant role in scientific society. While much sound research has nurtured this growth, continued advancement will only be realized through the support of active research in the areas of characterization and application.